UNIVERSITY OF CALIFORNIA
RIVERSIDE

LC-MS/MS/MS Quantification of Oxidatively Induced DNA Lesions

A Dissertation submitted in partial satisfaction
of the requirements for the degree of

Doctor of Philosophy

in

Chemistry

by

Candace Rae Guerrero

Spring 2014

Dissertation Committee:
Dr. Yinsheng Wang, Chairperson
Dr. Wenwan Zhong
Dr. Huiwang Ai

The Dissertation of Candace Rae Guerrero is approved:

_____

_____

_____

Committee Chairperson

University of California, Riverside

ACKNOWLEDGEMENTS

Over the duration of my graduate career, I have had the great opportunity to learn and grow as a scientist and individual. There are many people responsible for this, and without their help and encouragement I would not be where I am.

First, I would like to thank my research adviser, Professor Yinsheng Wang, for his much needed guidance and encouragement pertaining to my research during my PhD study at UCR. He challenged me to think "outside the box" which improved my skills for thinking independently as an analytical chemist and mass spectrometrist. His patience and support throughout the last six years has allowed me tackle lingering problems as well as to grow and evolve as researcher. Thank you Dr. Wang, the journey has been worthwhile.

I would like to express my gratitude to my committee, Professors Wenwan Zhong and Huiwang Ai. Thank you for taking your time reading my dissertation and offering your suggestions. I appreciate all your efforts in promoting my success.

I would also like to take a moment to thank current and previous members of the Wang lab. I would like to extend my thanks to Dr. Nicholas Amato, Dr. Renee Williams, Shuo Liu, Lijuan Fu, and Eric Stephens for all of your help and discussions over the years with my research projects. Special thanks goes to Dr. Nicholas Amato, Dr. Renee Williams and Dr. Fan Zhang for your friendships that have uplifted me and motivated me along the way.

I would like to say thank you to God and my parents. Without my Parent's love, encouragement, and setting the bar, I could not have done this. You are my best friends and I love you more than you will ever know. To my partner, Courtney Mitchell, you are the most amazing person in my life. So often you accompanied me on nights I worked so I would not be alone. You are my rock and I can only hope one day I can repay you for all your patience. A million thank yous are not enough.

Lastly, the year I started at UCR my grandmother, Juanita Phelps, passed away. Throughout the years, she has traveled across the country to watch my softball games and attended all of my school events. In her final days, she watched me graduate from college and I know she is watching down now. I love you Grandma and I dedicate this entire process and dissertation to you. You are forever my role model for love, happiness, hard work, and dedication.

COPYRIGHT ACKNOWLEDGEMENTS

The text and figures in Chapter 2, and Appendix A, in part or in full, are a reprint of the material as it appears in **Chem. Res. Toxicol.,** 2013, 26, 9, p. 1361-1366. The co-author (Dr. Yinsheng Wang) in that publication directed and supervised the research which forms the basis for this chapter. The co-author (Dr. Jin Wang) listed in that publication provided technical expertise with the purification of isotopically labeled standards.

The text and figures in Chapter 3, and Appendix B, in part or in full, are a reprint of the material as it appears in **Anal. Chem.,** 2011, 83, p. 2201-2209. The co-author (Dr. Yinsheng Wang) in that publication directed and supervised the research which forms the basis for this chapter. The co-author (Dr. Jin Wang) listed in that publication provided technical expertise with analyte identification and quantification. The co-author (Dr. Bifeng Yuan) listed in that publication provided technical expertise in Real-time qRT-PCR. The co-authors (Dr. Ralf Bahde and Sanjeev Gupta) listed in that publication provided technical expertise in the growing and harvesting of rat tissues.

ABSTRACT OF THE DISSERTATION

LC-MS/MS/MS Quantification of Oxidatively Induced DNA Lesions

by

Candace Rae Guerrero

Doctor of Philosophy, Graduate Program in Chemistry
University of California, Riverside, June 2014
Dr. Yinsheng Wang, Chairperson

Endogenous and exogenous sources can induce reactive oxygen species (ROS), which can inflict damage to DNA. This damage has been linked to aging, cancer, and other human diseases. In this dissertation, we focus on several DNA lesions, which remain unexplored with regards to their induction by ROS via the Fenton-type reaction. We employed a highly sensitive and robust LC-MS/MS/MS coupled with stable isotope dilution method to aid us in the research at hand.

In Chapter 2, we investigated the induction of the (5'*R*) and (5'*S*) 8,5'-cyclopurine-2'-deoxynucleosides by ROS *in vitro*. Fenton-type reaction constitutes a relevant source of endogenous ROS since transition metal ions in the reduced state can react with H_2O_2, which is a byproduct of normal aerobic metabolism, to generate a highly reactive ·OH. Our results demonstrated that under increasing concentrations of Fenton-type reagents,

both diastereomers cPu were generated in a dose-dependent manner, with the (5'*R*)-isomers being preferentially generated. This supported earlier findings that the (5'*R*) diastereomers of the purine cyclonucleosides are repaired more efficiently in mammalian cells than the (5'*S*) counterparts.

In Chapter 3, we described the accumulation of cPu in tissues of Long-Evan Cinnonmon rats, which bear a deletion in the *Atp7b* gene thus sharing many attributes of Wilson's disease. Wilson's disease entails defective excretion of copper ions into the bile, in which patients often suffer from hepatic, neurological and renal abnormalities following copper toxicosis. Therefore, this was a viable system to assess the induction of cPu from *in vivo* Fenton-type reactions. Our results showed that cPu accumulation occurred in age-dependent manner in liver and brain tissues.

In Chapter 4, we assessed the conversion of 5-methyl-2'-deoxycytidine (5-mdC) to its oxidative derivatives by Fenton-type reagents. A Tet/TDG-mediated pathway has been demonstrated to induce active cytosine demethylation in mammals through enzymatic oxidation and subsequent cleavage. Our results suggested ROS may induce demethylation without the use of Tet, potentially compromising the integrity of the genome and gene regulation. We showed that all three oxidation products of 5-mdC were induced in a dose-dependent manner.

TABLE OF CONTENTS

LIST OF FIGURES

LIST OF TABLES

LISTS OF SCHEMES

Chapter 1

Introduction

In order for an organism to exhibit normal cell growth and metabolism, it must have the ability to achieve and maintain homeostasis.[1] There are a variety of cellular mechanisms that contribute to the overall homeostatic state of an organism; these include both enzymatic and non-enzymatic systems. However, both endogenous and exogenous sources, such as reactive oxygen species (ROS), can play a significant role in disrupting cellular homeostasis, directly resulting in detrimental consequences for the organism.

1.1 Reactive Oxygen Species

ROS such as superoxide anion ($O_2^{\cdot -}$), hydroxyl radical ($\cdot OH$), and hydrogen peroxide (H_2O_2), are known to be major contributors to the onset of aging, cancer, and other diseases in humans.[1, 2] ROS is generated both by exogenous sources, such as ultraviolet light (UV), ionizing radiation (IR), chemotherapeutics, and environmental toxins, and also by endogenous sources which transpires by intracellular metabolism via oxidative phosphorylation in mitochondria, long chain fatty acids breakdown by peroxisomes, and host defense mechanisms employed by inflammatory cells.[3-6] Despite the origins of ROS, damage can arise from direct or indirect mechanisms.[6-15]

To a degree, endogenous ROS generation is critical for maintaining homeostasis. For example, phagocytes produce ROS for host defense mechanisms in fighting infections. Additionally, the stimulation of growth factors can generate cytosolic ROS to regulate cell proliferation responses.[16] In general, scientific investigations support endogenous ROS production for their use as signaling molecules for a variety of biological purposes.[17-19]

ROS encompass an assortment of chemical species, with much of the focus on the extremely reactive ·OH. Due to their instability, which in turn results in their high reactivity, the superoxide anion and hydroxyl radical are extremely short-lived. For example, the ·OH in aqueous solution exhibits a half-life of less than 1 ns.[20] However, hydrogen peroxide is a type of ROS that is long-lived and is freely diffusible in the cellular environment. Regardless of the life span, ROS are deleterious due to their reactivity with carbohydrates, lipids, proteins, and nucleic acids (DNA and RNA). As a result, extensive damage to these macromolecules readily occurs. In order to achieve homeostasis in the presence of ROS generation, the cell is equipped with elaborate defense mechanisms to counteract the excessive accumulation of ROS.

There are two specific defense mechanisms in which ROS regulation can be achieved. The first includes enzymatic systems, of which enzymatic scavengers actively covert highly reactive ROS to less reactive metabolites. One example is superoxide dismutase, which converts the $O_2^{\bullet -}$ into H_2O_2. The freely diffusible H_2O_2 can then be converted into water and O_2 by catalase and/or peroxidases.[21, 22] Additionally,

Peroxiredoxins, a family of peroxide scavengers, are also known to regulate ROS levels.[23] The second type of defense mechanisms includes various non-enzymatic small molecules such as glutathione, ascorbate, and pyruvate that serve as antioxidants, functioning as ROS scavengers. Unfortunately, when these antioxidant defense mechanisms fail to maintain the desired level of ROS required for homeostasis, many physiological functions are impaired. Specifically, when the cell experiences elevated levels of ROS, which is referred to as oxidative stress, macromolecules such as nucleic acids can quickly react with ROS, resulting in oxidative DNA damage.

1.2 Oxidative DNA Damage

1.2.1 Non-Bulky vs. Bulky Lesions

Oxidative damage can affect virtually every component of a cell. Much attention over the years has been focused on oxidative damage to lipids and proteins (including ROS induced carbonyl derivatives).[24] However, several efforts seeking to understand disease and aging have reported an increase in ROS-induced damage to DNA.[25] Therefore, it is speculated that the relatively high levels of oxidatively-induced DNA damage could be due to either the proximity of DNA to the primary source of the oxidant generation and/or lack of sufficient DNA repair mechanisms. For these reasons, the aims set forth in this dissertation will focus on ROS-induced DNA damage.

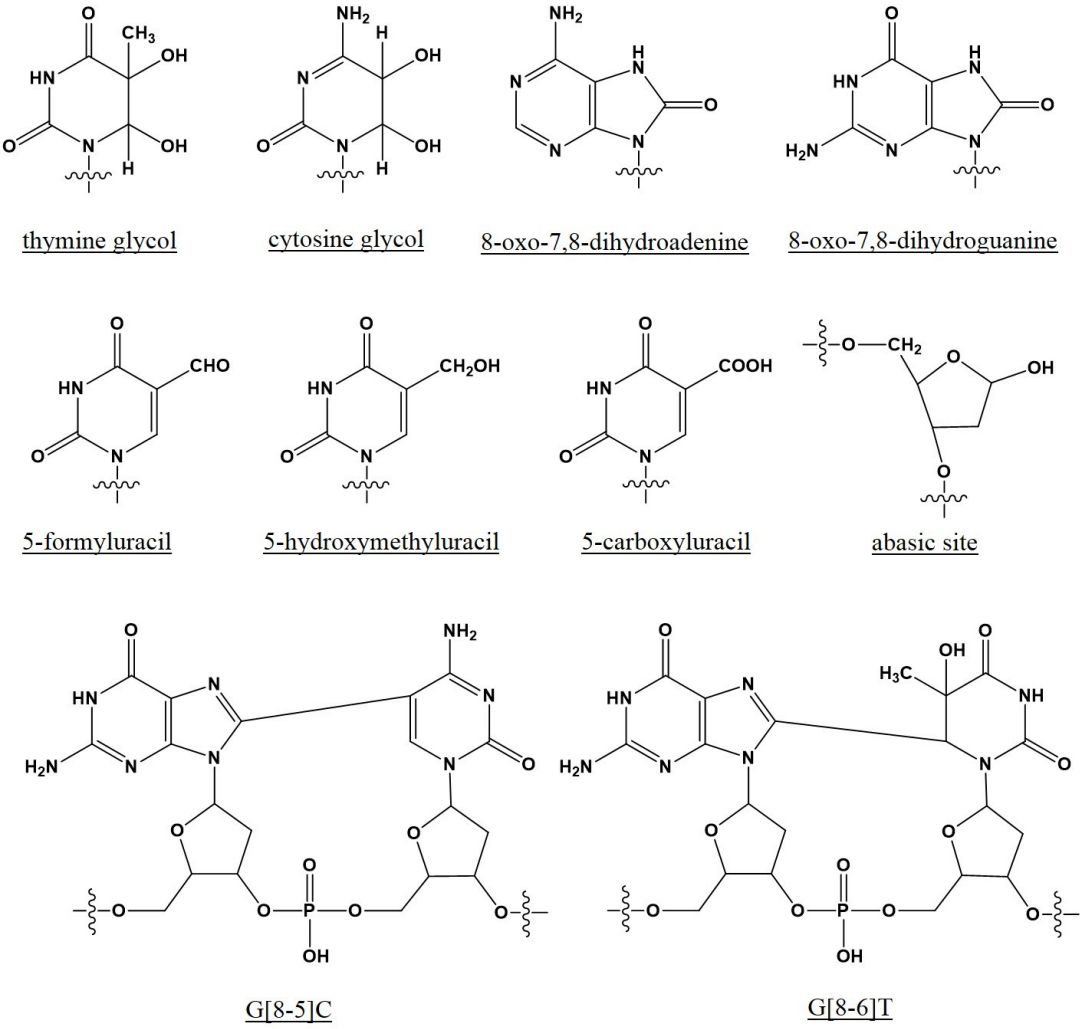

Figure 1.1. Structures of some representative ROS-induced single-nucleobase and bulky lesions.

Despite being short-lived, highly reactive ·OH can be induced via a Fenton-like reaction both endogenously and exogenously. These radicals can then (i) oxidize the double bonds of the heterocyclic DNA bases, (ii) abstract an H-atom from the methyl position of thymine or 5-methylcytosine (5-mdC), or (iii) abstract an H-atom from the carbon atoms of the 2'-deoxyribose. Generally, these lesions are categorized in two subsets; non-bulky and bulky lesions (Figure 1.1).

Non-bulky (or single–nucleobase) lesions are generally viewed as modifications to the nucleobase rather than the sugar-phosphate backbone. One of the most efficiently generated single-nucleobase lesion is 8-oxo-7,8-dihydro-2'-deoxyguanosine (8-oxodG). Other non-bulky lesions include 5-formyl-2'-deoxyuridine (5-fodU), thymine glycol, and cytosine glycol.[26] These modifications usually do not introduce distortions to the DNA double helical structure and can be induced on all four nucleobases, with a preference for guanine. The repair of these single-nucleobase lesions is commonly achieved by the base excision repair (BER) pathway. Alternatively, modifications resulting from ·OH attack that result in helical distortions are often referred to as bulky lesions. Some examples of these bulky lesions are illustrated in Figure 1.1. Bulky lesions, such as cyclopurine 2'-deoxynucleosides, which are recognized by the nucleotide excision repair (NER) pathway are discussed in section 1.3.2 below.

1.2.2 Oxidative Derivatives of 5-Methylcytosine

Although there are a multitude of ROS-induced single-nucleobase lesions, several oxidatively induced nucleosides evaluated in the past few years have gained a significant amount of attention. The 5-methylcytosine (5-mC) lends itself to be an acceptable target for ·OH via a hydrogen atom abstraction from the methyl group residing on the C5 position of the heterocyclic ring.[21] Consequently, the carbon-centered radical generated at the C5 position can react with molecular O_2 to form the peroxyl radical, which can be further reduced to generate 5-hydroxymethylcytosine (5hmC).[26] Subsequent oxidation to this methyl group yields 5-formylcytosine (5-foC) and 5-carboxylcytosine (5-caC). Because of the role of 5-mC in gene regulation,[27] ROS inflicted damage to 5-mC may be problematic for both genomic integrity and gene expression.

Recently, ten-eleven translocation (Tet) proteins were shown to oxidize 5-mC to 5-hmC, 5-hmC to 5-foC, and 5-foC to 5-caC (Scheme 1.1).[25, 28, 29] Tet-mediated oxdidation and the subsequent action by the BER machinery represents the first active demethylation pathway of 5-mC in mammals. Briefly, 5-mC can be oxidized by the Tet family proteins to produce 5-hmC, 5-foC, and 5-caC. Thymine DNA glycosylase (TDG) can then recognize and cleave both 5-foC and 5-caC, leading to the formation of an abasic site, which can be repaired by the BER pathway resulting in the incorporation of an unmodified cytosine. Thus, unwarranted demethylation in promoter regions of genes stimulated by ROS has the potential to impact gene regulation by inadvertently turning "ON" genes.

Scheme 1.1. Tet-mediated pathway for the demethylation of 5-mdC.

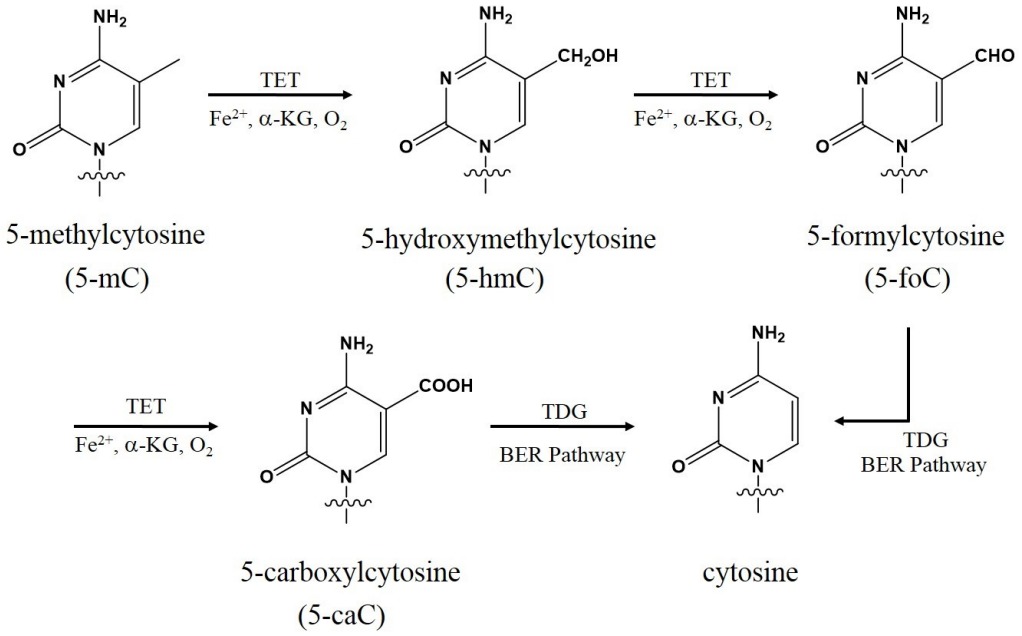

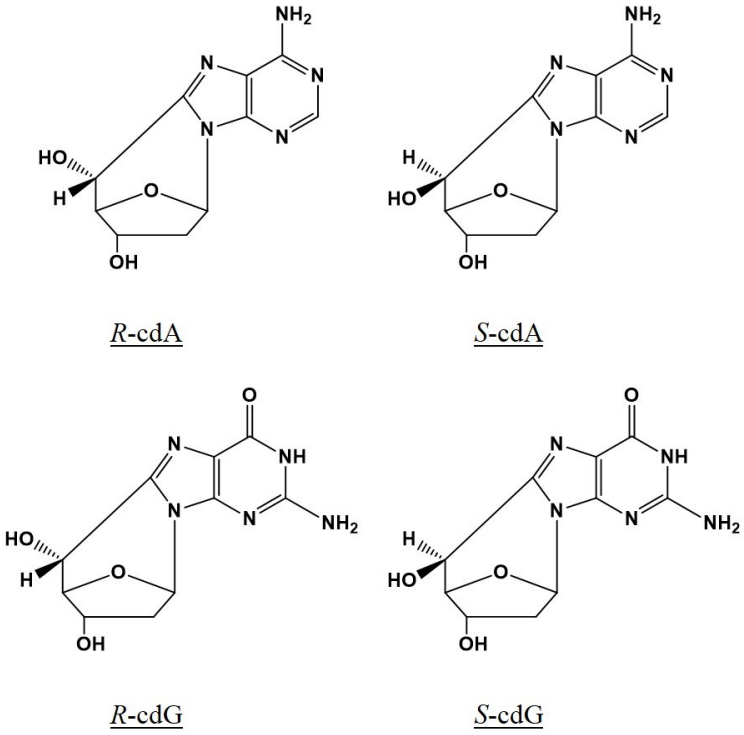

Figure 1.2. The chemical structures of ROS-induced 8,5'-cyclopurine-2'-deoxynucleosides.

1.2.3 8,5'-Cyclopurine-2'-deoxynucleosides

Bulky lesions, such as 8,5'-cyclopurine-2'-deoxynucleosides (cPus), have been shown to accumulate in mammalian tissues and are readily induced by X- or γ-irradiation in human cells (Figure 1.2).[30-35] These lesions possess a covalent bond between the C8-position of the nucleobase and C5'-position of the sugar, resulting in helical distortion of the DNA backbone. Depending on the configuration of the covalent addition at the C5'-position, cPus exist in *R*- and *S*- diastereomeric forms (Figure 1.2). 2'- Deoxyadenosine (dA) and 2'-deoxyguanosine (dG) can be converted to 8,5'-cyclopurine-2'-deoxyadenosine (cdA) and 8,5'-cyclopurine-2'-deoxyguanosine (cdG), respectively. This is facilitated by the ·OH-mediated hydrogen abstraction from the C5'-position resulting in a C5'-centered sugar radical which can undergo intramolecular cyclization with the C8-position of the purine nucleobase.[26, 36]

Biological relevance has been placed on these lesions due to their complexity with regard to repair and their highly mutagenic effects. For many years, it was assumed that a majority of oxidatively-induced DNA damage was repaired by the BER pathway. However, many studies with cPus have demonstrated that helical distortions in DNA induced by the C5' and C8 covalent linkage renders the *N*-glycosidic bond resistant towards acid-induced hydrolysis.[37-39] If fact, the NER pathway is required for the appropriate excision and repair of cdA and cdG.[40-42] While cdA and cdG are excised by NER with similar efficiencies, the *R*-diastereomers are excised with efficiencies that are approximately 2 fold higher than the *S*-isomers.[42] The unsuccessful repair of these lesions

by NER can lead to transcriptional stalling and nucleotide misincorporation. Recent studies have shown that cdA and cdG generate mutations during both replication (via the translesion synthesis pathway) and transcription, which may contribute to the development of human diseases.[40, 43-46]

1.3 DNA Repair

As previously mentioned, there are several cellular mechanisms for the detection and repair of oxidatively generated DNA damage. In order to maintain genomic integrity, there are two major excision repair pathways which include BER and NER.

1.3.1 Base Excision Repair

Non-bulky lesions, such as 8-oxodG, 5-fodU, and 5-fodC are substrates for the BER pathway. Usually these substrates, as well as others that are recognized by the BER pathway, characteristically contain damage localized on the nucleobase portion of the nucleic acid. Consequently, these lesions generally do not impose helical distortions to the DNA backbone. In addition to lesions resulting from nucleobase damage, the BER pathway of most organisms can also remove DNA adducts such as alkylated thymidine, abasic (AP) sites, and even single-strand breaks.

The BER pathway successfully removes and efficiently repairs DNA damage by using a total of five enzymatic reactions.[47-50] Specifically, DNA glycosylases recognize the damaged nucleobase, initiating the BER enzymatic cascade. There are a variety of DNA glycosylases, demonstrating either monofunctional or bifunctional activites. Once the DNA lesions are recognized by DNA glycosylases, the lesions then undergo

enzymatic cleavage at the *N*-glycosidic bond, generating an AP site. Next, DNA AP endonuclease (APE1) can cleave the phosphodiester backbone of the AP site, generating a nick at the 5'-position of the AP site. This nick consists of a free 3'OH and a 5' 2-deoxyribose phosphate (5-dRP) termini.[51] DNA polymerase β (Pol β) subsequently removes 5-dRP and fills the gap with the appropriate nucleotide.[52-55] Finally, DNA ligase III (Lig III) catalyzes the formation of the phosphodiester bond, restoring the oligonucleotide back to its undamaged state.[56] For the scope of this dissertation, only the short-patch BER mechanism utilizing monofunctional DNA glycosylases will be addressed. A general overview is illustrated in Scheme 1.2.

1.3.2 Nucleotide Excision Repair

The NER pathways is a pivotal process in which bulky adducts or helix-distorting lesions are removed. Deficiencies in this repair pathway contribute to diseases such as xeroderma pigmentosum (XP) and Cockayne's syndrome.[57, 58] If left unrepaired by NER pathway, these lesions can halt DNA replication.

Typically, the UV-DDB and XPC-RAD23 complexes identify and bind to the DNA lesions that mediate helix distortions, commencing the NER pathway.[20, 59-61] As a result of the formation of these DNA-protein complexes, several other proteins (XPA, RPA, and TFIIH) are recruited, which facilitate the unwinding of the double-stranded

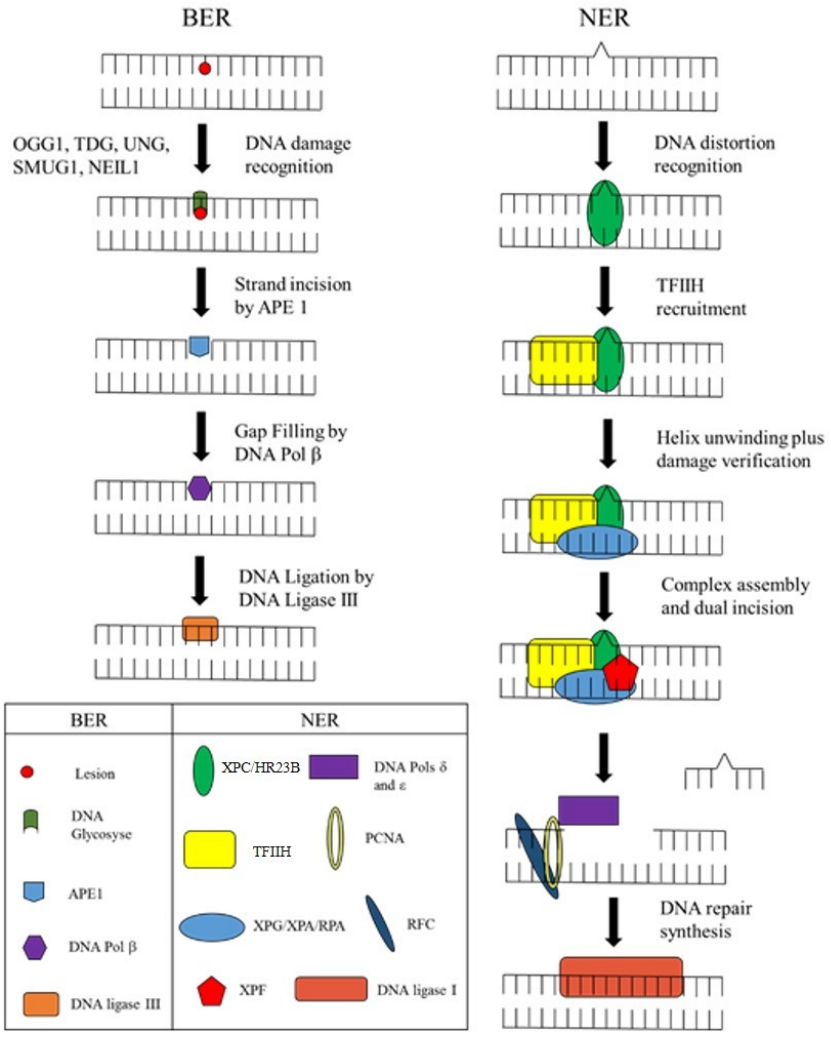

Scheme 1.2. Cartoon illustration highlighting the key steps and enzymes involved in the BER and NER pathways. This representation is modeled after Figure 2 of Brierley and Martin 2013.[25]

DNA double helix and reconfirms the presence of DNA damage. Subsequently, a pre-incision complex consisting of ERCC1-XPF and XPG, is recruited to excise the lesion which is used as the template for DNA synthesis. Finally, DNA ligase I can seal the remaining nick (Scheme 1.2).[62, 63]

1.4 Metal-induced Oxidative Stress

As discussed previously, homeostasis is essential for healthy cellular activity. Particularly, transition metals like iron (Fe) and copper (Cu) are vital for a wide variety of biological functions. These functions include, but are not limited to, cell growth, oxygen utilization, immune system response, gene expression, and the electron transport system.[51] There are extensive mechanisms for metal-ion uptake, storage, and secretion that function to control intracellular concentrations of free metal ions required to maintain homeostasis.[64-68]

When homeostasis is disrupted, metals have the capability to interact with proteins and DNA that are not associated with their normal functions.[52] There have been a considerable amount of literature devoted to the investigations about the negative implications of transition metal accumulation in cells and their ability to inflict damage to proteins and DNA.[51, 55, 57, 58, 69] The aberrant accumulation of metal ions can lead to the unregulated metal-mediated generation of free ROS.

One transition metal that is highly regulated in humans for cellular homeostasis is iron. Predominately, iron is present in biological systems as Fe(II) or Fe(III). “Free iron”

is rarely available in the body due to its reactivity with molecular oxygen, which can readily generate undesired ROS. Thus, iron is usually bound to heme proteins (hemoglobin, myoglobin, and cytochrome), iron storage proteins (ferritin and hemosiderin), or iron-containing enzymes.[65] Only approximately 0.1% of iron is stationed in the plasma. Specifically, exchangeable iron ,which is required for many biological functions, is shielded by a variety of chelating agents and proteins such as transferrin, to both foster the facile transport of iron in cells and the protection against iron-mediated ROS production. Overall, the regulation of iron is performed by iron regulatory proteins which monitor the uptake and storage of iron.

Copper, which exists in cells as Cu(II) or Cu(I), is an indispensable transition metal that participates in the electron transport chain (ETC) for ATP synthesis. Besides its role in the ETC, copper serves as a co-factor for several enzymes involved in redox reactions, such as superoxide dismutase and cytochrome *c* oxidase.[51] Furthermore, copper also serves as a structure metal in chromatin and can establish stable complexes with DNA.[16-19] Similar to iron, "free" copper is rarely present in cells, as its accumulation can have a deleterious impact on cellular damage. Copper is regulated at homeostasis by absorption and excretion mechanisms, of which roughly 80% of copper stored in the liver is released through the biliary pathway.[68]

Despite the known regulatory pathways for both iron and copper, there are existing mechanisms in which these metals can become "free", mediating the formation of an assortment of ROS [$O_2^{\cdot -}$, $^{\cdot}OH$, and peroxyl radicals ($ROO^{\cdot}$)]. Significant levels of endogenously generated $^{\cdot}OH$ is a result of Fenton-like reactions, which have previously

been demonstrated to generate ROS-induced DNA damage *in vitro*.[69, 70] These *in vitro* experiments have revealed that ascorbate can act as a reducing agent towards transition metals such as iron and copper. In doing so, these metals can be effectively reduced to Fe(II) and/or Cu(I) under physiological conditions where ascorbic acid exists as a monoanion. While ascorbate's prooxidant properties hold true *in vitro*, research by Suh et al.[71] demonstrated this is not the case in their *in vivo* conditions. Under excessive oxidative stress *in vivo*, $O_2^{\cdot -}$ formation can generate "free iron" *in vivo* from iron-containing molecules, such as ferritin.[72] Additionally, $O_2^{\cdot -}$ is also capable of reducing Cu(II) to Cu(I) due to the involvement of copper in redox dependent reactions with enzymes, such as superoxide dismutase.

During normal aerobic metabolism, superoxide radicals can be generated via the coupling of electrons leaking from the ETC to molecular oxygen.[73] It has been reported about that 1-3% of the molecular oxygen present in the mitochondria can be converted to superoxide radicals.[73-75] Superoxide dismutase then readily converts the generated superoxide radicals into H_2O_2 and oxygen molecules.[36] As previously mentioned, H_2O_2 is freely diffusible in a cellular environment; therefore, H_2O_2 can reach the nucleus and react with transition metals Fe(II) and Cu(I), yielding the extremely reactive hydroxyl radical via a Fenton-type reaction (Equations 1-2).[76] While this is not the only reaction that can occur, copper and/or iron can complex with DNA, thereby increasing the susceptibility of DNA to $\cdot OH$-induced damage.[16, 17, 22]

Equation 1: $Fe(II) + H_2O_2 \rightarrow Fe(III) + \cdot OH + OH^-$

Equation 2: $Cu(I) + H_2O_2 \rightarrow Cu(II) + \cdot OH + OH^-$

1.5 LC-MS^n Approaches for Assessing DNA Damage

Over the years, mass spectrometry has proven itself to be extremely useful for the identification and structure elucidation of DNA lesions generated from oxidative damage. When mass spectrometry is coupled with liquid chromatography, it can not only be used as a qualitative method, but also as a highly robust quantitative approach to assessing DNA damage induced by ROS or other genotoxic agents. Before the mainstream adoption of LC-MS methods for the analysis of DNA damage, methods such as [^{32}P]-labeling, GC-MS, gel electrophoresis, immunoassays, and ligation-mediated polymerase chain reaction were all previously used, but proven to have many disadvantages. An illustration of these methods was reported in a review by Himmelstein et al.,[77] who reported that these assays lack the quantitative advantage of LC-MS. Specifically, they require large sample amounts and often several derivatization steps. For these reasons, the research set forth in this dissertation will utilize LC-MS^n couple with stable isotope dilution for identifying and quantifying lesions of interest.

1.5.1 Enzymatic Digestion

Assay optimization and reproducibility are crucial for quantifying DNA lesions. The overall goal of quantifying DNA lesions at the nucleoside level depends

predominately on the enzymatic digestion methods utilized. Varying from adduct to adduct, and depending on whether the lesion is bulky or non-bulky, the efficiency of enzymatic hydrolysis at the phosphodiester bond varies. In Chapters 1 and 2, we discuss quantification of cPus which induce helical distortions to the phosphate backbone, which could be problematic for the efficient release of these nucleosides by enzymatic digestion. In Chapter 3, we discuss the non-bulky, oxidized 5-mdC derivatives, which should not influence their enzymatic release from double-stranded DNA

Based on previous publications, a four-enzyme cocktail was used to promote the successful release of cross-linked products. Therefore, we chose to optimize this protocol for the release of similar cross-linked lesions, including cPu.[65, 68, 71] The four-enzyme cocktail consists of nuclease P1 (NP1), calf spleen phosphodiesterase (ExoPII), calf intestinal alkaline phosphatase (CIP), and snake venom phosphodiesterase (ExoPI). First NP1 and ExoPII are mixed with the intact DNA under acidic conditions. Due to the presence of residual adenine deaminase(s) present in commercial enzyme preparations, the conditions were optimized by adding the demaninase inhibitor, *erythro*-9-(2-hydroxy-3-nonyl)adenine (EHNA) hydrochloride, to minimize the coversion of dA to 2'-deoxyinosine (dI).[78] NP1, an endonuclease, cleaves on the 3'-side of any internal phosphodiester bond resulting in 5'-phosphates attached to adjacent nucleosides. ExoPII, a specific exonuclease hydrolytically removes the terminal nucleotide residues from the 5'-side of the phosphodiester bond. Once treatment with NP1 and ExoPII is administered, the aqueous environment is shifted to an alkaline pH, and CIP and ExoPI are added. ExoPI, similar as ExoPII creates nucleoside-5'-phosphates, as well as NP1, but

specifically works in the 3'→5' direction. The combination of these three enzymes results in nucleoside 5'-monophosphates which can be further hydrolyzed by CIP to mononucleosides.

1.5.2 Stable Isotope Dilution

Stable isotope dilution (SID) offers several benefits for the identification and quantification of DNA lesions. By synthesizing an isotopically labeled standard of a desired analyte, one can control which atoms are isotopically labeled, permitting for accurate structure elucidation and fragmentation pathway identification. While differing in molecular weight, chemical properties are conserved for the heavy- and light-isotope containing species therefore the same structural and molecular interactions are exhibited for these isotopomers.[69] For LC-MS applications, these characteristics allow for the unambiguous identification of DNA lesions by sharing the same LC elution times, while still differentiating the target lesion from the isotope-labeled standard based on the unique transitions observed during their fragmentation. The SID methods work exceptionally well particularly because both the isotope-labeled standard and analyte exhibit very similar, if not the same ionization efficiencies, yielding precise quantification.

1.5.3 Enrichment

For analytes of low abundance, such as cPus and cadC, regardless of the enzymatic digestion procedures and the istope-labeled standard utilized, the LC-MS analyte signal can be suppressed by highly abundant unmodified nucleosides. For this reason, we used an off-line enrichment protocol in which unwanted salts and canonical

nucleosides are removed, resulting in a cleaner sample matrix.[58, 69, 79] Samples are subjected to reversed-phase high performance liquid chromatography (RP-HPLC) and each analyte is collected in a predetermined retention time window; this minimizes ion suppression and isobaric interferences, allowing for optimal signal for each modified nucleoside investigated.

1.6 Scope of this Dissertation

This dissertation focuses on the identification and quantification of oxidatively induced single-nucleobase lesions and bulky lesions using LC-MS coupled with SID methods. In Chapter 2, the ability of Fenton-like reactions to facilitate the generation of cPus lesions *in vitro* is investigated. For this study, analytical methods exploiting LC-MS^3 coupled with stable isotope dilution are used to identify and quantify cPus in calf thymus DNA treated with various concentrations of Fenton-type reagents. The observed yields for cdA and cdG exhibited a dose-dependent response, with marked increase displayed at concentrations of 800 and 1600 μM H_2O_2. Futhermore, *R*-diastereomers of cdA and cdG are preferentially produced over *S*-isomers.

In Chapter 3, I explored further into the formation of the cPu lesions from endogenous ROS by using an *in vivo* system representative of Fenton-like conditions. Long Evans Cinnamon (LEC) rats bearing a deletion in the *Atp7b* gene have hepatic damage arising from copper accumulation, of which the damage increases with age. We reason that these rats are suitable models for *in vivo* Fenton-like conditions due to the

excess copper accumulations. In this work, we established that cPus and single-nucleobase lesions indeed accumulated in these tissues. Furthermore, we demonstrated that the levels of both diastereomers of cdA display age-dependent accumulation, as observed with the LEC-/- tissues compared to 3-month control LEA rats. Finally, cPus accumulation was found to be tissue-specific.

In Chapter 4, we further explored the generation of ROS-induced lesions by studying the oxidation of 5-mdC to its oxidatized derivatives, 5-hmdC, 5-fodC, and 5-cadC. *In vitro* experiments revealed that Fenton-type reactions can induce dose-dependent formation these lesions. We found that 5-fodC and 5-cadC levels are induced at comparable levels. This, together with the presence of 10-fold lower levels of 5-cadC relative to 5-fodC, suggest the more efficient removal of 5-cadC than 5-fodC *in vivo*. These *in vitro* experiments suggests the potential involvement of ROS induced active cytosine demethylation.

References

(1) Finkel, T., and Holbrook, N. J. (2000) Oxidants, oxidative stress and the biology of ageing. *Nature*, ***408***, 239-247.

(2) Lindahl, T. (1999) DNA lesions generated *in vivo* by reactive oxygen species, their accumulation and repair. *NATO ASI Ser.*, ***Ser. A 302***, 251-257.

(3) Imlay, J. A., and Linn, S. (1988) DNA damage and oxygen radical toxicity. *Science*, ***240***, 1302-1309.

(4) Lewis, C. D., and Laemmli, U. K. (1982) Higher order metaphase chromosome structure: evidence for metalloprotein interactions. *Cell*, ***29***, 171-181.

(5) George, A. M., Sabovljev, S. A., Hart, L. E., Cramp, W. A., Harris, G., and Hornsey, S. (1987) DNA quaternary structure in the radiation sensitivity of human lymphocytes--a proposed role of copper. *Br. J. Cancer Suppl.*, ***8***, 141-144.

(6) Georgellis, A., Montelius, J., and Rydstrom, J. (1987) Evidence for a free-radical-dependent metabolism of 7,12-dimethylbenz(*a*)anthracene in rat testis. *Toxicol. Appl. Pharmacol.*, ***87***, 141-154.

(7) Box, H. C., Budzinski, E. E., Dawidzik, J. D., Wallace, J. C., Evans, M. S., and Gobey, J. S. (1996) Radiation-induced formation of a crosslink between base moieties of deoxyguanosine and thymidine in deoxygenated solutions of d(CpGpTpA). *Radiat. Res.*, ***145***, 641-643.

(8) Box, H. C., Budzinski, E. E., Dawidzik, J. B., Gobey, J. S., and Freund, H. G. (1997) Free radical-induced tandem base damage in DNA oligomers. *Free Radic. Biol. Med.*, ***23***, 1021-1030.

(9) Budzinski, E. E., Dawidzik, J. B., Rajecki, M. J., Wallace, J. C., Schroder, E. A., and Box, H. C. (1997) Isolation and characterization of the products of anoxic irradiation of d(CpGpTpA). *Int. J. Radiat. Biol.*, ***71***, 327-336.

(10) Box, H. C., Budzinski, E. E., Dawidzik, J. B., Wallace, J. C., and Iijima, H. (1998) Tandem lesions and other products in X-irradiated DNA oligomers. *Radiat. Res.*, ***149***, 433-439.

(11) Romieu, A., Bellon, S., Gasparutto, D., and Cadet, J. (2000) Synthesis and UV photolysis of oligodeoxynucleotides that contain 5-(phenylthiomethyl)-2'-deoxyuridine: A specific photolabile precursor of 5-(2'-deoxyuridilyl)methyl radical. *Org. Lett.*, ***2***, 1085-1088.

(12) Bellon, S., Ravanat, J. L., Gasparutto, D., and Cadet, J. (2002) Cross-linked thymine-purine base tandem lesions: synthesis, characterization, and measurement in gamma-irradiated isolated DNA. *Chem. Res. Toxicol.*, ***15***, 598-606.

(13) Zhang, Q., and Wang, Y. (2003) Independent generation of 5-(2'-deoxycytidinyl)methyl radical and the formation of a novel cross-link lesion between 5-methylcytosine and guanine. *J. Am. Chem. Soc.*, ***125***, 12795-12802.

(14) Zhang, Q., and Wang, Y. (2004) Independent generation of the 5-hydroxy-5,6-dihydrothymidin-6-yl radical and its reactivity in dinucleoside monophosphates. *J. Am. Chem. Soc.*, ***126***, 13287-13297.

(15) Wang, Y. (2008) Bulky DNA lesions induced by reactive oxygen species. *Chem. Res. Toxicol.*, ***21***, 276-281.

(16) Agarwal, K., Sharma, A., and Talukder, G. (1989) Effects of copper on mammalian cell components. *Chem. Biol. Interact.*, ***69***, 1-16.

(17) Drouin, R., Rodriguez, H., Gao, S. W., Gebreyes, Z., O'Connor, T. R., Holmquist, G. P., and Akman, S. A. (1996) Cupric ion/ascorbate/hydrogen peroxide-induced DNA damage: DNA-bound copper ion primarily induces base modifications. *Free Radic. Biol. Med.*, ***21***, 261-273.

(18) Bach, D., and Miller, I. R. (1967) Polarographic investigation of binding of Cu++ and Cd++ by DNA. *Biopolymers*, ***5***, 161-172.

(19) Bryan, S. E., and Frieden, E. (1967) Interaction of copper(II) with deoxyribonucleic acid below 30 degrees. *Biochemistry*, ***6***, 2728-2734.

(20) Pastor, N., Weinstein, H., Jamison, E., and Brenowitz, M. (2000) A detailed interpretation of OH radical footprints in a TBP-DNA complex reveals the role of dynamics in the mechanism of sequence-specific binding. *J. Mol. Biol.*, ***304***, 55-68.

(21) Evans, M. D., Dizdaroglu, M., and Cooke, M. S. (2004) Oxidative DNA damage and disease: induction, repair and significance. *Mutat. Res.*, ***567***, 1-61.

(22) Netto, L. E., Ferreira, A. M., and Augusto, O. (1991) Iron(III) binding in DNA solutions: complex formation and catalytic activity in the oxidation of hydrazine derivatives. *Chem. Biol. Interact.*, ***79***, 1-14.

(23) He, Y. F., Li, B. Z., Li, Z., Liu, P., Wang, Y., Tang, Q., Ding, J., Jia, Y., Chen, Z., Li, L., Sun, Y., Li, X., Dai, Q., Song, C. X., Zhang, K., He, C., and Xu, G. L. (2011) Tet-mediated formation of 5-carboxylcytosine and its excision by TDG in mammalian DNA. *Science*, ***333***, 1303-1307.

(24) Stadtman, E. R. (1992) Protein oxidation and aging. *Science*, ***257***, 1220-1224.

(25) Brierley, D. J., and Martin, S. A. (2013) Oxidative stress and the DNA mismatch repair pathway. *Antioxid. Redox Signal.*, ***18***, 2420-2428.

(26) Steenken, S. (1989) Purine bases, nucleosides, and nucleotides: aqueous solution redox chemistry and transformation reactions of their radical cations and e- and OH adducts. *Chemical Reviews*, ***89***, 503-520.

(27) Jaenisch, R., and Bird, A. (2003) Epigenetic regulation of gene expression: how the genome integrates intrinsic and environmental signals. *Nat. Genet.*, ***33 Suppl***, 245-254.

(28) McCord, J. M., Keele, B. B., Jr., and Fridovich, I. (1971) An enzyme-based theory of obligate anaerobiosis: the physiological function of superoxide dismutase. *Proc. Natl. Acad. Sci. U.S.A.*, ***68***, 1024-1027.

(29) Chae, H. Z., Kang, S. W., and Rhee, S. G. (1999) Isoforms of mammalian peroxiredoxin that reduce peroxides in presence of thioredoxin. *Methods Enzymol.*, ***300***, 219-226.

(30) Belmadoui, N., Boussicault, F., Guerra, M., Ravanat, J. L., Chatgilialoglu, C., and Cadet, J. (2010) Radiation-induced formation of purine 5',8-cyclonucleosides in isolated and cellular DNA: high stereospecificity and modulating effect of oxygen. *Org. Biomol. Chem.*, ***8***, 3211-3219.

(31) Wang, J., Yuan, B., Guerrero, C., Bahde, R., Gupta, S., and Wang, Y. (2011) Quantification of oxidative DNA lesions in tissues of Long-Evans Cinnamon rats by capillary high-performance liquid chromatography−tandem mass spectrometry coupled with stable isotope-dilution method. *Anal. Chem.*, ***83***, 2201-2209.

(32) Dizdaroglu, M., Dirksen, M. L., Jiang, H. X., and Robbins, J. H. (1987) Ionizing-radiation-induced damage in the DNA of cultured human cells. Identification of 8,5-cyclo-2-deoxyguanosine. *Biochem. J.*, ***241***, 929-932.

(33) Pouget, J. P., Frelon, S., Ravanat, J. L., Testard, I., Odin, F., and Cadet, J. (2002) Formation of modified DNA bases in cells exposed either to gamma radiation or to high-LET particles. *Radiat. Res.*, ***157***, 589-595.

(34) D'Errico, M., Parlanti, E., Teson, M., de Jesus, B. M., Degan, P., Calcagnile, A., Jaruga, P., Bjoras, M., Crescenzi, M., Pedrini, A. M., Egly, J. M., Zambruno, G., Stefanini, M., Dizdaroglu, M., and Dogliotti, E. (2006) New functions of XPC in the protection of human skin cells from oxidative damage. *EMBO J.*, ***25***, 4305-4315.

(35) Boussicault, F., Kaloudis, P., Caminal, C., Mulazzani, Q. G., and Chatgilialoglu, C. (2008) The fate of C5' radicals of purine nucleosides under oxidative conditions. *J. Am. Chem. Soc.*, ***130***, 8377-8385.

(36) Ito, S., Shen, L., Dai, Q., Wu, S. C., Collins, L. B., Swenberg, J. A., He, C., and Zhang, Y. (2011) Tet proteins can convert 5-methylcytosine to 5-formylcytosine and 5-carboxylcytosine. *Science*, ***333***, 1300-1303.

(37) Das, R. S., Samaraweera, M., Morton, M., Gascon, J. A., and Basu, A. K. (2012) Stability of N-glycosidic bond of (5'*S*)-8,5'-cyclo-2'-deoxyguanosine. *Chem. Res. Toxicol.*, ***25***, 2451-2461.

(38) Huang, H., Das, R. S., Basu, A. K., and Stone, M. P. (2011) Structure of (5'*S*)-8,5'-cyclo-2'-deoxyguanosine in DNA. *J. Am. Chem. Soc.*, ***133***, 20357-20368.

(39) Theruvathu, J. A., Jaruga, P., Dizdaroglu, M., and Brooks, P. J. (2007) The oxidatively induced DNA lesions 8,5'-cyclo-2'-deoxyadenosine and 8-hydroxy-2'-deoxyadenosine are strongly resistant to acid-induced hydrolysis of the glycosidic bond. *Mech. Ageing Dev.*, ***128***, 494-502.

(40) Brooks, P. J., Wise, D. S., Berry, D. A., Kosmoski, J. V., Smerdon, M. J., Somers, R. L., Mackie, H., Spoonde, A. Y., Ackerman, E. J., Coleman, K., Tarone, R. E., and Robbins, J. H. (2000) The oxidative DNA lesion 8,5'-(*S*)-cyclo-2'-deoxyadenosine is repaired by the nucleotide excision repair pathway and blocks gene expression in mammalian cells. *J. Biol. Chem.*, ***275***, 22355-22362.

(41) Kuraoka, I., Bender, C., Romieu, A., Cadet, J., Wood, R. D., and Lindahl, T. (2000) Removal of oxygen free-radical-induced 5',8-purine cyclodeoxynucleosides from DNA by the nucleotide excision-repair pathway in human cells. *Proc. Natl. Acad. Sci. U.S.A.*, ***97***, 3832-3837.

(42) Pfaffeneder, T., Hackner, B., Truss, M., Munzel, M., Muller, M., Deiml, C. A., Hagemeier, C., and Carell, T. (2011) The discovery of 5-formylcytosine in embryonic stem cell DNA. *Angew Chem. Int. Ed. Engl.*, ***50***, 7008-7012.

(43) You, C., Dai, X., Yuan, B., Wang, J., Wang, J., Brooks, P. J., Niedernhofer, L. J., and Wang, Y. (2012) A quantitative assay for assessing the effects of DNA lesions on transcription. *Nat. Chem. Biol.*, ***8***, 817-822.

(44) Jasti, V. P., Das, R. S., Hilton, B. A., Weerasooriya, S., Zou, Y., and Basu, A. K. (2011) (5'S)-8,5'-cyclo-2'-deoxyguanosine is a strong block to replication, a potent pol V-dependent mutagenic lesion, and is inefficiently repaired in Escherichia coli. *Biochemistry*, ***50***, 3862-3865.

(45) Marietta, C., Gulam, H., and Brooks, P. J. (2002) A single 8,5'-cyclo-2'-deoxyadenosine lesion in a TATA box prevents binding of the TATA binding

protein and strongly reduces transcription in vivo. *DNA Repair (Amst)*, ***1***, 967-975.

(46) Abraham, J., and Brooks, P. J. (2011) Divergent effects of oxidatively induced modification to the C8 of 2'-deoxyadenosine on transcription factor binding: 8,5'(S)-cyclo-2'-deoxyadenosine inhibits the binding of multiple sequence specific transcription factors, while 8-oxo-2'-deoxyadenosine increases binding of CREB and NF-kappa B to DNA. *Environ. Mol. Mutagen.*, ***52***, 287-295.

(47) Sijbers, A. M., de Laat, W. L., Ariza, R. R., Biggerstaff, M., Wei, Y. F., Moggs, J. G., Carter, K. C., Shell, B. K., Evans, E., de Jong, M. C., Rademakers, S., de Rooij, J., Jaspers, N. G., Hoeijmakers, J. H., and Wood, R. D. (1996) Xeroderma pigmentosum group F caused by a defect in a structure-specific DNA repair endonuclease. *Cell*, ***86***, 811-822.

(48) Kelman, Z. (1997) PCNA: structure, functions and interactions. *Oncogene*, ***14***, 629-640.

(49) Aboussekhra, A., Biggerstaff, M., Shivji, M. K., Vilpo, J. A., Moncollin, V., Podust, V. N., Protic, M., Hubscher, U., Egly, J. M., and Wood, R. D. (1995) Mammalian DNA nucleotide excision repair reconstituted with purified protein components. *Cell*, ***80***, 859-868.

(50) Araujo, S. J., Tirode, F., Coin, F., Pospiech, H., Syvaoja, J. E., Stucki, M., Hubscher, U., Egly, J. M., and Wood, R. D. (2000) Nucleotide excision repair of DNA with recombinant human proteins: definition of the minimal set of factors, active forms of TFIIH, and modulation by CAK. *Genes Dev.*, ***14***, 349-359.

(51) Valko, M., Rhodes, C. J., Moncol, J., Izakovic, M., and Mazur, M. (2006) Free radicals, metals and antioxidants in oxidative stress-induced cancer. *Chem. Biol. Interact.*, ***160***, 1-40.

(52) Nelson, N. (1999) Metal ion transporters and homeostasis. *EMBO J.*, ***18***, 4361-4371.

(53) Halliwell, B., and Gutteridge, J. M. (1990) The antioxidants of human extracellular fluids. *Arch. Biochem. Biophys.*, ***280***, 1-8.

(54) Prasad, R., Beard, W. A., Strauss, P. R., and Wilson, S. H. (1998) Human DNA polymerase beta deoxyribose phosphate lyase. Substrate specificity and catalytic mechanism. *J. Biol. Chem.*, ***273***, 15263-15270.

(55) Halliwell, B., and Gutteridge, J. M. (1990) Role of free radicals and catalytic metal ions in human disease: an overview. *Methods Enzymol.*, ***186***, 1-85.

(56) Halliwell, B. (1990) How to characterize a biological antioxidant. *Free Radic. Res. Commun.*, ***9***, 1-32.

(57) Stohs, S. J., and Bagchi, D. (1995) Oxidative mechanisms in the toxicity of metal ions. *Free Radic. Biol. Med.*, ***18***, 321-336.

(58) Mates, J. M. (2000) Effects of antioxidant enzymes in the molecular control of reactive oxygen species toxicology. *Toxicology*, ***153***, 83-104.

(59) Bosco, M. C., Rapisarda, A., Reffo, G., Massazza, S., Pastorino, S., and Varesio, L. (2003) Macrophage activating properties of the tryptophan catabolite picolinic acid. *Adv. Exp. Med. Biol.*, ***527***, 55-65.

(60) Horowitz, J. M., Pastor, D. M., Goyal, A., Kar, S., Ramdeen, N., Hallas, B. H., and Torres, G. (2003) BAX protein-immunoreactivity in midbrain neurons of Parkinson's disease patients. *Brain Res. Bull*, ***62***, 55-61.

(61) Moser, J., Volker, M., Kool, H., Alekseev, S., Vrieling, H., Yasui, A., van Zeeland, A. A., and Mullenders, L. H. (2005) The UV-damaged DNA binding protein mediates efficient targeting of the nucleotide excision repair complex to UV-induced photo lesions. *DNA Repair (Amst)*, ***4***, 571-582.

(62) Jiang, Y., Hong, H., Cao, H., and Wang, Y. (2007) In vivo formation and in vitro replication of a guanine-thymine intrastrand cross-link lesion. *Biochemistry*, ***46***, 12757-12763.

(63) Volker, M., Mone, M. J., Karmakar, P., van Hoffen, A., Schul, W., Vermeulen, W., Hoeijmakers, J. H., van Driel, R., van Zeeland, A. A., and Mullenders, L. H. (2001) Sequential assembly of the nucleotide excision repair factors in vivo. *Mol. Cell*, ***8***, 213-224.

(64) Kakhlon, O., and Cabantchik, Z. I. (2002) The labile iron pool: characterization, measurement, and participation in cellular processes(1). *Free Radic. Biol. Med.*, ***33***, 1037-1046.

(65) Jomova, K., and Valko, M. (2011) Advances in metal-induced oxidative stress and human disease. *Toxicology*, ***283***, 65-87.

(66) Schafer, F. Q., and Buettner, G. R. (2001) Redox environment of the cell as viewed through the redox state of the glutathione disulfide/glutathione couple. *Free Radic. Biol. Med.*, ***30***, 1191-1212.

(67) Liochev, S. I., and Fridovich, I. (1994) The role of O2.- in the production of HO.: in vitro and in vivo. *Free Radic. Biol. Med.*, ***16***, 29-33.

(68) Gaetke, L. M., and Chow, C. K. (2003) Copper toxicity, oxidative stress, and antioxidant nutrients. *Toxicology*, ***189***, 147-163.

(69) Hong, H., Cao, H., Wang, Y., and Wang, Y. (2006) Identification and quantification of a guanine-thymine intrastrand cross-link lesion induced by Cu(II)/H_2O_2/ascorbate. *Chem. Res. Toxicol.*, ***19***, 614-621.

(70) Cao, H., and Wang, Y. (2007) Quantification of oxidative single-base and intrastrand cross-link lesions in unmethylated and CpG-methylated DNA induced by Fenton-type reagents. *Nucleic Acids Res.*, ***35***, 4833-4844.

(71) Suh, J., Zhu, B. Z., and Frei, B. (2003) Ascorbate does not act as a pro-oxidant towards lipids and proteins in human plasma exposed to redox-active transition metal ions and hydrogen peroxide. *Free Radic. Biol. Med.*, ***34***, 1306-1314.

(72) Lech, T., and Sadlik, J. K. (2007) Copper concentration in body tissues and fluids in normal subjects of southern Poland. *Biol. Trace Elem. Res.*, ***118***, 10-15.

(73) Campian, J. L., Qian, M., Gao, X., and Eaton, J. W. (2004) Oxygen tolerance and coupling of mitochondrial electron transport. *J. Biol. Chem.*, ***279***, 46580-46587.

(74) Boveris, A., and Chance, B. (1973) The mitochondrial generation of hydrogen peroxide. General properties and effect of hyperbaric oxygen. *Biochem. J.*, ***134***, 707-716.

(75) Handy, D. E., and Loscalzo, J. (2012) Redox regulation of mitochondrial function. *Antioxid. Redox Signal.*, ***16***, 1323-1367.

(76) Cadet, J., Delatour, T., Douki, T., Gasparutto, D., Pouget, J. P., Ravanat, J. L., and Sauvaigo, S. (1999) Hydroxyl radicals and DNA base damage. *Mutat. Res.*, ***424***, 9-21.

(77) Himmelstein, M. W., Boogaard, P. J., Cadet, J., Farmer, P. B., Kim, J. H., Martin, E. A., Persaud, R., and Shuker, D. E. (2009) Creating context for the use of DNA adduct data in cancer risk assessment: II. Overview of methods of identification and quantitation of DNA damage. *Crit. Rev. Toxicol.*, ***39***, 679-694.

(78) Lim, K. S., Jenner, A., and Halliwell, B. (2006) Quantitative gas chromatography mass spectrometric analysis of 2'-deoxyinosine in tissue DNA. *Nat. Protoc.*, ***1***, 1995-2002.

(79) Hong, H., and Wang, Y. (2005) Formation of intrastrand cross-link products between cytosine and adenine from UV irradiation of d((Br)CA) and duplex DNA containing a 5-bromocytosine. *J. Am. Chem. Soc.*, ***127***, 13969-13977.

Chapter 2

Induction of 8,5'-Cyoclopurine-2'-dexynucleosides in Isolated DNA by Fenton-type Reagents

2.1 Abstract

Exposure of aqueous solutions of DNA to X- or γ-rays, which induces hydroxyl radical as one of the major reactive oxygen species (ROS), can result in the generation of a battery of single-nucleobase and bulky DNA lesions. These include the (5'*R*) and (5'*S*) diastereomers of 8,5'-cyclo-2'-deoxyadenosine (cdA) and 8,5'-cyclo-2'-deoxyguanosine (cdG), which were also found to be present at appreciable levels in DNA isolated from mammalian cells and tissues. However, it remains unexplored how efficiently the cdA and cdG can be induced by Fenton-type reagents. By employing HPLC coupled with tandem mass spectrometry (LC-MS/MS/MS) with the use of the isotope-dilution technique, here we demonstrated that treatment of calf thymus DNA with Cu(II) or Fe(II), together with H_2O_2 and ascorbate, could lead to dose-responsive formation of both the (5'*R*) and (5'*S*) diastereomers of cdA and cdG, though the yields of cdG were 2-4 orders of magnitude lower than that of 8-oxo-7,8-dihydro-2'-deoxyguanosine. This result suggests that Fenton reaction may constitute an important endogenous source for the formation of the cPu lesions. Additionally, the (5'*R*) diastereomers of cdA and cdG were induced at markedly higher levels than the (5'*S*) counterparts. This latter finding, in conjunction with the previous observations of similar or greater levels of the (5'*S*) than

(5'*R*) diastereomers of the two lesions in mammalian tissues, furnishes an additional line of evidence to support the more efficient repair of the (5'*R*) diastereomers of the purine cyclonucleosides in mammalian cells.

2.2 Introduction

Reactive oxygen species (ROS) are constantly induced by endogenous and exogenous sources and they can result in damage to DNA.[1, 2] For instance, exposure of DNA to γ- or X-rays can lead to the formation of a variety of single-nucleobase and bulky DNA lesions.[3-11] During normal aerobic metabolism, electrons leaking from the electron transport chain in mitochondria may couple with molecular O_2 to yield superoxide ($O_2^{\cdot -}$), which can be subsequently converted to H_2O_2 by superoxide dismutase. Being freely diffusible in the cellular environment, H_2O_2 may reach the nucleus and react with DNA-bound transition metal ions [e.g. Fe(II) or Cu(II)] to yield the highly reactive hydroxyl radical (•OH) via the Fenton-type reaction.[12] Along this line, earlier studies by Linn and co-workers[13-15] demonstrated the capability of Fenton-type reagents in inducing oxdatively generated lesions of DNA.

The importance of the Fenton-type reaction in human disease is manifested by genetic disorders associated with defects in handling transition metal ions, including Wilson's disease[16] and iron overload disease.[17] In this vein, we found previously that deficiency in the orthologue of human Wilson's disease gene (i.e., Atp7b) and the ensuing aberrant accumulation of copper ions in hepatocytes led to elevated levels of

oxidatively induced 8,5'-cyclo-2'-deoxyadenosine (cdA) and 8,5'-cyclo-2'-deoxyguanosine (cdG) lesions in liver tissues of Long-Evans Cinnamon (LEC) rats.[18]

The cdA and cdG are unique oxidatively induced DNA lesions owing to the presence of an additional C-C bond between the C8 of the purine base and the C5' of the 2-deoxyribose in the same nucleoside (Scheme 2.1). This additional covalent linkage induces helical distortion to DNA and renders the *N*-glycosidic bond resistant toward acid-induced hydrolysis.[19-22] Thus, cPu lesions are attractive substrates for nucleotide excision repair (NER), but they are poor substrates for DNA glycosylase-mediated base excision repair (BER).[23-25] Both the (5'*R*) and (5'*S*) diastereomers of cdA inhibit primer extension by T7 DNA polymerase as well as human DNA polymerase δ.[23, 26, 27] Nevertheless, results from steady-state kinetic measurements showed that yeast and human polymerase η-mediated nucleotide incorporation opposite (5'*S*)-cdA and (5'*S*)-cdG was largely efficient and accurate.[28] In addition, cdA and cdG strongly impede DNA transcription in mammalian cells and induce transcription mutagenesis.[23, 24, 26]

Recent studies have shown that both (5'*R*) and (5'*S*) diastereomers of cdA and cdG have been detected *in vitro* and *in vivo,*[18, 29-37] Nevertheless, it remains to be established how efficiently these lesions can be induced in DNA by Fenton-type reagents. Here we treated calf thymus DNA with Cu(II)/H_2O_2/ascorbate or Fe(II)/H_2O_2/ascorbate and analyzed the enzymatic digestion products of DNA by LC-MS/MS or LC-MS/MS/MS. We found that Fenton-type reagents could induce dose-dependent

Scheme 2.1. Chemical structures of synthesized ^{15}N-labeled nucleosides. The "N" in bold represents ^{15}N.

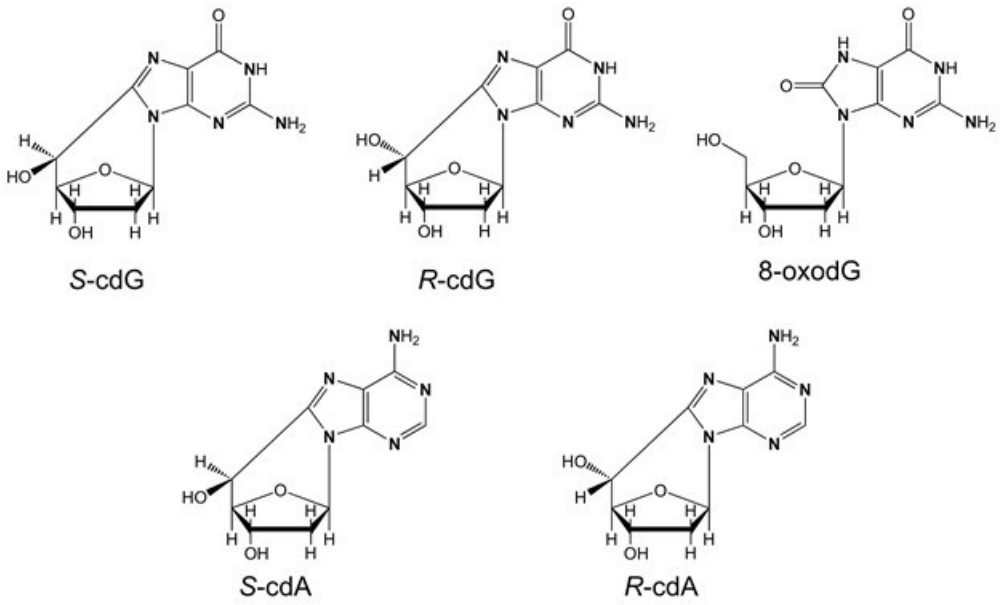

Table 2.1. Concentrations of Fenton Type Reagents Employed for the Treatment of Calf Thymus DNA. [a]

	Control	A	B	C	D	E
Cu(II)/Fe(II) (μM)	200	12.5	25	50	100	200
H_2O_2 (μM)	0	100	200	400	800	1600
Ascorbate (mM)	0	1.0	2.0	4.0	8.0	16.0

[a]All reactions were carried out in a 250-μL solution containing 75 μg of calf thymus DNA.

formation of cdA and cdG, with the (5'R) diastereomer being produced much more efficiently than its (5'S) counterpart.

2.3 Experimental Procedures

2.3.1 Materials

$CuCl_2$, $(NH_4)_2Fe(SO_4)_2 \bullet 6H_2O$, L-methionine, L-ascorbic acid, calf thymus DNA, nuclease P1, alkaline phosphatase, and phosphodiesterases 1 and 2 were purchased from Sigma-Aldrich (St. Louis, MO). Hydrogen peroxide (30%) and *erythro*-9-(2-hydroxy-3-nonyl)adenine (EHNA) hydrochloride were obtained from Fisher Scientific (Fair Lawn, NJ) and Tocris Bioscience (Ellisville, MO), respectively. The uniformly ^{15}N-labeled 8-oxodG, cdA and cdG were synthesized previously (Structures shown in Scheme 1).[18, 38]

2.3.2 Treatment of Calf Thymus DNA

Commercially available calf thymus DNA was desalted by ethanol precipitation. The DNA pellet was redissolved in a solution containing 25 mM NaCl and 50 mM phosphate (pH 7.0), and the DNA was annealed by heating the solution to 90°C for 5 min followed by cooling slowly to room temperature.

Aliquots of DNA (75 μg) were incubated with $CuCl_2$ or $(NH_4)_2Fe(SO_4)_2$ (12.5-200 μM), H_2O_2 (0.1-1.6 mM), and ascorbate (1-16 mM) in a 250-μL solution containing 25 mM NaCl and 50 mM phosphate (pH 7.0) at room temperature under aerobic conditions for 60 min. Chemicals used in the Fenton-type reagent treatment of DNA were

freshly prepared in doubly distilled water. Detailed concentrations of individual Fenton reagents used for the reactions are shown in Table 1. After 60 min, the reactions were terminated by adding excess L-methionine, and the DNA samples were again desalted by ethanol precipitation.

2.3.3 Enzymatic Digestion of DNA

To the above desalted DNA samples were added 8 units of nuclease P1, 0.01 unit of phosphodiesterase 2, 20 nmol of EHNA and a 20-μL solution containing 300 mM sodium acetate (pH 5.6) and 10 mM zinc chloride. EHNA was added to the enzymatic digestion mixture to prevent the possible deamination induced by residual contamination of adenine deaminase present in some commercial preparations of enzymes used in DNA digestion.[39] After a 48-hr incubation at 37°C, 8 units of alkaline phosphatase, 0.02 unit of phosphodiesterase 1, and 40 μL of 0.5 M Tris-HCl (pH 8.9) were added to the digestion mixture. The solution was further incubated at 37°C for 2 h, after which the enzymes were removed by chloroform extraction and the solution dried by Speed-vac. DNA samples were then reconstituted in doubly distilled water and their concentration measured using UV-absorption spectrophotometry. To the mixture were then added uniformly [15N]-labeled 8-oxodG (500 fmol), *R*-cdG (200 fmol), *S*-cdG (100 fmol), *R*-cdA (100 fmol), and *S*-cdA (40 fmol, Scheme 1). The resulting aliquots were subjected directly to LC-MS/MS analysis (for 8-oxodG), or HPLC enrichment prior to LC-MS/MS/MS analysis (for cdA and cdG).

2.3.4 HPLC Enrichment

A 4.6×250 mm Alltima HP C18 column (5 μm in particle size, Grace Davison, Deerfield, IL) was used for the enrichment of the oxidatively induced cPu lesions from the enzymatic digestion products of DNA. The flow rate was 1 mL/min, and the mobile phases were 10 mM ammonium formate (solution A) and methanol (solution B). A gradient of 25 min 0-2% B, 1 min at 2% B, 14 min 2-5% B, 1 min 5-15% B, and 20 min at 15% B was employed. The HPLC fractions eluting at 12-18, 31.5-41.5, 42.5-50.5, 63-71.5 min were pooled for *R*-cdG, *R*-cdA, *S*-cdG, and *S*-cdA, respectively (Figure S1). The collected fractions were dried in the Speed-vac, redissolved in H_2O, and subjected to LC-MS/MS/MS analysis.

2.3.5 LC-MS/MS Analysis of 8-oxodG

A 3×100 mm Hypersil Gold column (5 μm in particle size, Thermo, San Jose, CA) and an Accela 600 HPLC pump (Thermo) were used, and the flow rate was 50 μL/min. A solution of 0.1% (v/v) formic acid in doubly distilled water (solution A) and a solution of 0.1% (v/v) formic acid in methanol (solution B) were employed as mobile phases. The gradient included 0-90% B in 30 min and 90% B in 5 min. The effluent from the LC column was directed to a TSQ Vantage triple quadrupole mass spectrometer (Thermo). The instrument was operated in multiple-reaction monitoring (MRM) mode, and the MRM transitions for 8-oxodG and its uniformly ^{15}N-labeled standard were *m/z* 284→168 and *m/z* 289→173, respectively.

2.3.6 LC-MS/MS/MS Analysis of cdA and cdG

An Agilent 1100 capillary HPLC pump (Agilent Technologies) and a 0.5×250 mm Zorbax SB-C18 column (particle size, 5 μm, Agilent) were used for the separation. A solution of 0.1% (v/v) formic acid in water (solution A) and a solution of 0.1% (v/v) formic acid in methanol (solution B) were used as mobile phases, and the gradient included 20 min 0-15% B, 10 min 15-35% B, and 10 min 35-60% B. The flow rate was 10 μL/min.

The effluent from the LC column was directed to an LTQ linear ion-trap mass spectrometer (Thermo), which monitored the fragmentation of the $[M+H]^+$ ions of labeled and unlabeled *R*-cdG, *S*-cdG, *R*-cdA, *S*-cdA, and the further fragmentation of the corresponding $[M+H-86]^+$ fragments found in MS/MS.

2.4 Results

2.4.1 LC-MS/MS/MS Identification and Quantification of cdA and cdG Lesions in Calf Thymus DNA Exposed with Cu(II)/H_2O_2/Ascorbate

We set out to investigate how efficiently the cdA and cdG lesions could be induced by Fenton-type reagents in isolated DNA. To this end, we treated calf thymus DNA with various concentrations of Cu(II)/H_2O_2/ascorbate (Table 2.1), digested the DNA with a cocktail of four enzymes, enriched cdA and cdG from the resulting nucleoside mixture and subjected them to LC-MS/MS or LC-MS^3 analysis by using the

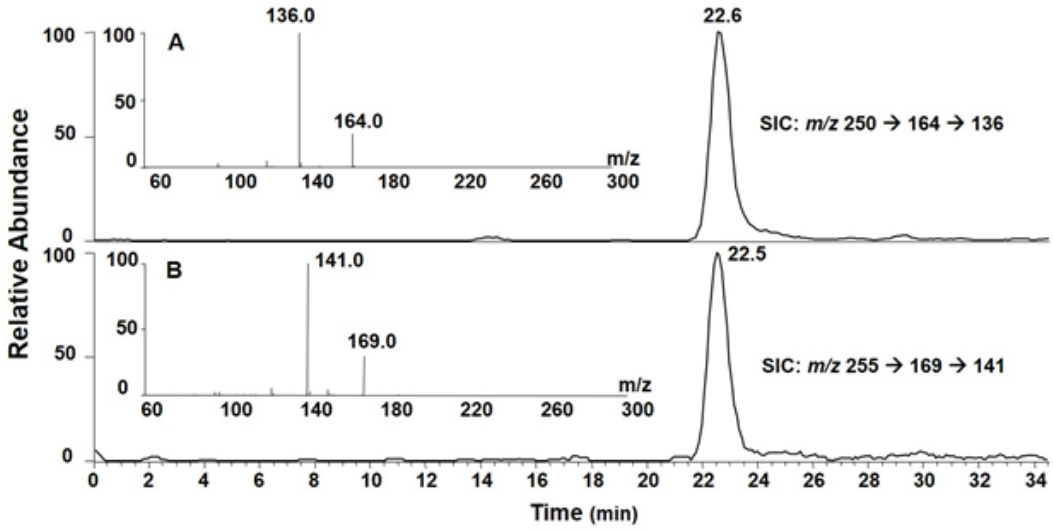

Figure 2.1. Selected-ion chromatograms (SICs) for monitoring the *m/z* 250→164→136 [A, for unlabeled (5'*S*)-cdA] and *m/z* 255→169→141 [B, for uniformly [^{15}N]-labeled (5'*S*)-cdA] transitions in the Cu(II)/H_2O_2/ascorbate-treated calf thymus DNA after enzymatic digestion. Shown in the insets are the positive-ion MS^3 spectra for the unlabeled and labeled (5'*S*)-cdA. The sample was treated under Conditions B listed in Table 2.1.

corresponding uniformly [^{15}N]-labeled nucleosides as internal standards (see Experimental Procedures).

In the LC-MS/MS/MS experiment, we monitored the *m/z* 250→164→136 and *m/z* 255→169→141 transitions for (5'*S*)-cdA and its uniformly [^{15}N]-labeled counterpart, respectively. The selected-ion chromatograms (SICs) and MS^3 spectra for the unlabeled and [^{15}N]-labeled (5'*S*)-cdA are displayed in Figure 2.1. The identity of the component eluting at 22.6 min in the SIC (Figure 2.1A and 2.1B) was found to be (5'*S*)-cdA by the co-elution, and similar fragment ions found in MS^3, of the analyte and its uniformly [^{15}N]-labeled standard. Ions of *m/z* 164 and *m/z* 169 arise from the neutral loss of a 86-Da fragment via cleavages of both the *N*-glycosidic linkage and the bond between the C5' and C4' of the 2-deoxyribose moiety of (5'*S*)-cdA and uniformly [^{15}N]-labeled (5'*S*)-cdA, respectively. Further cleavage of the ion of *m/z* 164 led to the elimination of a CO molecule to give the major fragment ion at *m/z* 136. Corresponding fragment ions were observed in the MS^3 of the ^{15}N-labeled (5'*S*)-cdA. (5'*R*)-cdA was found to yield the same fragment ions in both MS/MS and MS^3 as (5'*S*)-cdA, though the two diastereomers exhibited different elution time on a reversed phase C18 column (Appendix A, Figure B2). Moreover, the amounts of (5'*R*)- and (5'*S*)-cdA are significantly lower in the control samples without hydrogen peroxide treatment (Figure 2.2 and Table A1 in Appendix A), supporting that Cu(II)/H_2O_2/ascorbate can induce the formation of these two lesions.

We also observed the presence of (5'*R*)- and (5'*S*)-cdG based on the peaks at 11.6 and 21.4 min found in the SIC for monitoring the *m/z* 266→180→163 transition (Figures A3 and A4 in Appendix A). These components exhibit identical retention times as their

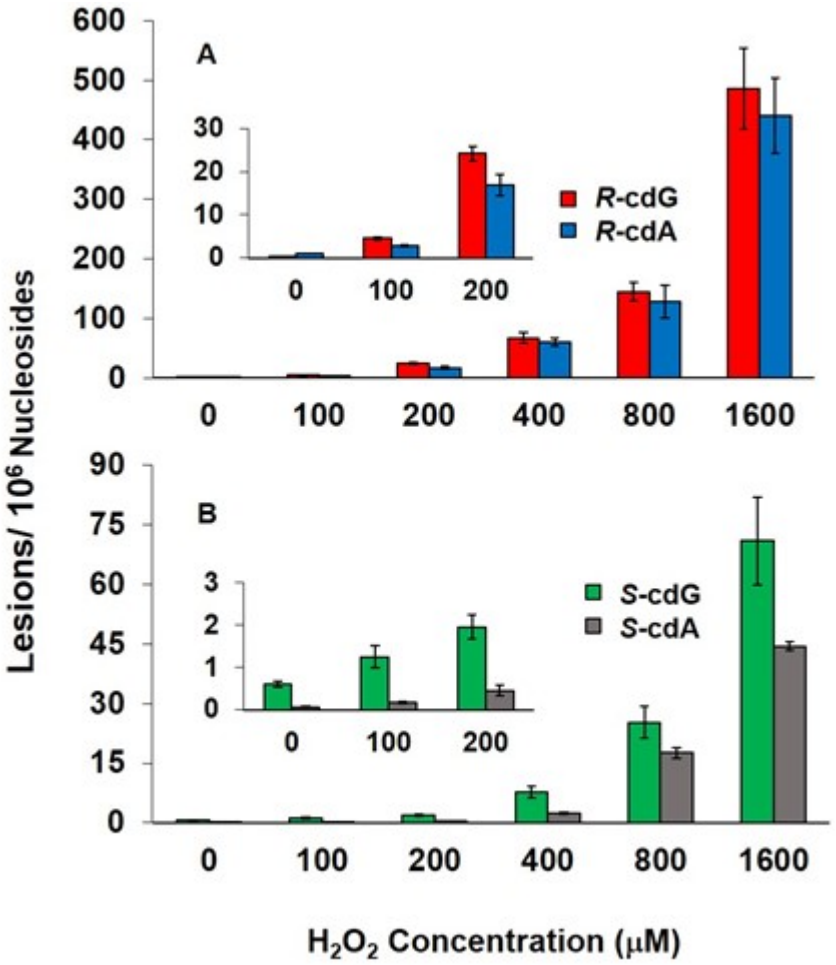

Figure 2.2. Cu(II)/H_2O_2/ascorbate-induced formation of cPu lesions in calf thymus DNA: (A) (5'*R*)-cdG and (5'*R*)-cdA; (B) (5'*S*)-cdG and (5'*S*)-cdA. The values represent the means ± S.D. of results from three independent experiments. The corresponding concentrations of Fe(II) and ascorbate are listed in Table 2.1.

respective isotope-labeled internal standards. Moreover, the major fragment ion at *m/z* 180 arises again from the cleavages of the C5'-C4' bond of 2-deoxyribose and the *N*-glycosidic bond in cdG.[40] Further fragmentation of the ion of *m/z* 180 yielded three major fragment ions of *m/z* 163, 152, and 135 in MS/MS/MS, which emanate from the neutral losses of NH_3, CO, and [NH_3 + CO], respectively (Figures A3 and A4 in Appendix A). The corresponding fragment ions were found in the MS^3 for both diastereomers of the internal standards (Figures A3 andS4). LC-MS^3 quantification results showed that the treatment of calf-thymus DNA with Cu(II)/H_2O_2/ascorbate induced the dose-dependent formation of both diastereomers of cdG (Figure 2.2 and Appendix A Table A1).

2.4.2 LC-MS/MS/MS Identification and Quantification of cdA and cdG Lesions Formed in Calf Thymus DNA Treated with Fe(II)/H_2O_2/Ascorbate

Iron is another biologically important transition metal that can participate in Fenton-type reactions.[13, 14, 41] Iron's ability to generate highly mutagenic oxidative lesions in genomic DNA has been linked with iron-induced carcinogenesis in iron-overload diseases.[17] Thus, we also assessed the formation of cadA and cdG lesions in calf thymus DNA treated with Fe(II)/H_2O_2/ascorbate (Table 2.1). It turned out that there is again a dose-dependent increase in the formation of the (5'*R*) and (5'*S*) diastereomers of cdA and cdG (Figure 2.3 and Table A2).

Comparison of the levels of the cdA and cdG lesions induced by the two Fenton systems revealed that the yields of cdA and cdG were lower when Cu(II) was replaced with Fe(II) under reaction conditions A through C (Figures 2.2 and 2.3 and Appendix A, Tables A1 and A2). However, we observed an opposite trend when the transition metal

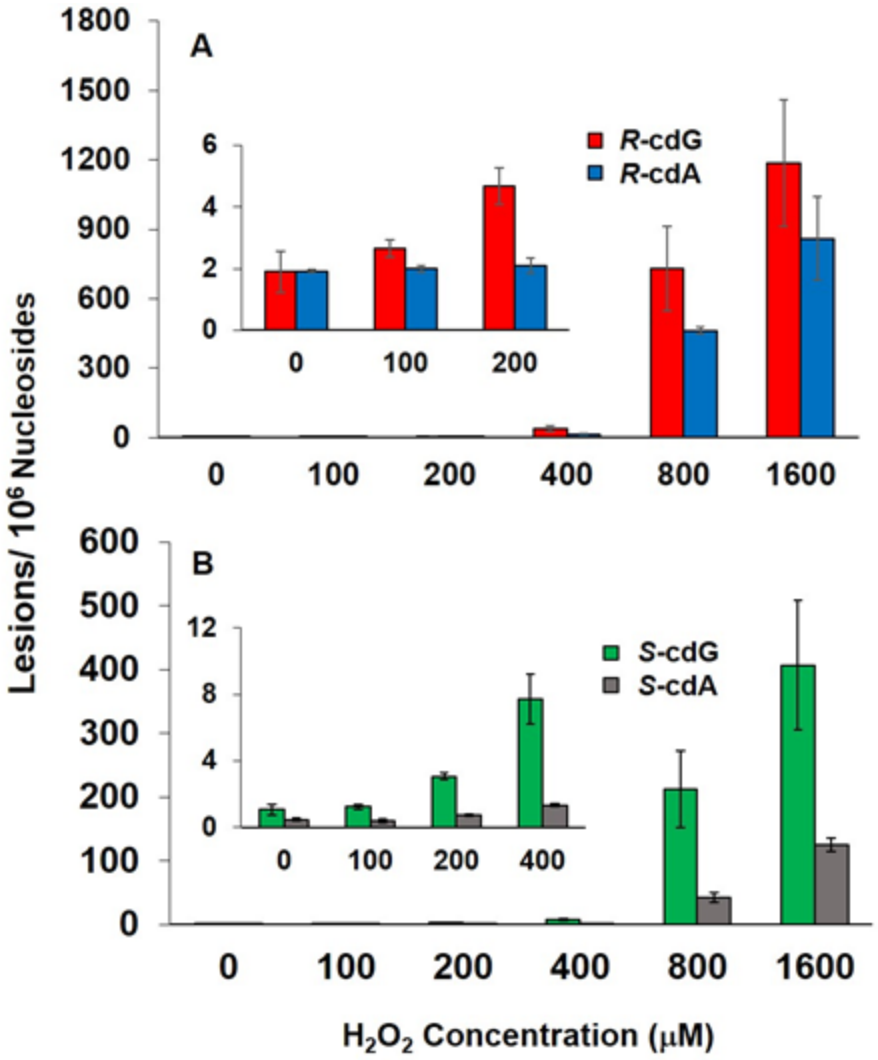

Figure 2.3. Fe(II)/H_2O_2/ascorbate-induced formation of cPu lesions in calf thymus DNA: (A) (5'*R*)-cdG and (5'*R*)-cdA; (B) (5'*S*)-cdG and (5'*S*)-cdA. The values represent the means ± S.D. of results from three independent experiments. The corresponding concentrations of Fe(II) and ascorbate are listed in Table 2.1.

ion concentrations exceeded 100 μM (i.e., conditions D and E, Figures 2.2 and 2.3 and Appendix A, Tables A1 and A2).

2.4.3 LC-MS/MS Quantification of 8-oxodG Formed in Calf Thymus DNA Treated with Fe(II)/H_2O_2/Ascorbate

Ionizing radiation-induced formation of cdA is thought to proceed through an •OH-mediated hydrogen abstraction from the C5' of the 2-deoxyribose. The resultant C5' radical then couples with the C8 of the purine base to form the additional covalent bond between the nucleobase and 2-deoxyribose in the same nucleoside. Viewing that •OH can also result in the formation of single-nucleobase lesions, it is important to compare the yields for the formation of cdA and cdG with respect to single-nucleobase lesions in both transition metal systems. Previous studies showed that Fenton reagents, Cu(II)/H_2O_2/ascorbate, can induce single-nucleobase lesion, 8-oxo-7,8-dihydro-2'-deoxyguanosine (8-oxodG) in isolated DNA.[38, 42] A comparison of the quantification results for Cu(II)/H_2O_2/ascorbate-induced cdG with these previously published quantification data of 8-oxodG under the same experimental condition[38] showed that cdG was induced at a level that is 2-4 orders of magnitude lower than 8-oxodG.

Here, we further assessed the generation of 8-oxodG via Fe(II)/ H_2O_2/ascorbate system, and our results revealed that the yield of 8-oxodG was ~50-2500 fold greater than the combined yield of the two diastereomers of cdG (Figures 2.3 and 2.4 and Appendix A, Tables A2 and A3).

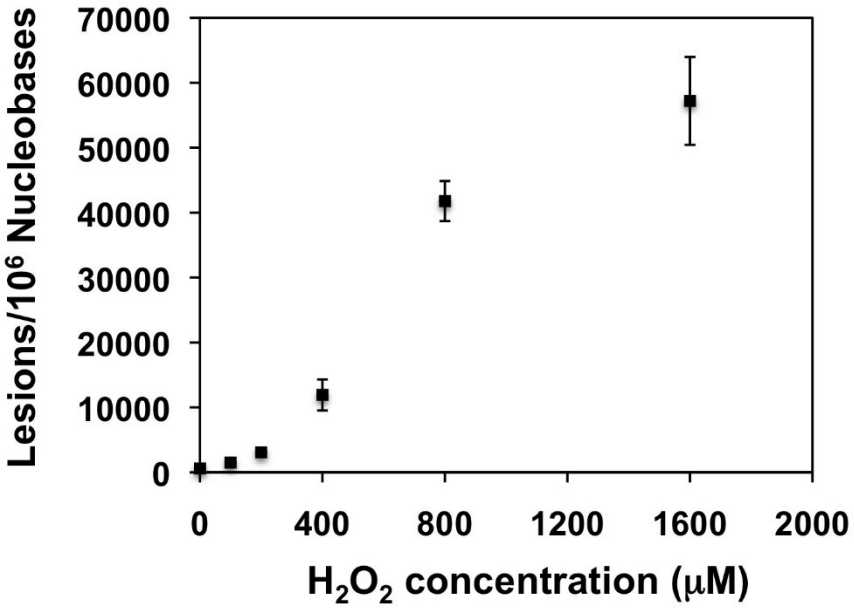

Figure 2.4. Fe(II)/H_2O_2/ascorbate-induced formation of 8-oxodG in calf thymus DNA. The values represent the means ± S.D. of results from three independent oxidation and quantification experiments.

It is worth nothing that Cu(II)/H_2O_2 was found to induce singlet oxygen ($^1O_2$) generation,[43, 44] and the incubation of Cu^+ or Cu^{2+} complex with H_2O_2 was observed to induce one-electron oxidation of DNA.[45] Both singlet oxygen and one-electron oxidation could result in the formation of 8-oxodG but not cdA and cdG. Ascorbate, however, is a known scavenger for singlet oxygen,[46] and the inclusion of excess amount of ascorbate in the reaction (Table 2.1) should also minimize one-electron oxidation of DNA by maintaining copper ion in the +1 oxidation state. Thus, we reason that the markedly lower yield observed for cdA and cdG than 8-oxodG is unlikely due to the involvement of singlet oxygen or one-electron oxidation.

2.5 Discussion

Here we demonstrated, by using LC-MS/MS/MS with the standard isotope dilution technique, that the treatment of isolated DNA with Cu(II)/H_2O_2/ascorbate or Fe(II)/H_2O_2/ascorbate can lead to the formation of both the (5'*R*) and (5'*S*) diastereomers of cdA and cdG. Additionally, the yields of cdA and cdG lesions exhibit a dose-dependent increase at low concentration ranges followed by a marked increase at 800 μM Cu(II) or Fe(II) (Figures 2.2 and 2.3 and Table A1 and A2 in Appendix A). These results are reminiscent of previous findings about the formation of intrastrand crosslink lesions in calf thymus DNA exposed with Fenton reagents under similar conditions,[38, 42] suggesting that binding to Cu(II) and Fe(II) may result in an alteration in DNA conformation. Although cdA and cdG can be detected in calf thymus DNA without treatment with Fenton reagents, which is consistent with the previous finding,[34] it is

apparent that Fe(II)/H_2O_2/ascorbate and Cu(II)/H_2O_2/ascorbate could induce the dose-responsive formation of these lesions. Our results also revealed that Fe(II)/H_2O_2/ascorbate at the two highest concentrations (conditions D and E) were at least ~ 2-8 fold as effective as Cu(II)/H_2O_2/ascorbate system in inducing the cadA and cdG lesions, though the latter is more efficient in inducing the cPu lesions at lower concentrations. Our observations with calf thymus DNA suggested that Fenton reaction may constitute an important endogenous source for the formation of cdA and cdG in mammalian tissues.

In keeping with previous results from treatment with γ rays,[29] our data demonstrated that treatment with Fenton reagents also led to the preferential formation of (5'*R*)- over (5'*S*)-diastereomers of both cdA and cdG. However, these results were inconsistent with another study showing preferential formation of (5'*S*)- over (5'*R*)-cdG in calf thymus DNA upon exposure to γ rays. The exact reason for this discrepancy is unclear, though it is possible that the less specific LC-MS or GC-MS technique used in the previous study[40] may lead to inaccurate measurements of the cdA and cdG lesions. Recent LC-MS/MS/MS quantification studies revealed that the (5'*S*) diastereomers of cdA and cdG are present at similar or higher levels than the corresponding (5'*R*) diastereomers in DNA isolated from mammalian tissues.[18, 36, 37] This result is in line with the more efficient repair of the (5'*R*) diastereomers than its (5'*S*) counterpart; indeed, it was observed that a substrate housing a (5'*R*)-cdA was cleaved more efficiently than the corresponding (5'*S*)-cdA substrate by NER activities in a mammalian nuclear extract.[23]

cdA and cdG are known substrates for NER, but not BER.[23, 24, 47] Our results showed that these lesions could be induced by Fenton-type reagents at efficiencies that are 2-4 orders of magnitude lower than that of 8-oxodG under the same experimental conditions (Figures 2.2-2.4). The detection of appreciable levels of cdA and cdG lesions in DNA isolated from mammalian tissues[18, 36, 37, 48] suggests that these lesions might be more resistant to repair than the oxidatively generated single-nucleobase lesions (e.g., 8-oxodG). In addition, cdA was a strong block to DNA polymerase δ,[23] and both cdA and cdG strongly inhibit transcription by RNA polymerase II *in vitro* and in mammalian cells.[24] Thus, these lesions could accumulate in patients with deficiency in NER and become cytotoxic. Neurons consume a vast amount of oxygen, rendering the central nervous system susceptible to ROS-induced DNA damage. In this vein, xeroderma pigmentosum (XP) patients suffer from a progressive, yet massive, neuron loss, which is accompanied with mental deterioration over a serveral of decades, and these patients also manifest an elevated frequency of internal cancers.[49] The induction of cdA and cdG lesions by Fenton-type reagents reported here provide important new knowledge toward understanding the role of these lesions in the pathological symptoms of XP patients or in deficiencies in handling transition metal ions, such as Cu(II) or Fe(II).

Appendix Materials

HPLC trace for the enrichment of cdA and cdG. LC-MS/MS/MS data and calibration curves for cdA and cdG. Table of numerical results of cdA, cdG, and 8-oxodG lesion levels. This material is found in Appendix A.

References

(1) Lindahl, T. (1999) DNA lesions generated *in vivo* by reactive oxygen species, their accumulation and repair. *NATO ASI Ser.*, ***Ser. A 302***, 251-257.

(2) Finkel, T., and Holbrook, N. J. (2000) Oxidants, oxidative stress and the biology of ageing. *Nature*, ***408***, 239-247.

(3) Box, H. C., Budzinski, E. E., Dawidzik, J. D., Wallace, J. C., Evans, M. S., and Gobey, J. S. (1996) Radiation-induced formation of a crosslink between base moieties of deoxyguanosine and thymidine in deoxygenated solutions of d(CpGpTpA). *Radiat. Res.*, ***145***, 641-643.

(4) Box, H. C., Budzinski, E. E., Dawidzik, J. B., Gobey, J. S., and Freund, H. G. (1997) Free radical-induced tandem base damage in DNA oligomers. *Free Radic. Biol. Med.*, ***23***, 1021-1030.

(5) Budzinski, E. E., Dawidzik, J. B., Rajecki, M. J., Wallace, J. C., Schroder, E. A., and Box, H. C. (1997) Isolation and characterization of the products of anoxic irradiation of d(CpGpTpA). *Int. J. Radiat. Biol.*, ***71***, 327-336.

(6) Box, H. C., Budzinski, E. E., Dawidzik, J. B., Wallace, J. C., and Iijima, H. (1998) Tandem lesions and other products in X-irradiated DNA oligomers. *Radiat. Res.*, ***149***, 433-439.

(7) Romieu, A., Bellon, S., Gasparutto, D., and Cadet, J. (2000) Synthesis and UV photolysis of oligodeoxynucleotides that contain 5-(phenylthiomethyl)-2'-deoxyuridine: A specific photolabile precursor of 5-(2'-deoxyuridilyl)methyl radical. *Org. Lett.*, ***2***, 1085-1088.

(8) Bellon, S., Ravanat, J. L., Gasparutto, D., and Cadet, J. (2002) Cross-linked thymine-purine base tandem lesions: synthesis, characterization, and measurement in gamma-irradiated isolated DNA. *Chem. Res. Toxicol.*, ***15***, 598-606.

(9) Zhang, Q., and Wang, Y. (2003) Independent generation of 5-(2'-deoxycytidinyl)methyl radical and the formation of a novel cross-link lesion between 5-methylcytosine and guanine. *J. Am. Chem. Soc.*, ***125***, 12795-12802.

(10) Zhang, Q., and Wang, Y. (2004) Independent generation of the 5-hydroxy-5,6-dihydrothymidin-6-yl radical and its reactivity in dinucleoside monophosphates. *J. Am. Chem. Soc.*, ***126***, 13287-13297.

(11) Wang, Y. (2008) Bulky DNA lesions induced by reactive oxygen species. *Chem. Res. Toxicol.*, ***21***, 276-281.

(12) Cadet, J., Delatour, T., Douki, T., Gasparutto, D., Pouget, J. P., Ravanat, J. L., and Sauvaigo, S. (1999) Hydroxyl radicals and DNA base damage. *Mutat. Res.*, ***424***, 9-21.

(13) Henle, E. S., Luo, Y., Gassmann, W., and Linn, S. (1996) Oxidative damage to DNA constituents by iron-mediated fenton reactions. The deoxyguanosine family. *J. Biol. Chem.*, ***271***, 21177-21186.

(14) Imlay, J. A., Chin, S. M., and Linn, S. (1988) Toxic DNA damage by hydrogen peroxide through the Fenton reaction in vivo and in vitro. *Science*, ***240***, 640-642.

(15) Imlay, J. A., and Linn, S. (1988) DNA damage and oxygen radical toxicity. *Science*, ***240***, 1302-1309.

(16) Ala, A., Walker, A. P., Ashkan, K., Dooley, J. S., and Schilsky, M. L. (2007) Wilson's disease. *Lancet.*, ***369***, 397-408.

(17) Toyokuni, S. (1996) Iron-induced carcinogenesis: the role of redox regulation. *Free Radic. Biol. Med.*, ***20***, 553-566.

(18) Wang, J., Yuan, B., Guerrero, C., Bahde, R., Gupta, S., and Wang, Y. (2011) Quantification of oxidative DNA lesions in tissues of Long-Evans Cinnamon rats by capillary high-performance liquid chromatography−tandem mass spectrometry coupled with stable isotope-dilution method. *Anal. Chem.*, ***83***, 2201-2209.

(19) Theruvathu, J. A., Jaruga, P., Dizdaroglu, M., and Brooks, P. J. (2007) The oxidatively induced DNA lesions 8,5'-cyclo-2'-deoxyadenosine and 8-hydroxy-2'-deoxyadenosine are strongly resistant to acid-induced hydrolysis of the glycosidic bond. *Mech. Ageing Dev.*, ***128***, 494-502.

(20) Das, R. S., Samaraweera, M., Morton, M., Gascon, J. A., and Basu, A. K. (2012) Stability of N-glycosidic bond of (5'*S*)-8,5'-cyclo-2'-deoxyguanosine. *Chem Res Toxicol*, ***25***, 2451-2461.

(21) Huang, H., Das, R. S., Basu, A. K., and Stone, M. P. (2011) Structure of (5'*S*)-8,5'-cyclo-2'-deoxyguanosine in DNA. *J. Am. Chem. Soc.*, ***133***, 20357-20368.

(22) Zaliznyak, T., Lukin, M., and de los Santos, C. (2012) Structure and stability of duplex DNA containing (5'S)-5',8-cyclo-2'-deoxyadenosine: an oxidatively generated lesion repaired by NER. *Chem. Res. Toxicol.*, ***25***, 2103-2111.

(23) Kuraoka, I., Bender, C., Romieu, A., Cadet, J., Wood, R. D., and Lindahl, T. (2000) Removal of oxygen free-radical-induced 5',8-purine cyclodeoxynucleosides from DNA by the nucleotide excision-repair pathway in human cells. *Proc. Natl. Acad. Sci. U.S.A.*, ***97***, 3832-3837.

(24) Brooks, P. J., Wise, D. S., Berry, D. A., Kosmoski, J. V., Smerdon, M. J., Somers, R. L., Mackie, H., Spoonde, A. Y., Ackerman, E. J., Coleman, K., Tarone, R. E., and Robbins, J. H. (2000) The oxidative DNA lesion 8,5'-(*S*)-cyclo-2'-deoxyadenosine is repaired by the nucleotide excision repair pathway and blocks gene expression in mammalian cells. *J. Biol. Chem.*, ***275***, 22355-22362.

(25) Pande, P., Das, R. S., Sheppard, C., Kow, Y. W., and Basu, A. K. (2012) Repair efficiency of (5'S)-8,5'-cyclo-2'-deoxyguanosine and (5'S)-8,5'-cyclo-2'-deoxyadenosine depends on the complementary base. *DNA Repair (Amst)*, ***11***, 926-931.

(26) Marietta, C., and Brooks, P. J. (2007) Transcriptional bypass of bulky DNA lesions causes new mutant RNA transcripts in human cells. *EMBO Rep.*, ***8***, 388-393.

(27) Kuraoka, I., Robins, P., Masutani, C., Hanaoka, F., Gasparutto, D., Cadet, J., Wood, R. D., and Lindahl, T. (2001) Oxygen free radical damage to DNA. Translesion synthesis by human DNA polymerase eta and resistance to exonuclease action at cyclopurine deoxynucleoside residues. *J. Biol. Chem.*, ***276***, 49283-49288.

(28) Swanson, A. L., Wang, J., and Wang, Y. (2012) Accurate and efficient bypass of 8,5'-cyclopurine-2'-deoxynucleosides by human and yeast DNA polymerase η. *Chem. Res. Toxicol.*, ***25***, 1682-1691.

(29) Belmadoui, N., Boussicault, F., Guerra, M., Ravanat, J. L., Chatgilialoglu, C., and Cadet, J. (2010) Radiation-induced formation of purine 5',8-cyclonucleosides in isolated and cellular DNA: high stereospecificity and modulating effect of oxygen. *Org. Biomol. Chem.*, ***8***, 3211-3219.

(30) Dizdaroglu, M. (1986) Free-radical-induced formation of an 8,5'-cyclo-2'-deoxyguanosine moiety in deoxyribonucleic acid. *Biochem. J.*, ***238***, 247-254.

(31) Dizdaroglu, M., Dirksen, M. L., Jiang, H. X., and Robbins, J. H. (1987) Ionizing-radiation-induced damage in the DNA of cultured human cells. Identification of 8,5-cyclo-2-deoxyguanosine. *Biochem. J.*, ***241***, 929-932.

(32) D'Errico, M., Parlanti, E., Teson, M., de Jesus, B. M., Degan, P., Calcagnile, A., Jaruga, P., Bjoras, M., Crescenzi, M., Pedrini, A. M., Egly, J. M., Zambruno, G., Stefanini, M., Dizdaroglu, M., and Dogliotti, E. (2006) New functions of XPC in the protection of human skin cells from oxidative damage. *EMBO J.*, ***25***, 4305-4315.

(33) Rodriguez, H., Jaruga, P., Leber, D., Nyaga, S. G., Evans, M. K., and Dizdaroglu, M. (2007) Lymphoblasts of women with BRCA1 mutations are deficient in cellular repair of 8,5'-cyclopurine-2'-deoxynucleosides and 8-hydroxy-2'-deoxyguanosine. *Biochem. J.*, ***46***, 2488-2496.

(34) Jaruga, P., and Dizdaroglu, M. (2008) 8,5'-Cyclopurine-2'-deoxynucleosides in DNA: mechanisms of formation, measurement, repair and biological effects. *DNA Repair (Amst)*, ***7***, 1413-1425.

(35) Kirkali, G., de Souza-Pinto, N. C., Jaruga, P., Bohr, V. A., and Dizdaroglu, M. (2009) Accumulation of (5'*S*)-8,5'-cyclo-2'-deoxyadenosine in organs of Cockayne syndrome complementation group B gene knockout mice. *DNA Repair (Amst)*, ***8***, 274-278.

(36) Wang, J., Clauson, C. L., Robbins, P. D., Niedernhofer, L. J., and Wang, Y. (2012) The oxidative DNA lesions 8,5'-cyclopurines accumulate with aging in a tissue-specific manner. *Aging Cell*, DOI: 10.1111/j.1474-9726.2012.00828.x.

(37) Tilstra, J. S., Robinson, A. R., Wang, J., Gregg, S. Q., Clauson, C. L., Reay, D. P., Nasto, L. A., St Croix, C. M., Usas, A., Vo, N., Huard, J., Clemens, P. R., Stolz, D. B., Guttridge, D. C., Watkins, S. C., Garinis, G. A., Wang, Y., Niedernhofer, L. J., and Robbins, P. D. (2012) NF-κB inhibition delays DNA damage–induced senescence and aging in mice. *J. Clin. Invest.*, ***122***, 2601-2612.

(38) Hong, H., Cao, H., Wang, Y., and Wang, Y. (2006) Identification and quantification of a guanine-thymine intrastrand cross-link lesion induced by Cu(II)/H_2O_2/ascorbate. *Chem. Res. Toxicol.*, ***19***, 614-621.

(39) Lim, K. S., Jenner, A., and Halliwell, B. (2006) Quantitative gas chromatography mass spectrometric analysis of 2'-deoxyinosine in tissue DNA. *Nat. Protoc.*, ***1***, 1995-2002.

(40) Jaruga, P., Birincioglu, M., Rodriguez, H., and Dizdaroglu, M. (2002) Mass spectrometric assays for the tandem lesion 8,5'-cyclo-2'-deoxyguanosine in mammalian DNA. *Biochem.*, ***41***, 3703-3711.

(41) Rai, P., Wemmer, D. E., and Linn, S. (2005) Preferential binding and structural distortion by Fe2+ at RGGG-containing DNA sequences correlates with enhanced oxidative cleavage at such sequences. *Nucleic Acids Res.*, ***33***, 497-510.

(42) Cao, H., and Wang, Y. (2007) Quantification of oxidative single-base and intrastrand cross-link lesions in unmethylated and CpG-methylated DNA induced by Fenton-type reagents. *Nucleic Acids Res.*, ***35***, 4833-4844.

(43) Yamamoto, K., and Kawanishi, S. (1989) Hydroxyl free radical is not the main active species in site-specific DNA damage induced by copper (II) ion and hydrogen peroxide. *J. Biol. Chem.*, ***264***, 15435-15440.

(44) Ma, W. J., Cao, E. H., and Qin, J. F. (1999) The involvement of singlet oxygen in copper-phenanthroline/H2O2-induced DNA base damage: a chemiluminescent study. *Redox Rep.*, ***4***, 271-276.

(45) Frelon, S., Douki, T., Favier, A., and Cadet, J. (2003) Hydroxyl radical is not the main reactive species involved in the degradation of DNA bases by copper in the presence of hydrogen peroxide. *Chem. Res. Toxicol.*, ***16***, 191-197.

(46) Shi, M., Xu, B., Azakami, K., Morikawa, T., Watanabe, K., Morimoto, K., Komatsu, M., Aoyama, K., and Takeuchi, T. (2005) Dual role of vitamin C in an oxygen-sensitive system: discrepancy between DNA damage and cell death. *Free Radic. Res.*, ***39***, 213-220.

(47) You, C., Dai, X., Yuan, B., Wang, J., Wang, J., Brooks, P. J., Niedernhofer, L. J., and Wang, Y. (2012) A quantitative assay for assessing the effects of DNA lesions on transcription. *Nat. Chem. Biol.*, ***8***, 817-822.

(48) Mitra, D., Luo, X., Morgan, A., Wang, J., Hoang, M. P., Lo, J., Guerrero, C. R., Lennerz, J. K., Mihm, M. C., Wargo, J. A., Robinson, K. C., Devi, S. P., Vanover, J. C., D'Orazio, J. A., McMahon, M., Bosenberg, M. W., Haigis, K. M., Haber, D. A., Wang, Y., and Fisher, D. E. (2012) An ultraviolet-radiation-independent pathway to melanoma carcinogenesis in the red hair/fair skin background. *Nature*, ***491***, 449-453.

(49) Cleaver, J. E., and Kraemer, K. H. (1989) *In The Metabolic Basis of Inherited Disease* McGraw-Hill, New York.

Chapter 3

Quantification of Oxidative DNA Lesions in Tissues of Long-Evans Cinnamon Rats by Capillary High-performance Liquid Chromatography-Tandem Mass Spectrometry Coupled with Stable Isotope-dilution Method

3.1 Abstract

Transition metal-driven Fenton reactions constitute an important endogenous source of reactive oxygen species (ROS). In genetic diseases characterized by aberrant accumulation of transition metal ions, excessive production of ROS is implicated in pathophysiological consequences, including DNA damage. Wilson's disease is an autosomal recessive disorder with copper toxicosis due to deficiency of the ATP7B protein, which is needed for excretion of copper ions into bile. The Long-Evans Cinnamon (LEC) rat bears a deletion in the Atp7b gene and serves as an excellent animal model for hepatic Wilson's disease. The purpose of our study was to develop suitable methods to identify oxidative DNA lesions in the setting of transition metal-related diseases. We used a sensitive capillary LC-ESI-MS/MS/MS coupled with the stable isotope dilution technique, and quantified several types of oxidative DNA lesions in the liver and brain of LEC rats. These lesions included 5-formyl-2'-deoxyuridine, 5-hydroxymethyl-2'-deoxyuridine, the 5'*R* and 5'*S* diastereomers of 8,5'-cyclo-2'-deoxyguanosine, and 8,5'-cyclo-2'-deoxyadenosine. Moreover, the levels of these DNA lesions in the liver and brain increased with age. This correlated with age-dependent

regulation of the expression of several DNA repair genes in the liver and brain of LEC rats. These results provided significant new knowledge for better understanding the implications of oxidative DNA lesions in transition metal-induced diseases, such as Wilson's disease, as well as in ageing and ageing-related pathological conditions.

3.2 Introduction

Reactive oxygen species (ROS) can be induced by both endogenous and exogenous sources and maintaining cellular ROS homeostasis is essential for normal cellular function; excess generation of ROS can cause damage to lipids, proteins and DNA [1]. Transition metal ion-mediated Fenton reactions constitute an important endogenous source of ROS [2]. Understanding the role of these processes in DNA damage will be particularly important for defining mechanisms of genotoxicity as well as for developing potential therapeutic interventions. This will be benefited by the availability of sensitive and effective diagnostic methods to characterize oxidative DNA lesions.

Among single-gene disorders of transition metal handling, Wilson's disease (WD) occupies a unique place due to defective excretion of copper into bile [3], along with hepatic, neurological and renal abnormalities following copper toxicosis [4, 5]. The WD gene encodes a copper-dependent P-type ATPase (ATP7B) and is highly expressed in the liver, kidney and placenta [4, 5]. Long-Evans Cinnamon (LEC) rat, which was found in an inbred colony of healthy Long-Evans Agouti (LEA) rats [6-8], bears a deletion in Atp7b gene [9] and shares many attributes of WD [8, 10], including hepatic damage arising from copper accumulation, which worsens with age [8, 11, 12]. Thus, LEC rat is an appropriate

animal model for examining the pathophysiology of liver injury in Wilson's disease [6, 8], and the LEA rat constitutes an excellent healthy control.

The accumulation of copper in tissues of LEC rats may lead to the aberrant generation of ROS and elevated formation of oxidative DNA lesions in tissues of LEC rats. In this context, 8-oxo-7,8-dihydro-2'-deoxyguanosine (8-oxodG) was found to be present at elevated levels in DNA of the liver, kidney and brain of LEC rats [13]. Nair et al. [14] found by immunoaffinity/^{32}P-postlabeling assays that hepatic levels of two DNA lesions arising as byproducts of lipid peroxidation, 1,N^6-etheno-2'-deoxyadenosine (εdA) and 3,N^4-etheno-2'-deoxycytidine (εdC), increased with age in LEC rats, peaking at 8-12 weeks. This suggested that progressive accumulation of oxidatively damaged DNA may contribute to losses of hepatocytes in WD. Moreover, additional oxidative DNA lesions may be contributing to liver damage in WD. Along this line, a Fenton-like reagent, Cu(II)/H_2O_2/ascorbate, was found to induce a spectrum of oxidatively generated DNA lesions, including single-nucleobase lesions (8-oxodG, 5-FodU and 5-HmdU) and intrastrand cross-link lesions [15, 16]. In alternative settings, quantification of 8-oxodG, 5-HmdU, 5-FodU, as well as cdG and cdA in cells after exposure to X- [17, 18] or γ-rays [19-21] or chemopreventive agents has been reported [22]. Similarly, cdG and cdA could be detected in mouse tissues [23-25].

The oxidatively induced DNA lesions, if left unrepaired, may accumulate and confer deleterious biological consequences. Along this line, 5-HmdU could induce T→C transition in cellular DNA [26-28], and 5-FodU could give rise to T→G and T→A transversions in mammalian cells [29]. Host cell reactivation assay and *in-vitro* cleavage

assay using mammalian cell nuclear extract revealed that cdA was a substrate for nucleotide excision repair (NER) [30, 31]. Additionally, cdA is a strong blockade to transcription in mammalian cells [30] and it could induce transcription mutagenesis [32]. Furthermore, both diastereomers of cdA inhibit primer extension by T7 DNA polymerase as well as human DNA polymerases η and δ [31, 33].

In the present study, we developed a sensitive capillary liquid chromatography-electrospray ionization-tandem mass spectrometry (LC-ESI-MS^3) method coupled with the stable isotope dilution technique and quantified the levels of 5-FodU, 5-HmdU, and the *R* and *S* diastereomers of cdG and cdA in DNA isolated from the liver and brain tissues of LEC and LEA rats. This provided information regarding the effect of Atp7b deficiency and ageing on the accumulation of endogenously induced DNA lesions in mammalian tissues.

3.3 Experimental Section

3.3.1 Materials

Nuclease P1 and phosphodiesterases 1 and 2 were purchased from Sigma-Aldrich (St. Louis, MO). Alkaline phosphatase and proteinase K were obtained from New England Biolabs (Ipswich, WA), and *erythro*-9-(2-hydroxy-3-nonyl)adenine (EHNA) hydrochloride was from Tocris Bioscience (Ellisville, MO).

Scheme 3.1. Chemical Structures of Oxidative DNA Lesions Measured in This Study[a]

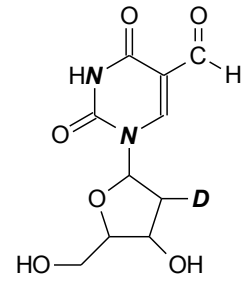

5-FodU

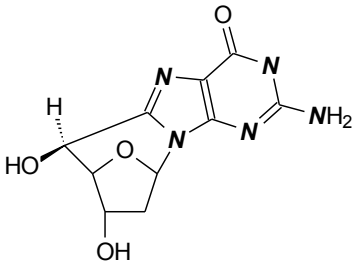

***S*-cdG**

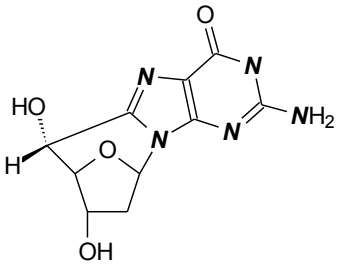

***R*-cdG**

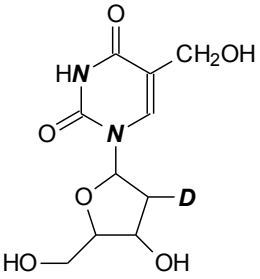

5-HmdU

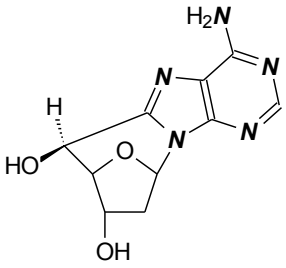

***S*-cdA**

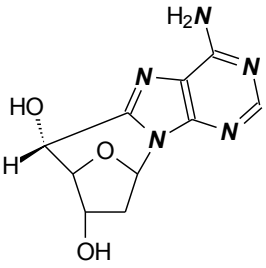

***R*-cdA**

[a]The "N" in bold italic font represents ^{15}N, and the site of deuterium atom incorporation is indicated with a "D".

3.3.2 Synthesis and Characterization of Compounds

The structures of the isotope-labeled DNA lesions used in the present study are shown in Scheme 3.1. The stable isotope-labeled 5-FodU and 5-HmdU were synthesized previously [16].

1,3,7,9-$^{15}N_4$-(2-Amino-^{15}N)]-8,5'-cyclo-2'-deoxyguanosine

The title compound was synthesized at a sub-milligram scale following published procedures for the preparation of un-labeled 8-bromo-2'-deoxyguanosine and cdG with some modifications. [34, 35] [1,3,7,9-$^{15}N_4$-(2-Amino-^{15}N)]-2'-deoxyguanosine (1 mg) was suspended in a mixture of acetonitrile (2.1 mL) and water (0.9 mL), to which was added *N*-bromosuccinimide (1.3 mg) solution in three portions. The mixture was stirred at room temperature for 1.5 h. After the solvent was removed, ethyl ether (1 mL) was added to the mixture. The solution was subsequently stirred at room temperature for 2 h and incubated at -20°C overnight. The mixture was then centrifuged and the supernatant discarded. The precipitate was washed twice with cold acetone and dried to give the uniformly ^{15}N-labeled 8-bromo-2'-deoxyguanosine.

A 1-mM solution of the above-prepared 8-bromo-2'-deoxyguanosine, dissolved in acetonitrile under argon atmosphere, was irradiated with 254-nm UV light from a TLC lamp (UVGL-58, UVP Inc., Upland, CA) at room temperature for 3 h. The resulting 5'*R* and 5'*S* diastereomers of [1,3,7,9-$^{15}N_4$-(2-amino-^{15}N)]-8,5'-cyclo-2'-deoxyguanosine were purified from the reaction mixture by HPLC. (Figure B1 in Appendix B). Exact mass measurements gave *m/z* 271.0741and *m/z* 271.0752 for the $[M + H]^+$ ions of the

uniformly 15N-labeled 5'*R*-cdG and 5'*S*-cdG, respectively which are in keeping with the calculated *m/z* of 271.0741. The high-resolution mass spectra (HRMS) were acquired on an Agilent 6510 Q-TOF LC-MS instrument equipped with an HPLC-Chip Cube MS interface as described previously.[36] The isotopic purity was found to be better than 99.9% based on LC-MS/MS analysis.

1,3,7,9-$^{15}N_4$-(2-amino-^{15}N)]-8,5'-cyclo-2'-deoxyadenosine

The isotope-labeled cdA was synthesized from the uniformly ^{15}N-labeled 2'-deoxyadenosine using the above-described procedures for the preparation of the two diastereomers of uniformly ^{15}N-labeled cdG (Figure B2 in Appendix B). Exact mass measurements yielded *m/z* 255.0801 and *m/z* 255.0796 for the $[M + H]^+$ ions of the uniformly 15N-labeled 5'*R*-cdA and 5'*S*-cdA, respectively, which are in keeping with the calculated *m/z* of 255.0792. the isotopic purity was found to be better than 99.1% based on LC-MS/MS analysis.

3.3.3 Animals

Breeding of rats was approved by the Animal Care and Use Committee at Albert Einstein College of Medicine. Rats were housed in the Institute for Animal Studies at Einstein under 14 h light/10 h dark cycles with unrestricted access to rodent chow (11.8 mg copper/kg; Ralson Purina, St. Louis, MO) and tap water. LEA rats were periodically backcrossed with LEC-/- rats to maintain their inbred status. LEA and LEC-/- rats were crossed to obtain heterozygous LEC+/- rats. The genotype of animals was verified by polymerase chain reaction (PCR) of genomic DNA from tail as described previously.[37]

Animals were housed without any manipulations for various time periods and sacrificed for collecting tissues in liquid nitrogen, which were stored under −80ºC. Grading of tissue changes was performed by histological examination of hematoxylin and eosin-stained tissue sections; the following changes in hepatocytes were graded, and mitosis.[38] The grades were summed with maximal possible score of 13 (see Results and Appendix B)

3.3.4 Extraction of Nuclear DNA

Genomic DNA was isolated using a high-salt method [39]. Briefly, rat tissue was ground under liquid nitrogen into fine powders in a mortar. The powders were subsequently transferred to a 50-mL centrifuge tube, to which was added a 5-mL lysis buffer containing 20 mM Tris (pH 8.1), 20 mM EDTA, 400 mM NaCl and 1% SDS (w/v) as well as 25 μL of proteinase K (20 mg/mL). The tube was incubated in a water bath at 55°C overnight. Next day, 0.5 volume of saturated NaCl solution was added to the digestion mixture, which was vortexed for 1 min, and then incubated at 55°C for 15 min. The mixture was centrifuged at ~10,000 rpm for 30 min and the supernatant was collected and centrifuged again under the same conditions. The nucleic acids in the supernatant were precipitated from ethanol. To the nucleic acid mixture was added 2.5 μL solution of RNase A (10 mg/mL) and 1 μL solution of RNase T1 (25 units/μL), and the solution was incubated at 37°C for 1 h followed by extraction with an equal volume of chloroform/isoamyl alcohol (24:1, v/v) twice. The DNA was then precipitated from the aqueous layer by ethanol. The mixture was subsequently centrifuged at 7,000 rpm for 15 min. The resulting DNA pellet was washed twice with 70% cold ethanol and allowed to

air-dry at room temperature for overnight. The pellet was then dissolved in TE buffer and the amount of nuclear DNA was quantified by using UV spectrophotometry.

3.3.5 Enzymatic Digestion of Nuclear DNA

Eight units of nuclease P1, 0.01 unit of phosphodiesterase 2, 20 nmol of EHNA and a 20-μL solution (pH 5.6) containing 300 mM sodium acetate and 10 mM zinc chloride were added to 80 μg of DNA. In this context, some enzymes used for DNA digestion were contaminated with adenine deaminase, which can induce the deamination of dA to 2'-deoxyinosine (dI). Because dI shared a very similar retention time as *S*-cdG during HPLC enrichment (Appendix B, Figure B3), the presence of considerable amount of dI in the digestion mixture diminished substantially the sensitivity for *S*-cdG measurement. Therefore, we added EHNA prior to the enzymatic digestion [40], which reduced the deamination of dA to less than 2%, facilitating *S*-cdG to be detected with adequate sensitivity. The above digestion was continued at 37°C for 48 h. To the digestion mixture were then added 8 units of alkaline phosphatase, 0.02 unit of phosphodiesterase 1 and 40 μL of 0.5 M Tris-HCl buffer (pH 8.9). The digestion mixture was incubated at 37°C for 2 h and subsequently neutralized by addition of formic acid. To the mixture were then added isotopically labeled standard lesions, which included 2.5 pmol of 5-FodU, 1.5 pmol of 5-HmdU, 80 fmol of *R*-cdG, 40 fmol of *S*-cdG, 60 fmol of *R*-cdA and 20 fmol of *S*-cdA (Scheme 3.1). The enzymes in the digestion mixture were subsequently removed by chloroform extraction. The resulting aqueous layer was dried, reconstituted in doubly distilled water, and subjected to off-line HPLC separation for the enrichment of the

lesions under study.

3.3.6 HPLC

A 4.6×250 mm Alltima HP C18 column (5 μm in particle size, Grace Davison, Deerfield, IL) was used for the enrichment of oxidatively induce DNA leisons from enzymatic digestion products of DNA. A solution of 10 mM ammonium formate (solution A) and methanol (solution B) were used as mobile phases, and the flow rate was 1 mL/min. A 90 min gradient of 42 min 0% B, 1 min 0-5% B, 32 min 5% B, 5 min 5-20% B, and 10 min 20% B was employed. A typical HPLC trace is depicted in Figure B1 of Appendix B. A minor RNA contamination (less than 5% for most DNA samples) was often observed for the DNA samples based on the chromatograms obtained during the HPLC enrichment. Correction for RNA contamination was made for each DNA sample according to the peak areas of adenosine and guanosine in the HPLC traces relative to those of 2'-deoxyadenosine (dA) and 2'-deoxyguanosine (dG). The HPLC fractions eluting at 8.5-10.0, 17.0-20.0, 21.0-24.0, 29.5-32.5, 32.5-36.0 and 56.0-63.0 min were pooled for *R*-cdG, 5-HmdU, *R*-cdA, *S*-cdG, 5-FodU and *S*-cdA, respectively. The collected fractions were dried in the Speed-vac, redissolved in H_2O, and injected for LC-MS/MS/MS analysis.

3.3.7 LC-MS/MS/MS Analysis

A 0.5×250 mm Zorbax SB-C18 column (particle size, 5 μm, Agilent) was used for the separation of the above-enriched lesion fractions, and the flow rate was 8.0 μL/min, which was delivered by using an Agilent 1100 capillary HPLC pump (Agilent

Technologies). A solution of 0.1% (v/v) formic acid in water (solution A) and a solution of 0.1% (v/v) formic acid in methanol (solution B) were used as mobile phases for the analyses of all the ROS-induced DNA lesions after HPLC enrichment, and a gradient of 5 min 0-20% B followed by 21 min 20-35% B was employed for the separation.

The effluent from the LC column was directed to an LTQ linear ion-trap mass spectrometer (Thermo Fisher Scientific), which was set up for monitoring the fragmentation of the labeled and unlabeled *R*-cdG, *S*-cdG, *R*-cdA and *S*-cdA in the positive-ion mode or the labeled and unlabeled 5-FodU and 5-HmdU in the negative-ion mode. The temperature for the ion transport tube was maintained at 275°C, the sheath gas flow rate was 15 arbitrary units, and no auxiliary gas was used. In the positive-ion mode, the spray voltage, capillary voltage and tube lens voltage were 4.5 kV, 5 V and 20 V, respectively; each MS^3 scan was composed of three microscans and maximum time for each microscan was 250 ms. In the negative-ion mode, the spray voltage, capillary voltage and tube lens were 4 kV, -10 V and -100 V, respectively; each scan had one microscan and the maximum scan time was 100 ms. Prior to analyzing the lesions isolated from tissue DNA samples, the sensitivities for detecting all these lesions were optimized by varying two working parameters of the LTQ mass spectrometer, i.e., normalized collision energy and activation Q (Table B1 of Appendix B). The detection limits (LOD and LOQ), calculated from the amounts of a lesion that could give rise to a signal-to-noise ratio (S/N) of 3 and 10 in the selected-ion chromatogram, respectively. The LOD and LOQ were determined based on three independent LC-MS^3 measurements preformed in three separate days (Table S1). A single LC-ESI-MS^3 measurement was

performed for each lesion released from each tissue genomic DNA.

3.3.8 Real-time Quantitative Reverse Transcription-Polymerase Chain Reaction (Real-time qRT-PCR)

mRNA was isolated from the liver and brain tissues of LEC rats with RNAeasy mini kit (Qiagen, Valencia, CA) following the vendor's recommended procedures. One μg of total RNA was subsequently reverse-transcribed with 1 μL iScript reverse transcriptase (Bio-Rad Laboratories, Hercules, CA) and 4 μL 5×iScript reaction mixture in a 20 μL-volume reaction. The reaction was carried out at 25°C for 5 min and at 42°C for 30 min, and the reverse transcriptase was then deactivated by heating at 85°C for 5 min.

Analyses of the transcripts for rat NTHL1, NEIL1, XPA, ERCC1, CSA and CSB were performed by real-time qRT-PCR using iQ^{TM} SYBR Green Supermix kit (Bio-Rad) according to the manufacturer's recommendations on a Bio-Rad iCycler system (Bio-Rad). The real-time PCR was performed by running at 95°C for 3 min and 45 cycles at 95°C for 15 s, 55°C for 30 s and 72°C for 45 s (The primer sequences are listed in Table B3 of Appendix B). The comparative cycle threshold (*Ct*) method was used for the relative quantification of gene expression [41]. The GAPDH gene was used as the internal control, which was included on each plate to correct for sample variations. The mRNA level of each gene in each sample was normalized to that of the internal control. Relative mRNA level with respect to 1-month old animal tissue was represented as $2^{-\Delta\Delta Ct}$, where $\Delta\Delta Ct = (Ct_{\text{gene of interest}} - Ct_{\text{internal control}})_{\text{3 or 6 month}} - (Ct_{\text{gene of interest}} - Ct_{\text{internal control}})_{\text{1 month}}$. Relative mRNA levels in 3 and 12 month old LEC+/- rats were calculated in a similar fashion. All data shown were the mean ± S.D. of three separate experiments.

3.4 Results

3.4.1 LC-MS^3 method for quantifying ROS-induced DNA lesions in rat tissues

For quantifying low levels of DNA lesions in isolated and cellular DNA, we enriched lesions from the enzymatic digestion mixture by off-line HPLC with an analytical column and then subjected lesion-containing fractions to LC-MS analysis on an LTQ linear ion-trap mass spectrometer [16, 42-44]. To achieve unambiguous identification and quantification of low levels of ROS-induced bulky lesions in complicated sample matrices [16, 42, 43], we employed MS^3 mode of detection using parameters detailed in Table S1. We also assessed analytical performance of LC-MS^3 monitored in the positive- or negative-ion mode (See Experimental Section) for all lesions (Appendix B, Table B1).

Here we describe detection of *S*-cdG to illustrate the application of LC-MS^3 for quantifying this lesion in rat tissues. The selected-ion chromatograms (SICs) and MS^3 spectra for unlabeled and ^{15}N-labeled *S*-cdG are shown in Figure 3.1. We monitored the *m/z* 266→180→163 and *m/z* 271→185→167 transitions for *S*-cdG and its uniformly ^{15}N-labeled counterpart, respectively. The identity of the component eluting at 13.6 min in the SIC depicted in Figure 3.1A was determined to be *S*-cdG based on its co-elution with ^{15}N-labeled *S*-cdG and similar fragment ions found in MS^3 of the analyte and its uniformly ^{15}N-labeled standard (Figure 3.1). As shown in Scheme 2, the ions of *m/z* 180 and 185 arise from cleavages of both the *N*-glycosidic linkage and the bond between the 5'-C and 4'-C of the 2-deoxyribose moiety of *S*-cdG and ^{15}N-labeled *S*-cdG, respectively [45]. Further fragmentation of the ion at *m/z* 180 gave rise to three major fragment ions at *m/z* 163, 152 and 135, which form from the neutral losses of NH_3, CO and [NH_3 + CO],

respectively. The corresponding fragment ions were found in the MS^3 of the internal standard. In addition, the relative abundances of these three major fragment ions emanating from the cleavage of the ions of *m/z* 180 and 185 were very similar, thereby confirming the identity of the component eluting at 13.6 min to be *S*-cdG. Other purine cyclonucleosides were assessed by LC-MS/MS/MS in a similar fashion (Figures B4-B6 in Appendix B). We also constructed calibration curves for the quantification of all these lesions from results of three independent sets of experiments performed in three separate days (Tables B5-B10 and Figures B7-B12 in Appendix B). The relatively small variation in measurement results highlighted the reproducibilities of the LC-MS/MS/MS method.

3.4.2 The levels of ROS-induced DNA lesions in liver and brain tissues of LEA and LEC rats

With the above LC-MS^3 method, we quantified all lesions in DNA isolated from rat liver and brain tissues. The data are summarized in Table B2 and plotted in Figures 3.2-3.3. Therein, the lesion levels are reported as number of lesions per 10^6 DNA nucleosides. To obtain these numbers, we converted the peak area ratios obtained in LC-MS^3 analysis to molar ratios, which were then multiplied by the amount of the corresponding labeled standards to give the amount of lesions in mole. The number of DNA nucleosides in the tissue genomic DNA was calculated by dividing the amount (μg) of DNA used for enzymatic digestion with the mean molecular weight of deoxyribonucleotides, 309 g/mol.

To manage the number of samples, we studied 3-month old LEA rats since liver copper remains normal in these animals without age-dependent changes. Similarly, no alteration

in liver histology was observed in LEA rats over age (Table S4). In addition, we established that biliary copper excretion is normally maintained in heterozygous LEC+/- rats and as a result liver copper content also remains normal. This was confirmed by normal liver histology in heterozygous LEC+/- rats, which was similar to LEA rats (Table S4). Nevertheless, we included heterozygous LEC+/- rats of 3 and 12 month ages in our studies of DNA lesions. By contrast, LEC rats begin to exhibit significant changes in hepatic copper content at early ages, and extensive copper-induced liver damage becomes apparent within several weeks of age (Table B4).

We next describe the levels of oxidatively induced DNA lesions in livers of LEA, LEC+/- and LEC-/- rats. First, we did not observe significant differences in the levels of oxidatively induced DNA lesions in 3-month old LEA and LEC+/- rats (Figures 3.2-3.4), which was in agreement with normal liver copper content and histological appearances. On the other hand, appreciably higher levels of 5-FodU, 5-HmdU, and both diastereomers of cdA were observed in the liver of 3-month old LEC-/- rats (Figures 3.2-3.4). The two diastereomers of cdG were present at slightly higher levels in liver of LEC significant. Additionally, we observed that the liver of 12-month old LEC+/- rats contained higher levels of ROS-induced lesions than corresponding 3-month old LEA or LEC +/- rats.We found greatest levels of 5-FodU and *S*-cdA in LEC-/- rats at 3-months of age compared with at 1- or 6-months of age, which may reflect changes associated with acute-on-chronic liver injury, which is a known feature of hepatitis in LEC-/- rats. However, no statistically significant difference was observed for other lesions among LEC-/- rats at various ages, except for *S*-cdG, which was present at higher levels in 6-

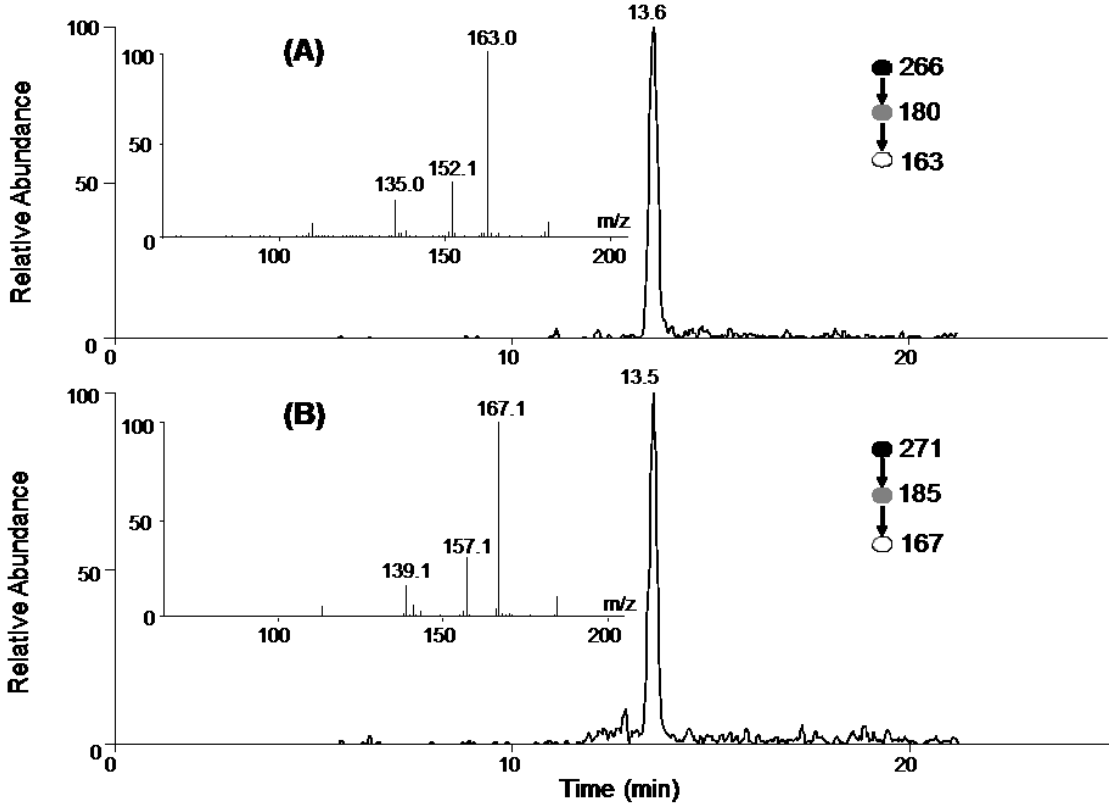

Figure 3.1. Selected-ion chromatograms (SICs) for monitoring the *m/z* 266→180→163 [A, for unlabeled *S*-cdG] and *m/z* 271→185→167 [B, for labeled *S*-cdG] transitions of the digestion mixture of genomic DNA from the liver tissue of a 6-month old LEC-/- rat. Shown in the insets are the positive-ion MS^3 spectra for the unlabeled and labeled *S*-cdG.

Scheme 3.2. Proposed Major Fragmentation Pathways for the $[M + H]^+$ Ion of Unlabeled *S*-cdG Observed in MS/MS and MS/MS/MS

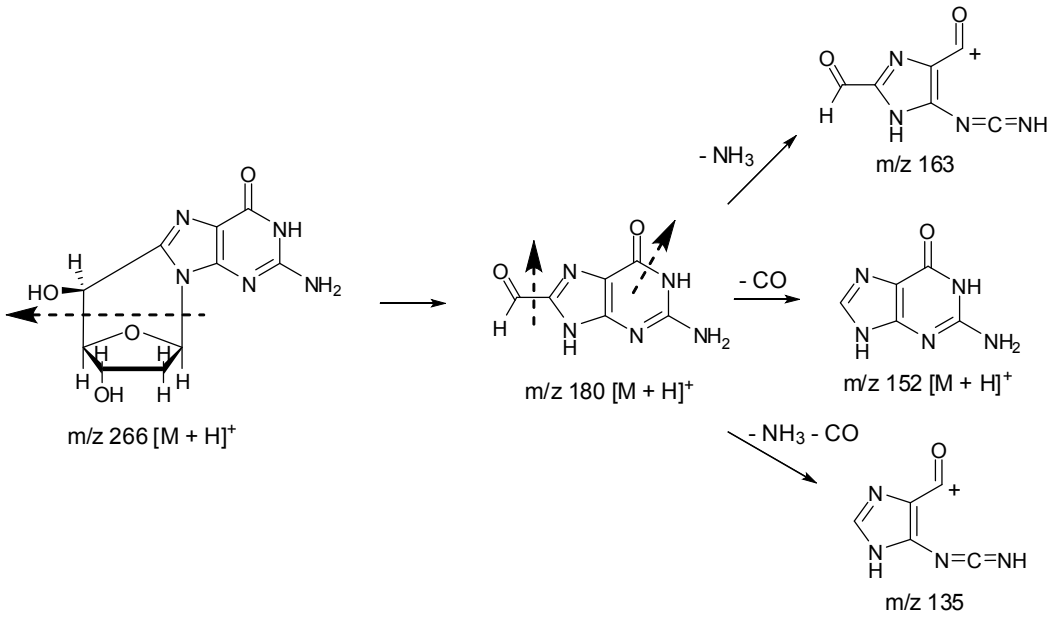

month old rats

While LEC rats exhibited extensive liver damage due to copper toxicosis, no neurological abnormalities or brain damage have been reported in these animals, which differs from WD in humans [46] and is attributable to the lack of copper accumulation in the brain of LEC rats. However, examination of oxidative DNA lesions in the brain of these rats revealed some similarities and differences with those in the liver. In this respect, we again observed similar levels of all quantified oxidative DNA lesions in 3-month old LEA and LEC+/- rats. Likewise, we found age-dependent accumulation of all quantified oxidative DNA lesions, except for *S*-cdG and *S*-cdA in brain of LEC+/- rats. In contrast to liver tissues, we observed a slightly higher level of 5-FodU in the brain of LEC-/- rats compared with LEA or LEC+/- rats. Furthermore, we found an age-dependent increase in the levels of all the quantified ROS-induced DNA lesions in brain of LEC-/- rats.

3.4.3 Real-time qRT-PCR for monitoring expression levels of genes involved in DNA repair

Previous studies revealed a decreased expression of some DNA repair genes in liver tissues of LEC rats in the acute hepatitis stage [47]. We reasoned that the altered expression of DNA repair genes may also have contributed to age-related levels of oxidative DNA lesions in the brain and liver tissues of LEC rats. Therefore, we studied six DNA repair genes, including two BER genes, NTHL1 and NEIL1, two NER genes, XPA and ERCC1, and two transcription-coupled repair genes, CSA and CSB [48].

Expression of NTHL1, NEIL1, XPA, and CSB was markedly lower in the liver of

3-month old LEC-/- rats compared with 1-month old LEC-/- rats, while the expression of

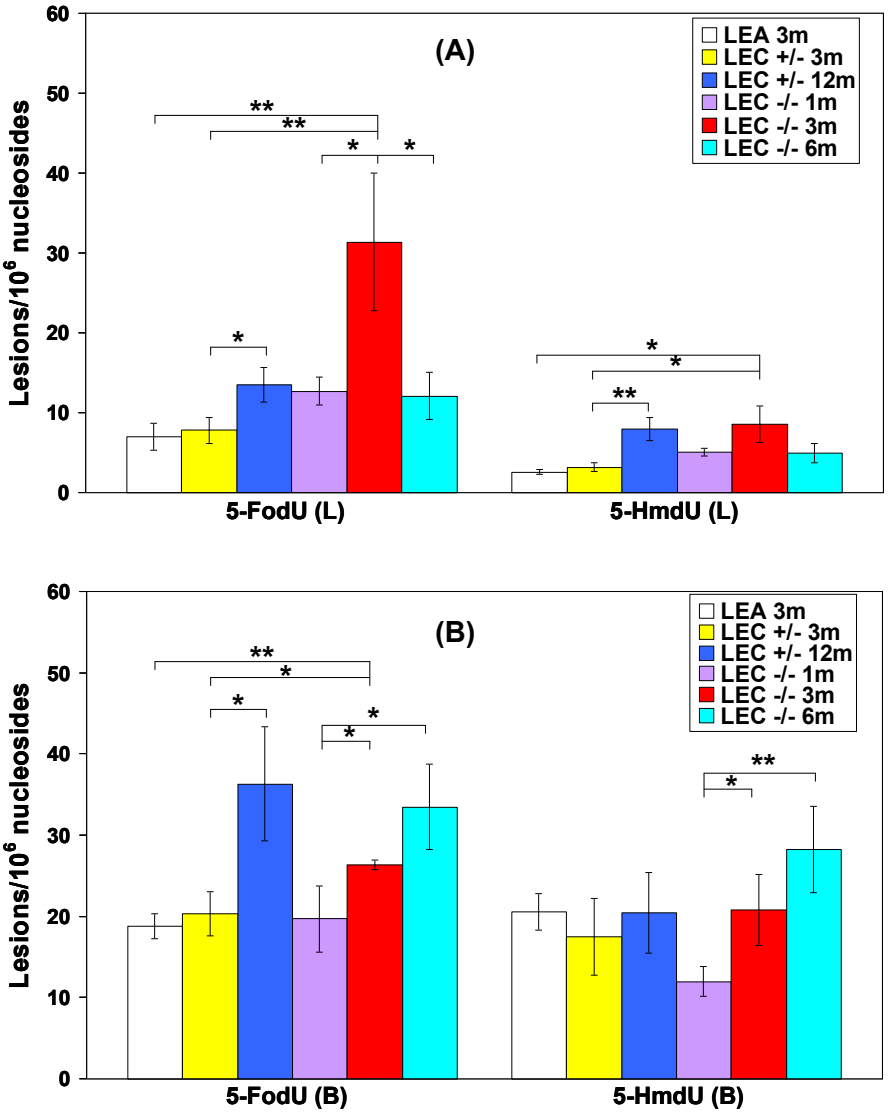

Figure 3.2. Levels of 5-FodU and 5-HmdU in genomic DNA isolated from the liver (L) and brain (B) of LEA (3m), LEC+/- (3m or 12m) and LEC-/- (1m, 3m or 6m) rats. The values represent the mean ± S.D. of results obtained from tissues of three rats. '*', $P < 0.05$; '**', $P < 0.01$; '***', $P < 0.001$. The P values were calculated by using paired t-test.

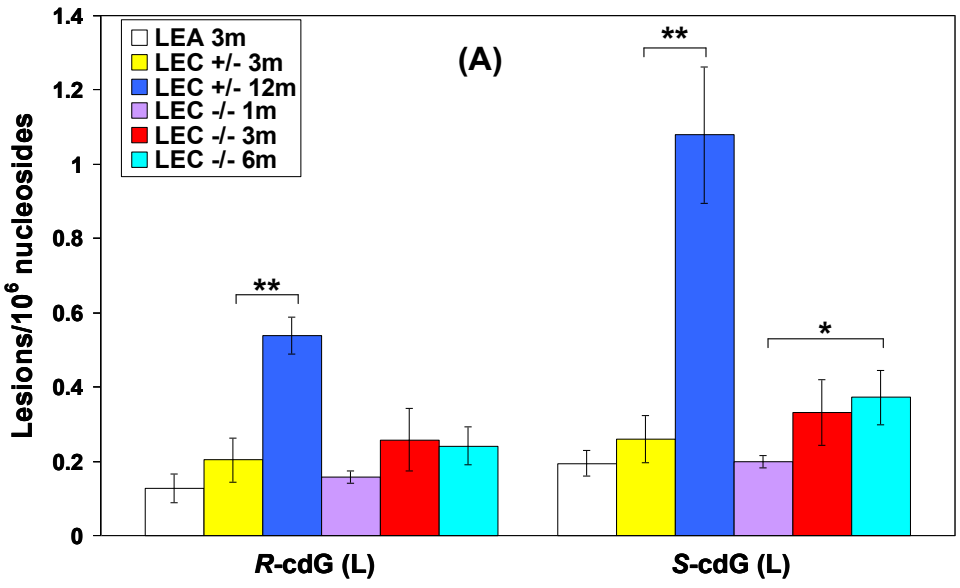
LEA 3m
LEC +/- 3m
LEC +/- 12m
LEC -/- 1m
LEC -/- 3m
LEC -/- 6m
(A)
Lesions/10^6 nucleosides
1.4
1.2
1
0.8
0.6
0.4
0.2
0
**
**
*
R-cdG (L)
S-cdG (L)

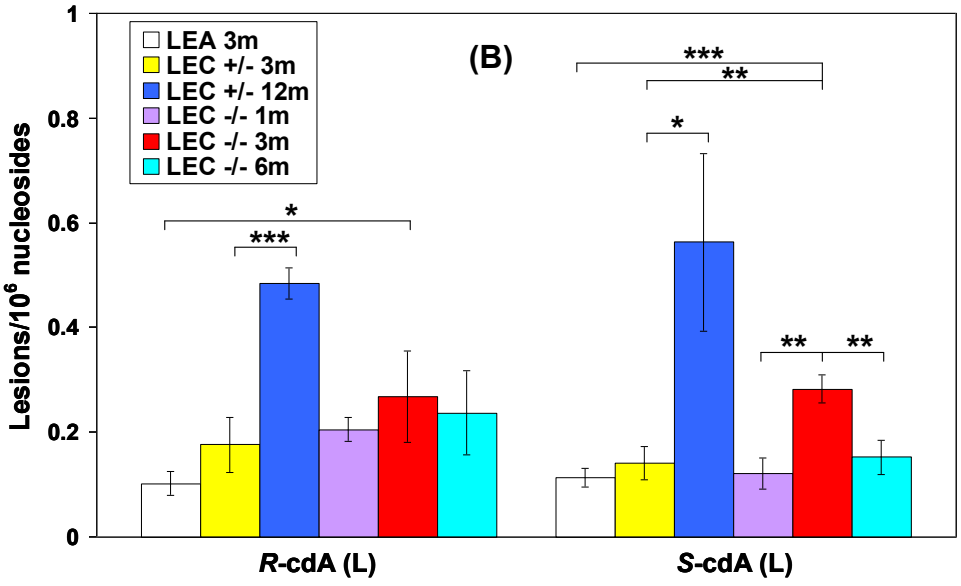
LEA 3m
LEC +/- 3m
LEC +/- 12m
LEC -/- 1m
LEC -/- 3m
LEC -/- 6m
(B)
Lesions/10^6 nucleosides
1
0.8
0.6
0.4
0.2
0
*
***
***
**
*
**
**
R-cdA (L)
S-cdA (L)

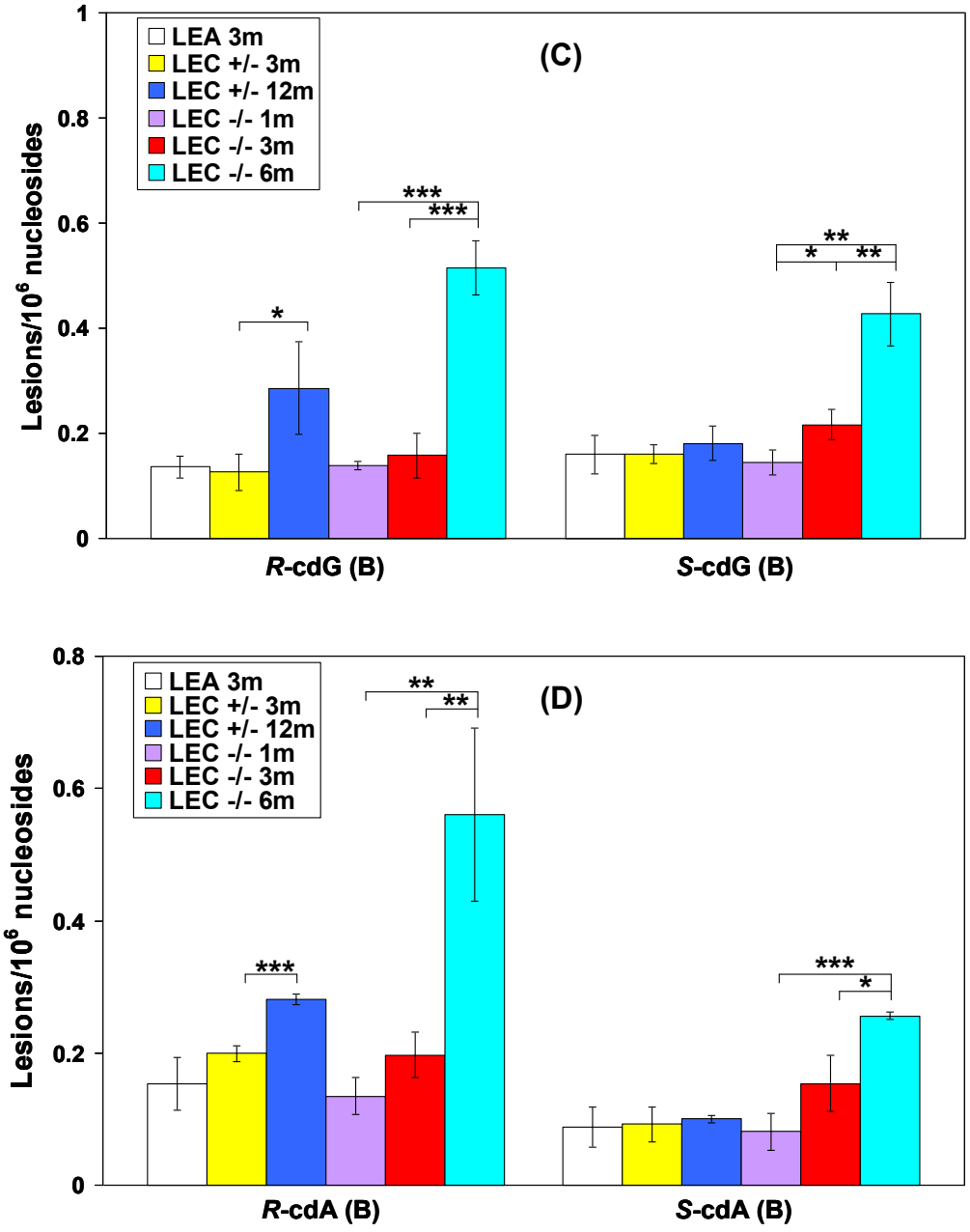

Figure 3.3. Levels of *R*-cdG, *S*-cdG, *R*-cdA and *S*-cdA in genomic DNA isolated from the livers (L) and brains (B) of LEA (3m), LEC+/- (3m or 12m) and LEC-/- (1m, 3m or 6m) rats. The values represent the mean ± S.D. of results obtained for tissue samples from three different rats. '*', $P < 0.05$; '**', $P < 0.01$; '***', $P < 0.001$. The *P* values were calculated by using paired *t*-test.

these genes was restored, fully or in part, in 6-month old LEC-/- rats (Figure 3.4). The transcript levels of CSA were not substantially different in liver of 1- and 3-month old LEC-/- rats, whereas the liver of 6-month old animals exhibited significantly higher expression of these two genes. On the other hand, expression of NTHL1 and CSA was slightly decreased in the brain of 3-month old LEC-/- rats. Furthermore, we found expression of NEIL1 increased with age, whereas expression of XPA, ERCC1 and CSB exhibited an age-dependent decrease in the brain of LEC-/- rats.

Together, the brain and liver of LEC-/- rats displayed different age-dependent expression of DNA repair genes, which may have been responsible, at least in part, for the differences in the profiles of DNA lesions in these tissues.

We also assessed, by employing real-time PCR analysis, the levels of expression of the above six DNA repair genes in the liver and brain tissues of 3 and 12 month old LEC +/- rats, respectively small differences were observed between the 3 and 12 month old LEC +/- rats, particularly for the brain tissues (Figure B13 in Appendix B). Thus, the higher levels of the oxidatively induced DNA lesions observed for the brain and liver tissues of 12 month old LEC +/- rats might reflect the age-associated accumulation of these lesions.

3.5 Discussion

In this study, we found MS^3 detection mode offered more reliable quantification of ROS-induced DNA lesions than the MS^2 mode that was employed to analyze these

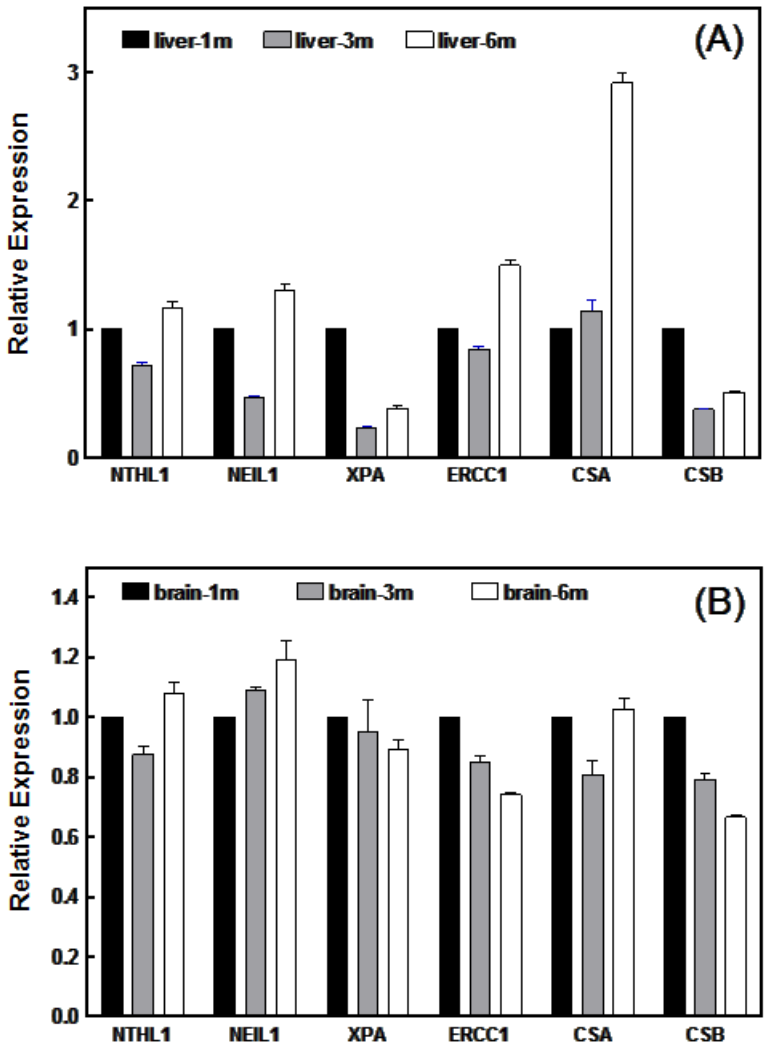

Figure 3.4. The mRNA levels of NTHL1, NEIL1, XPA, ERCC1, CSA and CSB in the liver (A) and brain (B) of LEC-/- (1m, 3m or 6m) rats. The results were obtained by real-time qRT-PCR with the use of GAPDH as standard. The data represent the mean ± S.D. of three separate experiments.

types of lesions in most previous studies.[23-25] For instance, Figure B5 shows the SICs and MS^3 results for monitoring *S*-cdA in a rat DNA sample, where two pairs of major fragment ions at *m/z* 136 and 119, and at *m/z* 141 and 123 were observed for the unlabeled and labeled *S*-cdA, respectively. Apart from these fragment ions, other ions emanating from isobaric interferences (e.g. the ions of *m/z* 151 and 152 in Figure S3B) were also detected. Similar interferences were observed for some other lesions quantified in the present study. Thus, MS^3 afforded more reliable detection of these lesions in cellular DNA. We found higher levels of 5-FodU, 5-HmdU, and two diastereomers of cdA in the liver of 3-month old LEC-/- than age-matched LEC+/- or LEA rats. This was in keeping with previous observation of greater 8-oxodG levels in LEC rats, especially at the acute hepatitis stage [13]. In contrast, LEC-/- rats deficient in Atp7b did not show greater levels of all the quantified ROS-induced lesions, except for 5-FodU in the brain, which was in agreement with the absence of gross neurological defects in these rats.[49]

We observed age-dependent increases in ROS-induced DNA lesions in liver and brain of LEC+/- rats and brain of LEC-/- rats (Figures 3.2-3.3). Randerath et al. [50] demonstrated by ^{32}P-postlabeling assays that bulky DNA lesions increase with age in animals. Some of these indigenous lesions ("I-compounds") were identical to those induced in isolated DNA exposed to Fenton-type reagents and the levels of these lesions were elevated in kidneys of rodents treated with prooxidant carcinogens [51]. Thus, these so-called "Type II-I compounds" were attributed to those induced by endogenous ROS [51]. Later, some of the Type-II I compounds found by ^{32}P-postlabeling assay were identified to be *S*-cdA with different flanking 5' nucleosides [52]. The covalent linkage between the

C8 carbon of adenine and the C5' carbon of 2-deoxyribose in the lesion inhibits cleavage of the flanking 5' phosphodiester bond by nucleases in the ^{32}P-post-labeling assay [52] However, the structures of other bulky DNA lesions demonstrated by the ^{32}P-post-labeling assay are yet to be established. Our studies showed that all four purine cyclonucleosides could be detected in animal tissues and all of them exhibited age-dependent increases in brain of LEC-/- rats and brain and liver of LEC+/- rats. Thus, aside from previously identified *S*-cdA, other bulky lesions, including *R*-cdA, *S*-cdG and *R*-cdG, should constitute new members of the Type II I-compound family. In this context, it is worth noting that we assessed the lesion levels in tissues of animals from a relatively small number of age groups. In the future, it will be important to expand the study to more age groups of rats and to other mammalian species.

Among our noteworthy findings were that we did not observe age-dependent increases in ROS-induced DNA lesions in the liver of LEC-/- rats. Indeed, the liver of 3-month old LEC-/- rats exhibited greater levels of 5-FodU and *S*-cdA than 1- and 6-month old LEC-/- rats. Similar age-associated prevalences of DNA lesions were previously observed for εdA and εdC in liver of LEC rats, where the levels of these two lesions peaked at 8-12 weeks [14]. Additionally, the age-dependent accumulation of εdA and εdC paralleled the liver copper content of these rats [14]. Also, accumulation of hepatic copper in LEC rats was shown to compromise the capacity for DNA repair. In the latter respect, the enzymatic activities and expression levels of two major DNA glycosylases, endonuclease III (NTHL1) and 8-oxoguanine DNA glycosylase (OGG1), were greatly diminished in LEC rat liver extracts during acute hepatitis at 16-18 weeks of age [47]. No

substantial differences in DNA repair activity or expression level of DNA repair genes were observed for LEA rats with ages ranging from 8 to 40 weeks [47]. In keeping with these previous findings, the transcript levels of NTHL1, NEIL1, XPA and CSB genes in 3-month old LEC-/- rats were lower than those in 1-month old LEC-/- rats. The products of the former two genes are important for repairing thymine methyl group oxidation products [53, 54], and NEIL1 is important for repairing cdA [55]. Additionally, cdA is a substrate for mammalian NER pathway [30, 31]. On the other hand, CSA and CSB are important in transcription-coupled repair; CSB plays a key role as a coupling factor to recruit NER proteins to lesion-stalled RNA polymerase II, whereas CSA is dispensable for this process [56]. Along this line, the CSB-/- mouse embryonic fibroblast (MEF) is 2-fold more sensitive to γ rays than wild-type MEF, whereas the CSA-/- MEF exhibited similar sensitivity as the wild-type counterpart [57]. In particular, CSB was also shown to be important in repairing *S*-cdA [58]. Therefore, diminished hepatic expression of NTHL1, NEIL1, XPA, and CSB in 3-month old LEC rats may have contributed to the elevated levels of 5-FodU and *S*-cdA in the liver of these rats.

It is worth discussing the relative levels of the ROS-induced purine cyclonucleosides with respect to 5-HmdU and 5-FodU. In this regard, our results (Figures 3.2-3.3) revealed that cdA and cdG levels were approximately 2 orders of magnitude lower than those of 5-FodU and 5-HmdU in the liver and brain of LEA and LEC rats. The relative levels of these lesions reflect a dynamic interplay between the rates of their formation and repair in animal tissues.

Taken together, the age- and genotype-dependent accumulation of oxidative DNA

lesions, as revealed in herein, should help in understanding the implications of oxidative DNA damage in the pathophysiology of WD, as well as in ageing and ageing-associated pathological conditions.

Appendix Materials

Instrument parameters for LC-MS/MS/MS analysis, LC-MS/MS/MS data, calibration curves, and histological grading for liver damage of rats used in this study. This material is in Appendix B.

References

(1) Finkel, T., and Holbrook, N. J. (2000) Oxidants, oxidative stress and the biology of ageing. *Nature*, ***408***, 239-247.

(2) Cadet, J., Delatour, T., Douki, T., Gasparutto, D., Pouget, J. P., Ravanat, J. L., and Sauvaigo, S. (1999) Hydroxyl radicals and DNA base damage. *Mutat. Res.*, ***424***, 9-21.

(3) Danks, D. M. (1989) *Disorders of copper transport*. McGraw-Hill, New York.

(4) Ala, A., Walker, A. P., Ashkan, K., Dooley, J. S., and Schilsky, M. L. (2007) Wilson's disease. *Lancet.*, ***369***, 397-408.

(5) Ferenci, P. (2005) Wilson's Disease. *Clin. Gastroenterol. Hepatol.*, ***3***, 726-733.

(6) Mori, M., Hattori, A., Sawaki, M., Tsuzuki, N., Sawada, N., Oyamada, M., Sugawara, N., and Enomoto, K. (1994) The LEC rat: a model for human hepatitis, liver cancer, and much more. *Am. J. Pathol.*, ***144***, 200-204.

(7) Sasaki, M., Yoshida, M. C., Kagami, K., Takeichi, N., Kobayashi, H., Dempo, K. and Mori, M. (1985) Spontaneous hepatitis in an inbred strain of long-evans rats. *Rat News Lett.*, ***14***, 4-6.

(8) Yoshida, M. C., Masuda, R., Sasaki, M., Takeichi, N., Kobayashi, H., Dempo, K., and Mori, M. (1987) New mutation causing hereditary hepatitis in the laboratory rat. *J. Hered.*, ***78***, 361-365.

(9) Wu, J., Forbes, J. R., Chen, H. S., and Cox, D. W. (1994) The LEC rat has a deletion in the copper transporting ATPase gene homologous to the Wilson disease gene. *Nat. Genet.*, ***7***, 541-545.

(10) Li, Y., Togashi, Y., Sato, S., Emoto, T., Kang, J. H., Takeichi, N., Kobayashi, H., Kojima, Y., Une, Y., and Uchino, J. (1991) Spontaneous hepatic copper accumulation in Long-Evans Cinnamon rats with hereditary hepatitis. A model of Wilson's disease. *J. Clin. Invest.*, ***87***, 1858-1861.

(11) Masuda, R., Yoshida, M. C., Sasaki, M., Dempo, K., and Mori, M. (1988) High susceptibility to hepatocellular carcinoma development in LEC rats with hereditary hepatitis. *Jpn. J. Cancer Res.*, ***79***, 828-835.

(12) Sawaki, M., Enomoto, K., Takahashi, H., Nakajima, Y., and Mori, M. (1990) Phenotype of preneoplastic and neoplastic liver lesions during spontaneous liver carcinogenesis of LEC rats. *Carcinogenesis*, ***11***, 1857-1861.

(13) Yamamoto, F., Kasai, H., Togashi, Y., Takeichi, N., Hori, T., and Nishimura, S. (1993) Elevated level of 8-hydroxydeoxyguanosine in DNA of liver, kidneys, and brain of Long-Evans Cinnamon rats. *Jpn. J. Cancer Res.*, ***84***, 508-511.

(14) Nair, J., Strand, S., Frank, N., Knauft, J., Wesch, H., Galle, P. R., and Bartsch, H. (2005) Apoptosis and age-dependent induction of nuclear and mitochondrial etheno-DNA adducts in Long-Evans Cinnamon (LEC) rats: enhanced DNA damage by dietary curcumin upon copper accumulation. *Carcinogenesis*, ***26***, 1307-1315.

(15) Cao, H., and Wang, Y. (2007) Quantification of oxidative single-base and intrastrand cross-link lesions in unmethylated and CpG-methylated DNA induced by Fenton-type reagents. *Nucleic Acids Res*, ***35***, 4833-4844.

(16) Hong, H., Cao, H., Wang, Y., and Wang, Y. (2006) Identification and quantification of a guanine-thymine intrastrand cross-link lesion induced by Cu(II)/H_2O_2/ascorbate. *Chem. Res. Toxicol.*, ***19***, 614-621.

(17) D'Errico, M., Parlanti, E., Teson, M., de Jesus, B. M., Degan, P., Calcagnile, A., Jaruga, P., Bjoras, M., Crescenzi, M., Pedrini, A. M., Egly, J. M., Zambruno, G., Stefanini, M., Dizdaroglu, M., and Dogliotti, E. (2006) New functions of XPC in the protection of human skin cells from oxidative damage. *EMBO J.*, ***25***, 4305-4315.

(18) D'Errico, M., Parlanti, E., Teson, M., Degan, P., Lemma, T., Calcagnile, A., Iavarone, I., Jaruga, P., Ropolo, M., Pedrini, A. M., Orioli, D., Frosina, G., Zambruno, G., Dizdaroglu, M., Stefanini, M., and Dogliotti, E. (2007) The role of CSA in the response to oxidative DNA damage in human cells. *Oncogene*, ***26***, 4336-4343.

(19) Dizdaroglu, M., Dirksen, M. L., Jiang, H. X., and Robbins, J. H. (1987) Ionizing-radiation-induced damage in the DNA of cultured human cells. Identification of 8,5-cyclo-2-deoxyguanosine. *Biochem. J.*, ***241***, 929-932.

(20) Pouget, J. P., Frelon, S., Ravanat, J. L., Testard, I., Odin, F., and Cadet, J. (2002) Formation of modified DNA bases in cells exposed either to gamma radiation or to high-LET particles. *Radiat. Res.*, ***157***, 589-595.

(21) Hong, H., and Wang, Y. (2007) Derivatization with Girard reagent T combined with LC-MS/MS for the sensitive detection of 5-formyl-2'-deoxyuridine in cellular DNA. *Anal. Chem.*, ***79***, 322-326.

(22) Bhimani, R. S., Troll, W., Grunberger, D., and Frenkel, K. (1993) Inhibition of oxidative stress in HeLa cells by chemopreventive agents. *Cancer Res.*, ***53***, 4528-4533.

(23) Jaruga, P., Xiao, Y., Nelson, B. C., and Dizdaroglu, M. (2009) Measurement of (5'R)- and (5'S)-8,5'-cyclo-2'-deoxyadenosines in DNA in vivo by liquid chromatography/isotope-dilution tandem mass spectrometry. *Biochem. Biophys. Res. Commun.*, ***386***, 656-660.

(24) Kirkali, G., de Souza-Pinto, N. C., Jaruga, P., Bohr, V. A., and Dizdaroglu, M. (2009) Accumulation of (5'*S*)-8,5'-cyclo-2'-deoxyadenosine in organs of Cockayne syndrome complementation group B gene knockout mice. *DNA Repair (Amst)*, ***8***, 274-278.

(25) Egler, R. A., Fernandes, E., Rothermund, K., Sereika, S., de Souza-Pinto, N., Jaruga, P., Dizdaroglu, M., and Prochownik, E. V. (2005) Regulation of reactive oxygen species, DNA damage, and c-Myc function by peroxiredoxin 1. *Oncogene*, ***24***, 8038-8050.

(26) Boorstein, R. J., and Teebor, G. W. (1988) Mutagenicity of 5-hydroxymethyl-2'-deoxyuridine to Chinese hamster cells. *Cancer Res.*, ***48***, 5466-5470.

(27) Bilimoria, M. H., and Gupta, S. V. (1986) Comparison of the mutagenic activity of 5-hydroxymethyldeoxyuridine with 5-substituted 2'-deoxyuridine analogs in the Ames Salmonella/microsome test. *Mutat. Res.*, ***169***, 123-127.

(28) Shirname-More, L., Rossman, T. G., Troll, W., Teebor, G. W., and Frenkel, K. (1987) Genetic effects of 5-hydroxymethyl-2'-deoxyuridine, a product of ionizing radiation. *Mutat. Res.*, ***178***, 177-186.

(29) Kamiya, H., Murata-Kamiya, N., Karino, N., Ueno, Y., Matsuda, A., and Kasai, H. (2002) Induction of T --> G and T --> A transversions by 5-formyluracil in mammalian cells. *Mutat. Res.*, ***513***, 213-222.

(30) Brooks, P. J., Wise, D. S., Berry, D. A., Kosmoski, J. V., Smerdon, M. J., Somers, R. L., Mackie, H., Spoonde, A. Y., Ackerman, E. J., Coleman, K., Tarone, R. E., and Robbins, J. H. (2000) The oxidative DNA lesion 8,5'-(*S*)-cyclo-2'-deoxyadenosine is repaired by the nucleotide excision repair pathway and blocks gene expression in mammalian cells. *J. Biol. Chem.*, ***275***, 22355-22362.

(31) Kuraoka, I., Bender, C., Romieu, A., Cadet, J., Wood, R. D., and Lindahl, T. (2000) Removal of oxygen free-radical-induced 5',8-purine cyclodeoxynucleosides from DNA by the nucleotide excision-repair pathway in human cells. *Proc. Natl. Acad. Sci. U. S. A.*, ***97***, 3832-3837.

(32) Marietta, C., and Brooks, P. J. (2007) Transcriptional bypass of bulky DNA lesions causes new mutant RNA transcripts in human cells. *EMBO Rep.*, ***8***, 388-393.

(33) Kuraoka, I., Robins, P., Masutani, C., Hanaoka, F., Gasparutto, D., Cadet, J., Wood, R. D., and Lindahl, T. (2001) Oxygen free radical damage to DNA. Translesion synthesis by human DNA polymerase η and resistance to exonuclease action at cyclopurine deoxynucleoside residues. *J. Biol. Chem.*, ***276***, 49283-49288.

(34) Gillet, L. C. J., and Scharer, O. D. (2002) Preparation of C8-amine and acetylamine adducts of 2 '-deoxyguanosine suitably protected for DNA synthesis. *Org. Lett.*, ***4***, 4205-4208.

(35) Jimenez, L. B., Encinas, S., Miranda, M. A., Navacchia, M. L., and Chatgilialoglu, C. (2004) The photochemistry of 8-bromo-2-deoxyadenosine. A direct entry to cyclopurine lesions. *Photochem. Photobiol. Sci.*, ***3***, 1042-1046.

(36) Xiong, L., and Wang, Y. (2010) Quantitative proteomic analysis reveals the perturbation of multiple cellular pathways in HL-60 cells induced by arsenite treatment. *J. Proteome. Res.*, ***9***, 1129-1137.

(37) Ahmed, S., Deng, J., and Borjigin, J. (2005) A new strain of rat for functional analysis of PINA. *Brain Res. Mol. Brain Res.*, ***137***, 63-69.

(38) Malhi, H., Bhargava, K. K., Afriyie, M. O., Volenberg, I., Schilsky, M. L., Palestro, C. J., and Gupta, S. (2002) 99mTc-mebrofenin scintigraphy for evaluating liver disease in a rat model of Wilson's disease. *J. Nucl. Med.*, ***43***, 246-252.

(39) Miller, S. A., Dykes, D. D., and Polesky, H. F. (1988) A simple salting out procedure for extracting DNA from human nucleated cells. *Nucleic Acids Res.*, ***16***, 1215.

(40) Lim, K. S., Jenner, A., and Halliwell, B. (2006) Quantitative gas chromatography mass spectrometric analysis of 2'-deoxyinosine in tissue DNA. *Nat. Protoc.*, ***1***, 1995-2002.

(41) Livak, K. J., and Schmittgen, T. D. (2001) Analysis of relative gene expression data using real-time quantitative PCR and the $2^{-\Delta\Delta CT}$ Method. *Methods*, ***25***, 402-408.

(42) Hong, H., Cao, H., and Wang, Y. (2007) Formation and genotoxicity of a guanine-cytosine intrastrand cross-link lesion in vivo. *Nucleic Acids Res*, ***35***, 7118-7127.

(43) Jiang, Y., Hong, H., Cao, H., and Wang, Y. (2007) In vivo formation and in vitro replication of a guanine-thymine intrastrand cross-link lesion. *Biochemistry*, ***46***, 12757-12763.

(44) Goodenough, A. K., Schut, H. A., and Turesky, R. J. (2007) Novel LC-ESI/MS/MS^n method for the characterization and quantification of 2'-deoxyguanosine adducts of the dietary carcinogen 2-amino-1-methyl-6-phenylimidazo[4,5-b]pyridine by 2-D linear quadrupole ion trap mass spectrometry. *Chem. Res. Toxicol.*, ***20***, 263-276.

(45) Jaruga, P., Birincioglu, M., Rodriguez, H., and Dizdaroglu, M. (2002) Mass spectrometric assays for the tandem lesion 8,5'-cyclo-2'-deoxyguanosine in mammalian DNA. *Biochemistry*, ***41***, 3703-3711.

(46) Lorincz, M. T. (2010) Neurologic Wilson's disease. *Ann. N. Y. Acad. Sci.*, ***1184***, 173-187.

(47) Choudhury, S., Zhang, R., Frenkel, K., Kawamori, T., Chung, F. L., and Roy, R. (2003) Evidence of alterations in base excision repair of oxidative DNA damage during spontaneous hepatocarcinogenesis in Long Evans Cinnamon rats. *Cancer Res.*, ***63***, 7704-7707.

(48) Friedberg, E. C., Walker, G. C., Siede, W., Wood, R. D., Schultz, R. A., and Ellenberger, T. (2006) *DNA Repair and Mutagenesis*. ASM Press, Washington, D.C.

(49) Ahn, T. B., Cho, S. S., Kim, D. W., and Jeon, B. S. (2005) Absence of nigrostriatal degeneration in LEC rats up to 20 weeks of age. *Neurol. Res.*, ***27***, 409-411.

(50) Randerath, K., Reddy, M. V., and Disher, R. M. (1986) Age- and tissue-related DNA modifications in untreated rats: detection by ^{32}P-postlabeling assay and possible significance for spontaneous tumor induction and aging. *Carcinogenesis*, ***7***, 1615-1617.

(51) Randerath, K., Randerath, E., Zhou, G. D., and Li, D. H. (1999) Bulky endogenous DNA modifications (I-compounds) - possible structural origins and functional implications. *Mutat. Res.*, ***424***, 183-194.

(52) Randerath, K., Zhou, G. D., Somers, R. L., Robbins, J. H., and Brooks, P. J. (2001) A ^{32}P-postlabeling assay for the oxidative DNA lesion 8,5 '-cyclo-2 '-deoxyadenosine in mammalian tissues - Evidence that four type II I-compounds are dinucleotides containing the lesion in the 3 ' nucleotide. *J. Biol. Chem.*, ***276***, 36051-36057.

(53) Zhang, Q. M., Yonekura, S., Takao, M., Yasui, A., Sugiyama, H., and Yonei, S. (2005) DNA glycosylase activities for thymine residues oxidized in the methyl

group are functions of the hNEIL1 and hNTH1 enzymes in human cells. *DNA Repair*, ***4***, 71-79.

(54) Miyabe, I., Zhang, Q. M., Kino, K., Sugiyama, H., Takao, M., Yasui, A., and Yonei, S. (2002) Identification of 5-formyluracil DNA glycosylase activity of human hNTH1 protein. *Nucleic Acids Res.*, ***30***, 3443-3448.

(55) Jaruga, P., Xiao, Y., Vartanian, V., Lloyd, R. S., and Dizdaroglu, M. (2010) Evidence for the involvement of DNA repair enzyme NEIL1 in nucleotide excision repair of (5'R)- and (5'S)-8,5'-cyclo-2'-deoxyadenosines. *Biochemistry*, ***49***, 1053-1055.

(56) Fousteri, M., Vermeulen, W., van Zeeland, A. A., and Mullenders, L. H. (2006) Cockayne syndrome A and B proteins differentially regulate recruitment of chromatin remodeling and repair factors to stalled RNA polymerase II in vivo. *Mol. Cell*, ***23***, 471-482.

(57) de Waard, H., de Wit, J., Andressoo, J. O., van Oostrom, C. T., Riis, B., Weimann, A., Poulsen, H. E., van Steeg, H., Hoeijmakers, J. H., and van der Horst, G. T. (2004) Different effects of CSA and CSB deficiency on sensitivity to oxidative DNA damage. *Mol. Cell. Biol.*, ***24***, 7941-7948.

(58) Kirkali, G., de Souza-Pinto, N. C., Jaruga, P., Bohr, V. A., and Dizdaroglu, M. (2009) Accumulation of (5'S)-8,5'-cyclo-2'-deoxyadenosine in organs of Cockayne syndrome complementation group B gene knockout mice. *DNA Repair*, ***8***, 274-278.

Chapter 4

Induction of 5-Methylcytosine Oxidative Products in Isolated DNA by Fenton-Type Reagents

4.1 Abstract

Recently, it was demonstrated that ten-eleven translocation (Tet) family dioxgenases and thymine DNA glycosylase (TDG) mediate an active demethylation pathway for 5-methylcytosine in mammals; in which Tet mediates the sequential oxidation of 5-mdC to 5-fodC and then to 5-cadC followed by TDG recognition and cleavage of 5-fodC and 5-cadC. Base excision repair can then restore the resulting AP site with an unmodified cytosine, completing demethylation of the initial 5-mdC. This is the first active demethylation pathway found in mammals. However, endogenous and exogenous ROS is capable of generating 5-hmdC and 5-fodC, which may compromise genome integrity and result in aberrant gene expression. Furthermore, it has not been demonstrated *in vitro*, whether 5-cadC can be induced by ROS. Fenton-type reactions are a major endogenous source of ROS that has been associated with aging, disease, and cancer. Here, we examined the formation of 5-mdC oxidation products in isolated DNA treated with Fenton-type reagents. We found that all three modified 5-mdC derivatives could be induced proportionally with respect to increasing concentrations of Fenton-type reagents. 5-hmdC levels were one order of magnitude higher than those of 5-fodC and 5-cadC. In addition, this is the first evidence indicating that ROS can induce the generation

5-cadC. Furthermore, it is possible that ROS can induce 5-fodC and 5-cadC which could be recognized by TDG suggesting potential path of inadvertent active demethylation.

4.2 Introduction

DNA methylation is essential for epigenetic signaling, which regulates many important biological processes including genomic imprinting, retrotransposon silencing, and X-chromosome inactivation.[1-4] This methylation usually is initiated by DNA methyltransferases 3a and 3b (DNMT3a and DNMT3b) during embryonic development, while DNA methyltransferase 1 (DNMT1) facilitates the maintenance of the DNA methylation pattern during cell division.[1] In mammals, methylation occurs at the C5 position of cytosine residues mainly at CpG dinucleotide sites.[5] Recently, it was reported that an enzyme-mediated demethylation pathway exists, which may enable the dynamic regulation of DNA cytosine methylation during development and cellular differentiation.[6] This active demethylation pathway occurs via the oxidation of 5-mdC by the ten-eleven translocation (Tet) family dioxygenases Tet1, Tet2, and Tet3, followed by the recognition and cleavage of the resulting oxidation products by thymine DNA glycosylase (TDG), yielding an unmethylated cytosine. Briefly, Tet1, Tet2, and Tet3 are responsible for sequential enzymatic oxidation of 5-methyl-2'-deoxycytidine (5-mdC) to 5-hydroxymethyl-2'-deoxycytidine (5-hmdC), 5-formyl-2'-deoxycytidine (5-fodC), and 5-carboxyl-2'-deoxycytidine (5-caC) (Scheme 4.1).[7-9] Furthermore, TDG is capable of cleaving 5-foC and 5-caC, and the resulting abasic sites can be recognized by the base-excision repair (BER) machinery, which ultimately leads to the incorporation of an

unmethylated cytosine at the initial 5-mdC site.[10] Together, these enzymes comprise the first active demethylation pathway known to regulate cytosine methylation in mammalian cells.

Alternatively, the 5-hmC and 5-foC are known to be products of oxidatively-induced DNA damage.[11] While active demethylation by the Tet family dioxygenases is suspected to maintain intracellular regulation for a variety of factors, we hypothesize that inadvertent demethylation may also occur via reactive oxygen species (ROS)-induced oxidation of 5-mdC, where the resulting 5-fodC and 5-cadC may also be recognized by TDG thereby giving rise to cytosine demethylation in a process that is independent of Tet enzymes.

Endogenous and exogenous ROS are continuously inflicting damage to proteins, lipids, and DNA. Exogenous ROS such as γ- and X-rays are well-known to damage DNA, generating lesions including 5-hmC and 5-foC. Normal aerobic metabolism can generate ROS. In this regard, approximately 1 - 3% of cellular O_2 combines with electrons leaking from the electron transport chain to yield superoxide anion radicals ($O_2^{-\cdot}$).[12-14] $O_2^{-\cdot}$ can then be converted to H_2O_2 by superoxide dismutase.[15] H_2O_2 is freely diffusible in the cellular environment and can react with DNA-bound transition metal ions, such as Cu(I) and Fe(II), yielding a highly reactive hydroxyl radical ($\cdot OH$) via a Fenton-type reaction (Equation 1).[16]

Equation 1: $Cu(I) + H_2O_2 \rightarrow Cu(II) + \cdot OH + OH^-$

Scheme 4.1. Chemical structures of oxidized derivatives of 5-mdC.

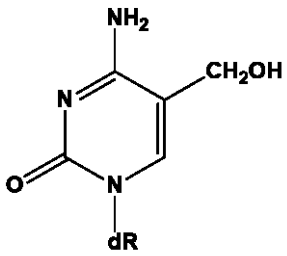

5-hmdC

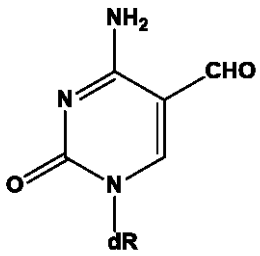

5-fodC

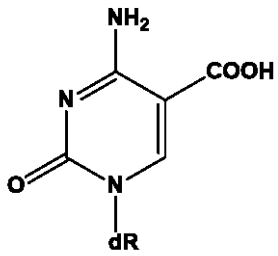

5-cadC

'dR' represents 2-deoxyribose

Transition metal ions serve as essential components for many intracellular and intercellular pathways. However, they have to be highly regulated to minimize their induction of ROS via the Fenton-type reaction. Several genetic disorders, such as Wilson's disease and iron overload disease, have deficiencies in regulating and maintaining homeostasis of transition metal ions.[17, 18] As a result, individuals with these diseases are known to be more susceptible to oxidatively-induced DNA damage. Previously we demonstrated that the bulky 8,5'-cyclo-2'-deoxyadenosine (cdA) and 8,5'-cyclo-2'-deoxyguanosine (cdG) lesions are induced in calf thymus DNA when treated with Fenton-type reagents.[19] Furthermore, we quantified the cadA and cdG levels in tissues of Long Evans Cinnamon (LEC) rats, which mimic the cellular conditions exhibited in patients with Wilson's disease. We found elevated levels of cdA and cdG in LEC rats compared to the controls.[20] This result supports transition metal ion-induced , oxidative DNA damage *in vitro* and *in vivo*. Lesions such as cdA and cdG pose threats to genomic integrity since they can impede DNA replication, transcription, and induce mutations in these processes.[21-23]

Previous studies have demonstrated the generation of 5-hmdC and 5-fodC in oligodeoxyribonucleotides (ODN) upon treatment with Fenton-like reagents.[11] In the present study, we employed LC-MS/MS/MS coupled with stable isotope-dilution method to identify and quantify 5-hmdC, 5-fodC, and 5-cadC in calf thymus DNA treated with Fenton-type reagents. Our results revealed a dose-dependent formation of all 5-mdC oxidative products. Specifically, to our knowledge, this is the first report demonstrating that 5-cadC can be induced at a similar level as 5-fodC by ROS *in vitro*.

4.3 Experimental Procedures

4.3.1 Materials

$CuCl_2$, $(NH_4)_2Fe(SO_4)_2 \cdot 6H_2O$, L-methionine, L-ascorbic acid, calf thymus DNA, nuclease P1, alkaline phosphatase, and phosphodiesterases 1 and 2 were purchased from Sigma-Aldrich (St. Louis, MO). Hydrogen peroxide (30%) and *erythro*-9-(2-hydroxy-3-nonyl)adenine (EHNA) hydrochloride were obtained from Fisher Scientific (Fair Lawn, NJ) and Tocris Bioscience (Ellisville, MO), respectively. The uniformly [^{15}N]-labeled 5-hmdC and 5-fodC were synthesized previously (Structures shown in Scheme 1).[24, 25]

4.3.2 Synthesis and Characterization of [4-amino-1,3-$^{15}N_3$]-5-Carboxyl-2'-deoxycytidine ([4-amino-1,3-$^{15}N_3$]-CadC)

The title compound was prepared at a micromole scale according to previously published methods for the synthesis of the corresponding unlabeled compound with slight modifications (Scheme 4.2).[26] [4-*amino*-1,3-$^{15}N_3$]-dC (3.0 mg, 13.0 μM) was dissolved in dimethylformamide (100 μL) and allowed to stir at room temperature (RT) for 10 min. Iodine (2.13 mg), followed by *m*-chloroperbenzoic acid (2.97 mg), was added and allowed to stir at RT for 1.5 h. The reaction mixture was then dried using a Speed-vacuum. The solid residues were reconstituted with water and filtered. The resulting [4-*amino*-1,3-$^{15}N_3$]-5-iodo-2'-deoxycytidine ([4-*amino*-1,3-$^{15}N_3$]-IdC) was purified by HPLC.

The purified [4-*amino*-1,3-$^{15}N_3$]-IdC was dissolved in methanol (500 μL) and bubbled with CO for 30 min. Subsequently, triphenylphosphine (1.37 mg), triethylamine

(2 μL) and tris(dibenzylideneacetone)dipalladium(0) (0.81 mg) were added. The reaction mixture was stirred overnight at 50 °C under CO atmosphere. The mixture was cooled to RT and the resulting solid was removed by filtration. The resulting [4-*amino*-1,3-$^{15}N_3$]-5-methoxycarbonyl-2'-deoxycytidine was readily converted to the desired [4-*amino*-1,3-$^{15}N_3$]-cadC by treating with 0.1 M K_2CO_3 in MeOH/H_2O at 40°C overnight. The latter compound was isolated from the reaction mixture by HPLC. The identity of [4-*amino*-1,3-$^{15}N_3$]-cadC was confirmed by LC-MS/MS analysis and by high-resolution MS analysis on an ESI-TOF instrument. The latter measurement gave *m/z* 273.0636 for the $[M - H]^-$ ion, whose calculated *m/z* was 273.0641.

4.3.3 Treatment of Calf Thymus DNA

Commercially available calf thymus DNA was desalted by ethanol precipitation and reconstituted in 25 mM NaCl and 50 mM phosphate (pH 7.0) buffer. The DNA was then slowly annealed by heating at 90°C for 5 min, followed by cooling slowly to room temperature.

Aliquots of DNA (75 μg) were incubated at room temperature under aerobic conditions for 60 min in a 250-μL of reaction buffer (25 mM NaCl, 50 mM phosphate, pH 7.0) containing various amounts of $CuCl_2$, H_2O_2 (0.1-1.6 mM) and ascorbate (1-16 mM). Chemicals used in the Fenton-type reagent treatment of DNA were freshly prepared in doubly distilled water. Detailed concentrations of individual Fenton reagents used for the reactions are shown in Table 1. After 60 min, the reactions were terminated

Table 4.1. Concentrations of Fenton-Type Reagents Employed for the Treatment of Calf Thymus DNA[a]

	Control	A	B	C	D
Cu(II) (μM)	200	12.5	25	50	100
H_2O_2 (μM)	0	100	200	400	800
ascorbate (mM)	0	1.0	2.0	4.0	8.0

[a]All reactions were carried out in a 250-μL solution containing 75 μg of calf thymus DNA.

by adding excess L-methionine. Finally, DNA samples were desalted by ethanol precipitation.

4.3.4 Enzymatic Digestion of DNA

To the above desalted DNA samples were added 8 units of nuclease P1, 0.01 unit of phosphodiesterase 2, 20 nmol of EHNA, and a 20-μL solution containing 300 mM sodium acetate (pH 5.6) and 10 mM zinc chloride. To prevent the potential deamination of adenine induced by residual contamination of adenine deaminase present in some commercial preparations of enzymes used for the DNA digestion, EHNA was added to the enzymatic digestion mixture.[27] After a 48-hr incubation at 37 °C, 8 units of alkaline phosphatase, 0.02 unit of phosphodiesterase 1, and 40 μL of 0.5 M Tris-HCl (pH 8.9) were added to the digestion mixture. The solution was further incubated at 37°C for 2 h, after which the enzymes were removed by chloroform extraction and the solution dried using the Speed vacuum. DNA samples were then reconstituted in doubly distilled water and concentrations determined using UV-absorption spectrophotometry. To aliquots of each mixture were added stable isotope-labeled 5-hmdC (300 fmol), 5-fodC (60 fmol), and 5-cadC (50 fmol), (Scheme 4.1). The resulting aliquots were subjected directly to LC-MS/MS analysis (mdC and hmdC), or HPLC enrichment prior to LC-MS/MS/MS analysis (fodC and cadC).

4.3.5 HPLC Enrichment

An Apollo C18 column (4.6×250 mm, 5 μm in particle size, Grace Davison, Deerfield, IL) was used for the enrichment of oxidatively induced 5-mdC products. The mobile phases consisted of 10 mM ammonium formate (solution A) and methanol (solution B). A gradient of 42 min 1% B, 1 min at 5% B, 17 min 5-15% B, and 10 min 15-90% B was employed at a flow rate of 1 mL/min. The HPLC fractions eluting at 2-8 min and 36-43 min were pooled for cadC and fodC, respectively (Appendix D1). The collected fractions were dried in the Speed vacuum, redissolved in H_2O, and finally subjected to LC-MS/MS/MS analysis.

4.3.6 LC-MS/MS/MS Analysis of 5-hmdC, 5-fodC, and 5-cadC

An Agilent 1100 capillary HPLC pump (Agilent Technologies) equipped with a SB-C18 Zorbax column (0.5×250 mm, 5 μm particle size, Agilent) was used for LC-MS separation. A solution of 0.1% (v/v) formic acid in water (solution A) and 0.1% (v/v) formic acid in methanol (solution B) were used as mobile phases. The optimized gradient used for LC separation included 0-20% B in 5 min, and 20-70% B in 25 min. The flow rate was 8 μL/min.

The eluent from the LC column was directly coupled to an LTQ linear ion-trap mass spectrometer (Thermo), of which the fragmentation of the $[M+H]^+$ ions of labeled and unlabeled hmdC, fodC, and cadC were monitored, as well as further fragmentation of the corresponding $[M+H-116]^+$ fragments found in MS/MS.

4.4 Results

4.4.1 LC-MS/MS/MS Method for Identification and Quantification of Oxidatively-Induced Derivatives of 5-mdC in Calf Thymus DNA Exposed to Cu(II)/H_2O_2/Ascorbate.

First we assessed how efficiently Fenton-type reagents could induce all three oxidized derivatives of 5-mdC. To this end, we treated calf thymus DNA with various concentrations of Cu(II)/H_2O_2/ascorbate (Table 4.1), which mimics the endogenous production of ROS via the Fenton-type reaction. The resulting DNA was digested to mononucleosides using a cocktail of four enzymes, and the 5-fodC and 5-cadC were enriched from the nucleoside mixture using off-line HPLC, and then analyzed by LC-MS^3 using an isotope-dilution method with [^{15}N]-labeled nucleoside standards. Lesion levels were calculated based on peak area ratios of analyte and labeled standards by using calibration curves constructed for each lesion (Appendix C2).

For the analysis of 5-hmdC, we chose to exclude off-line enrichment prior to subjecting to LC-MS/MS/MS due to its relatively high abundance. In the LC-MS^3, we monitored the *m/z* 258→142→124 and 261→144→126 transitions for 5-hmdC and its [^{15}N]-labeled counterpart, respectively. The selected-ion chromatograms (SICs) and MS^3 spectra for unlabeled and labeled 5-hmdC are shown in Figure 4.1. The identity of 5-hmdC was confirmed by the co-elution of components at 20.7 min and by similar fragment ions observed for the unlabeled analyte and the [^{15}N]-labeled standard in Figure 4.1A and B, respectively. Specifically, the ions of *m/z* 142 and *m/z* 144 arise from the neutral loss of a 116-Da fragment, which is associated with the cleavage of the *N*-glycosidic bond and the subsequent loss of the 2-deoxyribose component from the

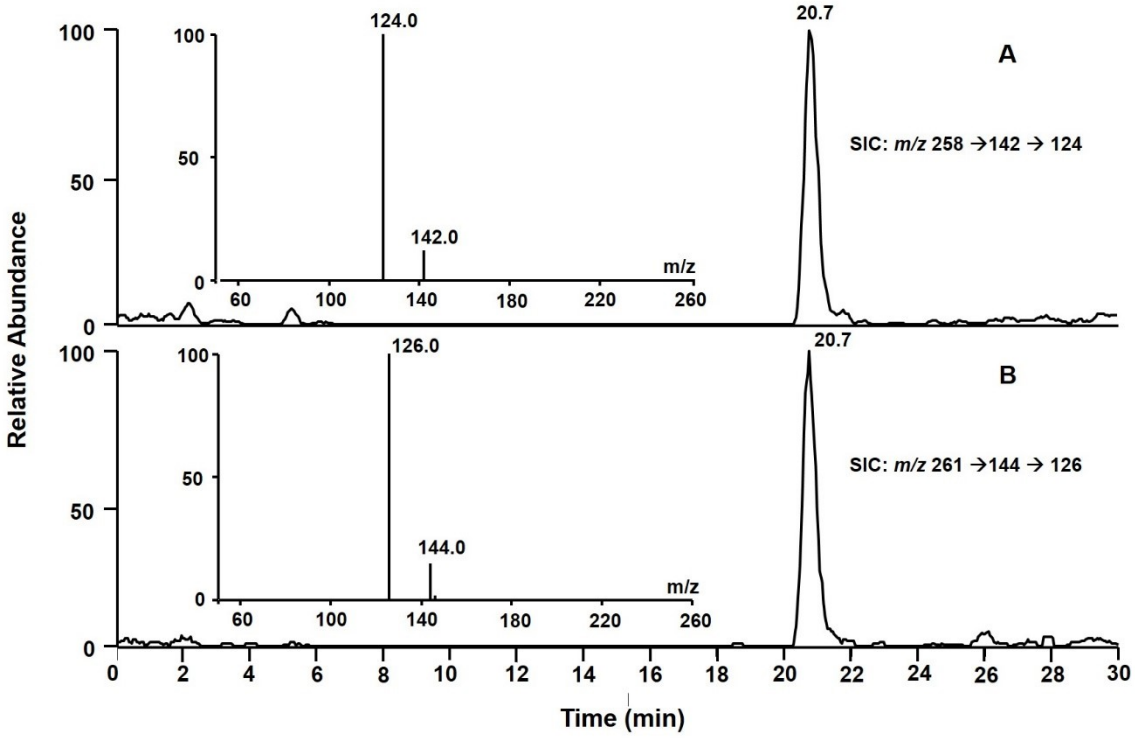

Figure 4.1. Selected-ion chromatograms (SICs) for monitoring the *m/z* 258→142→124 [A, for unlabeled 5-hmdC], and *m/z* 261→144→126 [B, for ^{15}N-labeled 5-hmdC] transitions in the Cu(II)/H_2O_2/ascorbate-treated calf thymus DNA after enzymatic digestion. MS^3 spectrum for unlabeled and labeled 5-hmdC are displayed in each inset. This representative SIC corresponds to calf thymus DNA treated under condition C listed in Table 4.1.

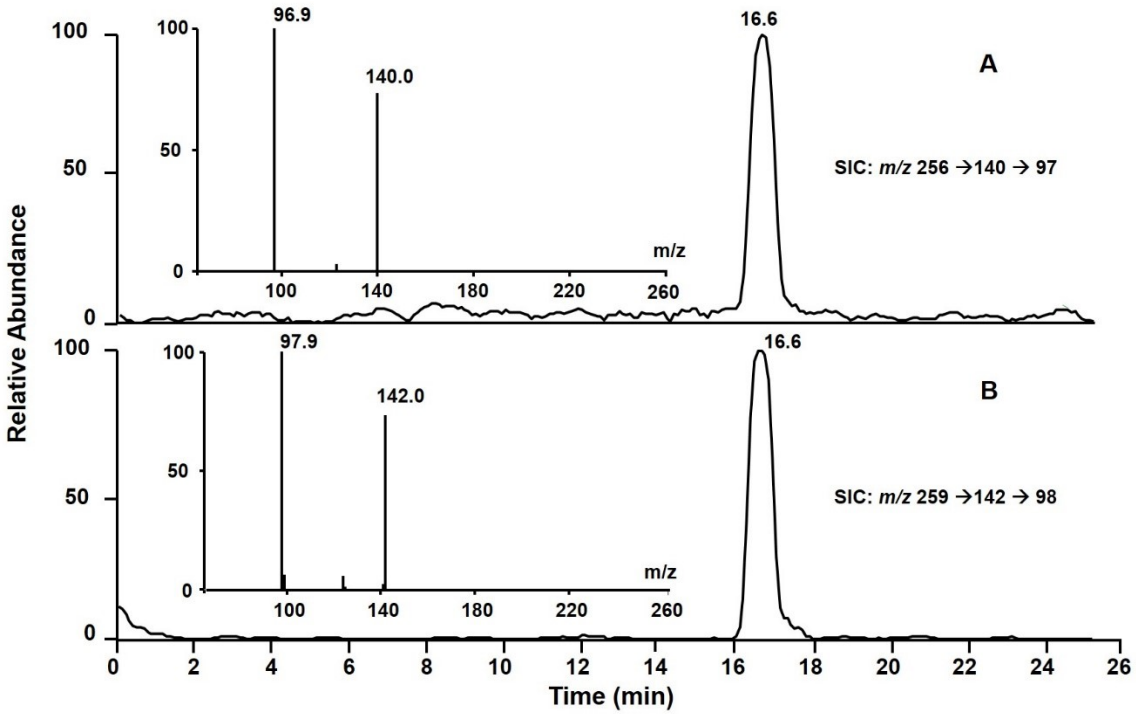

Figure 4.2. Selected-ion chromatograms (SICs) for monitoring the *m/z* 256→140→97 [A, for unlabeled 5-fodC], and *m/z* 259→142→98 [B, for ^{15}N-labeled 5-fodC] transitions in the Cu(II)/H_2O_2/ascorbate-treated calf thymus DNA after enzymatic digestion. MS^3 spectrum for unlabeled and labeled for 5-fodC are displayed in each inset. This representative SIC corresponds to calf thymus DNA treated under condition D listed in Table 4.1.

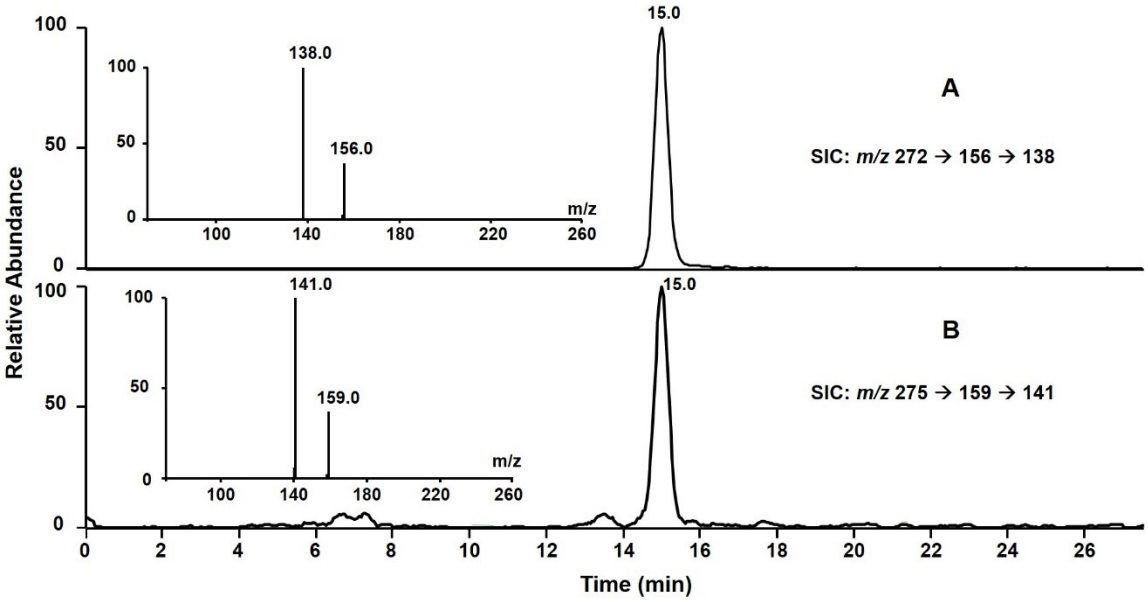

Figure 4.3. Selected-ion chromatograms (SICs) for monitoring the *m/z* 272→156→138 [A, for unlabeled 5-cadC], and *m/z* 275→159→141 [B, for ^{15}N-labeled 5-cadC] transitions in the Cu(II)/H_2O_2/ascorbate-treated calf thymus DNA after enzymatic digestion. MS^3 spectrum for unlabeled and labeled for 5-cadC are displayed in each inset. This representative SIC corresponds to calf thymus DNA treated under condition C listed in Table 4.1.

$[M + H]^+$ ions of 5-hmdC and [^{15}N]-labeled 5-hmdC, respectively. Further cleavage of the ion of *m/z* 142 leads to the elimination of a H_2O molecule to produce a major fragment ion at *m/z* 124. [^{15}N]-labeled 5-hmdC exhibited the same fragment ions for the neutral losses of the 116-Da moiety and additional loss of H_2O to give product ions of *m/z* 144 and *m/z* 126, respectively.

The subsequent oxidation of 5-mdC to 5-hmdC continues on to yield 5-fodC. Due to the relatively lower level of formation of 5-fodC and 5-cadC, we chose to employ off-line HPLC enrichment to provide a cleaner sample matrix for introduction into the LC-MS. For precise validation and quantification of the 5-fodC, we monitored the *m/z* 256→140→97 and *m/z* 259→142→98 transitions for 5-fodC and [^{15}N]-labeled 5-fodC, respectively. Figure 4.2 displays representative the SICs for both the analyte and stable isotope-labeled 5-fodC, in which both components co-elute at 16.6 min. Ions of *m/z* 140 and *m/z* 142 result from the loss of a 2-deoxyribose moiety from the $[M + H]^+$ ions of the unlabeled and [^{15}N]-labeled 5-fodC, respectively. Furthermore, collisional activation of the ions of *m/z* 140 and *m/z* 142 leads to the loss of a HNCO moiety yielding fragment ions of *m/z* 97 and *m/z* 98 for 5-fodC and [^{15}N]-labeled 5-fodC, respectively.

The final oxidative lesion generated from the subsequent oxidation of 5-mdC is 5-cadC. For this lesion, we also employed the off-line HPLC enrichment in order to improve the detection sensitivity of 5-cadC, in addition to removing buffer salts and isobaric interferences from the sample matrix. To achieve reliable quantification of 5-cadC, we monitored the *m/z* 272→156→138 and *m/z* 275→159→141 transitions for unlabeled and [^{15}N]-labeled 5-cadC, respectively. SICs for 5-cadC showed the co-elution

of analyte and [^{15}N]-labeled standard at 15.0 min (Figure 4.3). Collisional activation of the ions of *m/z* 272 and *m/z* 275 again leads to the loss of a 2-deoxyribose for both the analyte and internal standard. Subjecting the daughter ions to further collisional activation resulted in the loss of a H_2O molecule.

4.4.2 Levels of 5-HmdC, 5-FodC, and 5-CadC Formed in Calf Thymus DNA Exposed with Fenton-type Reagents

For each Fenton-type condition we quantified 5-hmdC, 5-fodC, and 5-cadC using the LC-MS^3 method detailed above. A summary of the results are given in Table C1 in Appendix C and plotted in Figures 4.4 and 4.5, where the levels of the modified nucleosides are reported as the number of lesions per 10^6 nucleosides. Our results showed that all three oxidatively-induced 5-mdC lesions were generated by Fenton-type reagents in calf thymus DNA in a dose-dependent manner. Levels for 5-hmdC exceeded 650 lesions per million nucleosides at the highest concentrations of Fenton-type reagents used (condition D, Figure 4.4). Furthermore, we compared 5-hmdC levels to previously published data for the induction of 5-hmdU and found that 5-hmdC levels were 3.5-fold lower than 5-hmdU levels under the same experimental conditions.[24] This result suggests that the oxidation of 5-mdC to 5-hmdC is more facile than the corresponding oxidation of thymine when considering that 5-mdC only constitutes ~1.5% of the calf thymus DNA content.[28, 29]

5-FodC and 5-cadC were induced at comparable efficiencies, with 5-fodC formed at higher levels at lower Fenton concentrations (conditions: Control, A and B; Figure 4.5), but induction levels were reversed in conditions C and D. Compared to 5-hmdC, 5-

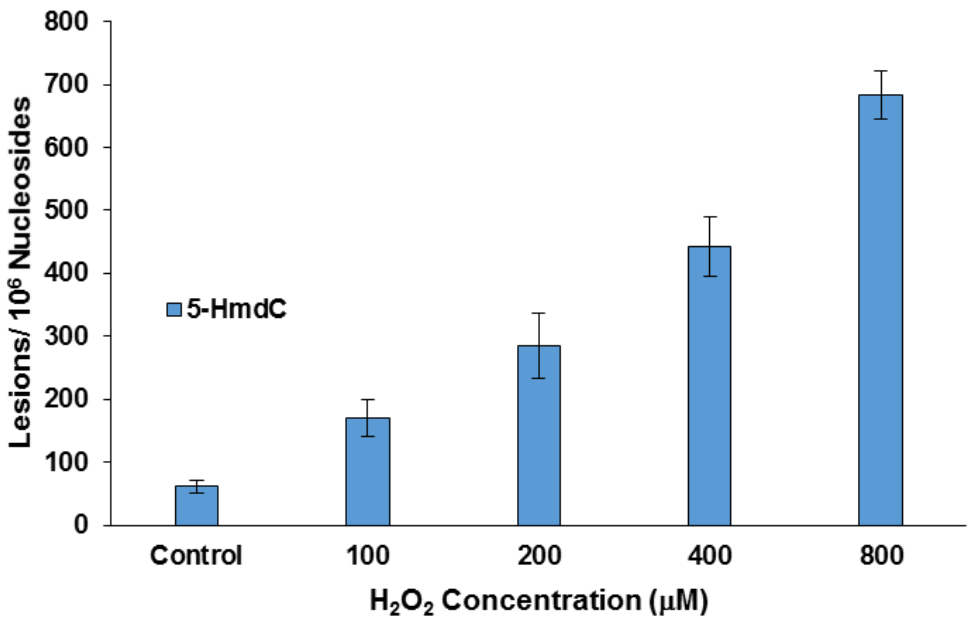

Figure 4.4. Cu(II)/H_2O_2/ascorbate-induced formation of 5-hmdC in calf thymus DNA. The values represent the mean $\pm$ SD of results from three independent experiments. The corresponding concentrations of Cu(II) and ascorbate are shown in Table 4.1.

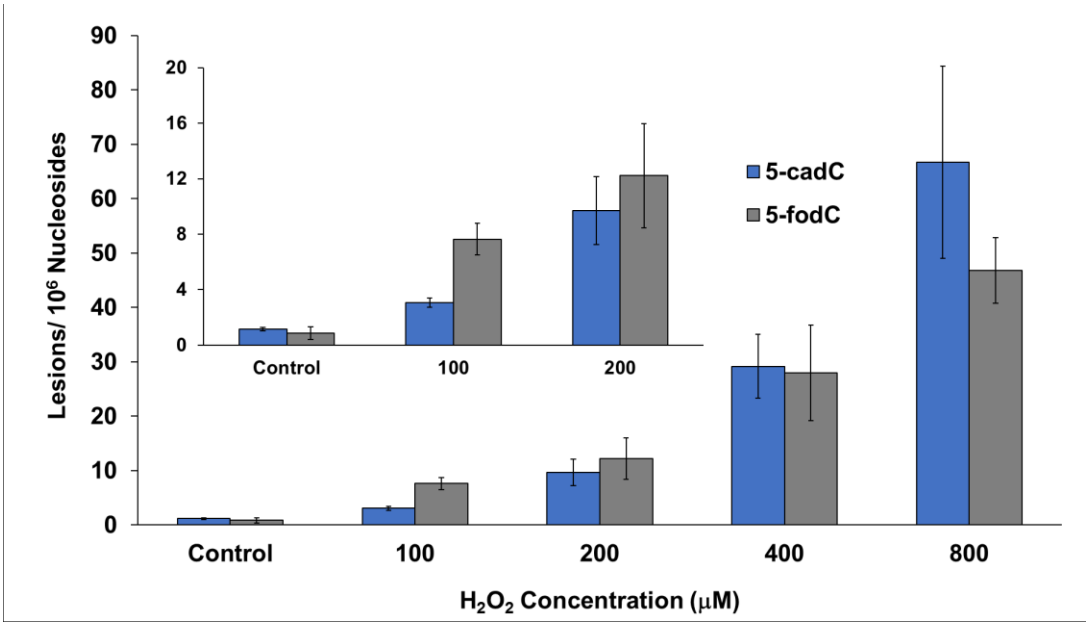

Figure 4.5. Cu(II)/H_2O_2/ascorbate-induced formation of 5-fodC and 5-cadC lesions in calf thymus DNA. The values represent the mean $\pm$ SD of results from three independent experiments. The corresponding concentrations of Cu(II) and ascorbate are shown in Table 4.1.

fodC and 5-cadC were induced at approximately 12-fold lower than in condition D. It is of note that, both 5-fodC and 5-cadC demonstrated profound increases with the concentrations of the Fenton-type reagents. In this vein, 5-fodC and 5-cadC were induced in condition D at levels that are 53- and 59-fold higher relative to the Control condition, respectively. On the other hand, the levels of 5-hmdC were only increased by 11-fold, when comparing the same conditions. This is mainly attributed to the presence of much higher levels of 5-hmdC than 5-fodC and 5-cadC in the initial calf thymus DNA, as observed previously for DNA isolated from mammalian cells and tissues.[30] Furthermore, 5-fodC and 5-cadC levels exceeded previously published levels for *S*-diastereomers for cdA and cdG under the similar experimental conditions.[19] This could suggest that while 5-fodC and 5-cadC are induced by Fenton-type reagents at relatively low levels compared to other single-nucleobase lesions, such as 8-oxodG or 5-fodU, it is still pertinent to understand the effects that oxidative damage can have on the genomic stability and gene regulation.

4.5 Discussion

By employing a robust and sensitive LC-MS/MS/MS couple with stable isotope dilution method, we were able to identify and quantify the levels of all three oxidatively damaged products of 5-mdC in isolated DNA treated with Cu(II)/H_2O_2/ascorbate. Our results indicated that 5-hmdC, 5-fodC and 5-cadC were generated in a dose-dependent manner. 5-HmdC was present at levels that are approximately 1 order of magnitude higher than 5-fodC and 5-cadC. In this context, Schiesser et al.[31] observed that the

conversion of 5-fodC and 5-cadC was minimal when a solution of 5-mdC was exposed to air at high temperature (60-80 °C).[31] Our observation of similar levels of formation of 5-fodC and 5-cadC suggests that, in the presence of Fenton-type reagents, the conversion of 5-fodC to 5-cadC or direct conversion of 5-hmdC to 5-cadC is a relatively efficient process.

When calf thymus DNA was treated with Control, A, and B conditions of Fenton-type reagents, we noticed higher 5-FodU accumulation compared to 5-cadC. However, in conditions C and D, levels of 5-cadC begins to supersede those of 5-FodC, suggesting that while the generation of 5-fodC is still occurring, the conversion of 5-fodC to 5-cadC occurs more efficiently under increased concentrations Fenton-type reagents. This is reminiscent of results from Berthod and Cadet[32], who reported that prolonged irradiation of thymidine in the presence of 2-methyl-1,4-naphthoquinone under aerobic conditions leads to depreciating 5-formyl-2-deoxyuridine (5-fodU) levels and elevated levels of 5-carboxy-2'-deoxyuridine (5-cadU). In this vein, Berthod and Cadet[32] also noted that that 5-cadU could also be induced by the ·OH-mediated decomposition of thymidine.

To our knowledge, this is the first time it has been demonstrated that 5-cadC can be induced *in vitro* by ROS via a Fenton-type reagent. Furthermore, the levels of 5-cadC and 5-fodC generated in calf thymus DNA are higher than the previously published results for *S*-diastereomers of cdA and cdG incubated with Cu(II)/H_2O_2/ascorbate.[19] When treated with 100 μM H_2O_2 (condition A), 5-fodC was generated at frequencies that are similar as *R*-cdA and *R*-cdG; however, at higher doses, 5-fodC and 5-cadC were produced at higher levels than those of *S*-cdA and *S*-cdG. Although these two lesions are

not induced at similar levels as other single-nucleobase lesions like 8-oxodG, small amounts could be detrimental to the integrity of the genome as in the case of *S*-cdA accumulation.[21, 33] There are numerous documented circumstances in which elevated copper concentrations accompany disease and cancer.[34] In this vein, we previously demonstrated that a deficiency in the orthologue of human Wilson's disease gene (i.e., *Atp7b*), which results in abnormal accumulation of copper ions in hepatocytes, resulted in elevated levels of oxidatively induced cdA and cdG lesions in liver tissues of LEC rats.[20] Therefore, since 5-fodC and 5-cadC are induced at either similar or higher rates *in vitro* compared to the *S*-diastereomers of cPus, future investigations seeking to unveil whether the 5-mdC oxidative derivatives are affected by copper accumulation *in vivo* should be pursued.

It was recently demonstrated that overexpression of catalytic domain human Tet-1 fostered marked increases in 5-hmdC, 5-FodC, and 5-cadC.[10, 30] In addition, TDG is known to exhibit high cleavage efficiencies for 5-fodC and 5-cadC and in its absence 5-cadC has been shown to accumulate in mouse embryonic stem cells.[10] TDG's inadequate recognition and subsequent cleavage of 5-hmdC is sometimes used to explain elevated levels of endogenous 5-hmdC.[35-37] There is also a recent hypothesis that 5-hmdC may serve as an epigenetic mark, thus induction of 5-hmdC could alter the epigenetic regulation of gene expression.[38] Aberrant epigenetic remodeling of gene expression has been associated with cancer development. Under normal cellular environments 5-hmdC is likely regulated; however, under conditions of oxidative stress, 5-hmdC generation and/or conversion to 5-fodC and 5-cadC may potentially perturb its further epigenetic

regulation. Regardless of Tet-mediated oxidation or ROS-induced oxidation, 5-hmdC, 5-fodC and 5-cadC find themselves in the middle of a 5-mdC active demethylation pathway where unwarranted oxidation of 5-mdC or 5-hmdC could lead to the restoration of unmethylated cytosine thus having adverse impacts on gene regulation.

In summary, we employed a sensitive LC-MS/MS/MS coupled with stable-isotope dilution methods for the quantification of 5-mdC oxidative products in isolated DNA treated with Fenton-type reagents. Our results illustrated a dose-dependent formation of all three methyl group oxidation products of 5-mdC in the presence of Cu(II)/H_2O_2/ascorbate. Additionally, to our knowledge, this is the first *in vitro* experiment demonstrating the ROS-induced formation of 5-cadC. We anticipate that under these conditions, which mimic endogenous Fenton-type conditions, the formation of 5-hmdC, 5-fodC, and 5-cadC are important not only for assessing oxidative DNA damage, but also for their potential roles in the TDG-mediated active demethylation pathway. It is suspected that ROS-induced damage may contribute to the onset of aging, cancer and other human diseases. Furthermore, ROS-induce active demethylation has the potential to generate aberrant epigenetic regulation, ultimately jeopardizing genomic integrity.

Appendix Materials

HPLC traces for the enrichment of 5-cadC and 5-fodC. Calibration curves for 5-hmdC, 5-fodC, and 5cadC.Table of numerical results for 5-hmdC, 5-fodC- and 5-cadC lesion levels. This material is in Appendix C

References

(1) Cedar, H., and Bergman, Y. (2009) Linking DNA methylation and histone modification: patterns and paradigms. *Nat. Rev. Genet.*, ***10***, 295-304.

(2) Suzuki, M. M., and Bird, A. (2008) DNA methylation landscapes: provocative insights from epigenomics. *Nat. Rev. Genet.*, ***9***, 465-476.

(3) Sasaki, H., and Matsui, Y. (2008) Epigenetic events in mammalian germ-cell development: reprogramming and beyond. *Nat. Rev. Genet.*, ***9***, 129-140.

(4) Bird, A. (2002) DNA methylation patterns and epigenetic memory. *Genes Dev.*, ***16***, 6-21.

(5) Jaenisch, R., and Bird, A. (2003) Epigenetic regulation of gene expression: how the genome integrates intrinsic and environmental signals. *Nat. Genet.*, ***33 Suppl***, 245-254.

(6) Ooi, S. K., and Bestor, T. H. (2008) The colorful history of active DNA demethylation. *Cell*, ***133***, 1145-1148.

(7) Ito, S., Shen, L., Dai, Q., Wu, S. C., Collins, L. B., Swenberg, J. A., He, C., and Zhang, Y. (2011) Tet proteins can convert 5-methylcytosine to 5-formylcytosine and 5-carboxylcytosine. *Science*, ***333***, 1300-1303.

(8) Pfaffeneder, T., Hackner, B., Truss, M., Munzel, M., Muller, M., Deiml, C. A., Hagemeier, C., and Carell, T. (2011) The discovery of 5-formylcytosine in embryonic stem cell DNA. *Angew Chem. Int. Ed. Engl.*, ***50***, 7008-7012.

(9) Wu, S. C., and Zhang, Y. (2010) Active DNA demethylation: many roads lead to Rome. *Nat. Rev. Mol. Cell Biol.*, ***11***, 607-620.

(10) He, Y. F., Li, B. Z., Li, Z., Liu, P., Wang, Y., Tang, Q., Ding, J., Jia, Y., Chen, Z., Li, L., Sun, Y., Li, X., Dai, Q., Song, C. X., Zhang, K., He, C., and Xu, G. L. (2011) Tet-mediated formation of 5-carboxylcytosine and its excision by TDG in mammalian DNA. *Science*, ***333***, 1303-1307.

(11) Cao, H., and Wang, Y. (2007) Quantification of oxidative single-base and intrastrand cross-link lesions in unmethylated and CpG-methylated DNA induced by Fenton-type reagents. *Nucleic Acids Res.*, ***35***, 4833-4844.

(12) Campian, J. L., Qian, M., Gao, X., and Eaton, J. W. (2004) Oxygen tolerance and coupling of mitochondrial electron transport. *J. Biol. Chem.*, ***279***, 46580-46587.

(13) Boveris, A., and Chance, B. (1973) The mitochondrial generation of hydrogen peroxide. General properties and effect of hyperbaric oxygen. *Biochem. J.*, ***134***, 707-716.

(14) Handy, D. E., and Loscalzo, J. (2012) Redox regulation of mitochondrial function. *Antioxid. Redox Signal.*, ***16***, 1323-1367.

(15) Finkel, T., and Holbrook, N. J. (2000) Oxidants, oxidative stress and the biology of ageing. *Nature*, ***408***, 239-247.

(16) Cadet, J., Delatour, T., Douki, T., Gasparutto, D., Pouget, J. P., Ravanat, J. L., and Sauvaigo, S. (1999) Hydroxyl radicals and DNA base damage. *Mutat. Res.*, ***424***, 9-21.

(17) Ala, A., Walker, A. P., Ashkan, K., Dooley, J. S., and Schilsky, M. L. (2007) Wilson's disease. *Lancet.*, ***369***, 397-408.

(18) Toyokuni, S. (1996) Iron-induced carcinogenesis: the role of redox regulation. *Free Radic. Biol. Med.*, ***20***, 553-566.

(19) Guerrero, C. R., Wang, J., and Wang, Y. (2013) Induction of 8,5'-Cyclo-2'-deoxyadenosine and 8,5'-cyclo-2'-deoxyguanosine in isolated DNA by Fenton-type reagents. *Chem. Res. Toxicol.*, ***26***, 1361-1366.

(20) Wang, J., Yuan, B., Guerrero, C., Bahde, R., Gupta, S., and Wang, Y. (2011) Quantification of oxidative DNA lesions in tissues of Long-Evans Cinnamon rats by capillary high-performance liquid chromatography−tandem mass spectrometry coupled with stable isotope-dilution method. *Anal. Chem.*, ***83***, 2201-2209.

(21) You, C., Dai, X., Yuan, B., Wang, J., Wang, J., Brooks, P. J., Niedernhofer, L. J., and Wang, Y. (2012) A quantitative assay for assessing the effects of DNA lesions on transcription. *Nat. Chem. Biol.*, ***8***, 817-822.

(22) Pednekar, V., Weerasooriya, S., Jasti, V. P., and Basu, A. K. (2014) Mutagenicity and Genotoxicity of (5′ S)-8,5′ -Cyclo-2′ -deoxyadenosine in Escherichia coli and Replication of (5′ S)-8,5′ -Cyclopurine-2′ -deoxynucleosides in Vitro by DNA Polymerase IV, Exo-Free Klenow Fragment, and Dpo4. *Chem. Res. Toxicol.*, ***27***, 200-210.

(23) Marietta, C., and Brooks, P. J. (2007) Transcriptional bypass of bulky DNA lesions causes new mutant RNA transcripts in human cells. *EMBO Rep.*, ***8***, 388-393.

(24) Hong, H., Cao, H., Wang, Y., and Wang, Y. (2006) Identification and quantification of a guanine-thymine intrastrand cross-link lesion induced by Cu(II)/H_2O_2/ascorbate. *Chem. Res. Toxicol.*, ***19***, 614-621.

(25) Cao, H., and Wang, Y. (2006) Collisionally activated dissociation of protonated 2'-deoxycytidine, 2'-deoxyuridine, and their oxidatively damaged derivatives. *J. Am. Soc. Mass Spectrom.*, ***17***, 1335-1341.

(26) Dai, Q., and He, C. (2011) Syntheses of 5-formyl- and 5-carboxyl-dC containing DNA oligos as potential oxidation products of 5-hydroxymethylcytosine in DNA. *Org. Lett.*, ***13***, 3446-3449.

(27) Lim, K. S., Jenner, A., and Halliwell, B. (2006) Quantitative gas chromatography mass spectrometric analysis of 2'-deoxyinosine in tissue DNA. *Nat. Protoc.*, ***1***, 1995-2002.

(28) Crain, P. F., and McCloskey, J. A. (1983) Analysis of modified bases in DNA by stable isotope dilution gas chromatography-mass spectrometry: 5-methylcytosine. *Anal. Biochem.*, ***132***, 124-131.

(29) Hu, J., Zhang, W., Ma, H., Cai, Y., Sheng, G., and Fu, J. (2010) Simultaneous determination of 8-hydroxy-2'-deoxyguanosine and 5-methyl-2'-deoxycytidine in DNA sample by high performance liquid chromatography/positive electrospray

ionization tandem mass spectrometry. *J. Chromatogr. B Analyt. Technol. Biomed. Life Sci.*, ***878***, 2765-2769.

(30) Liu, S., Wang, J., Su, Y., Guerrero, C., Zeng, Y., Mitra, D., Brooks, P. J., Fisher, D. E., Song, H., and Wang, Y. (2013) Quantitative assessment of Tet-induced oxidation products of 5-methylcytosine in cellular and tissue DNA. *Nucleic Acids. Res.*, ***41***, 6421-6429.

(31) Schiesser, S., Pfaffeneder, T., Sadeghian, K., Hackner, B., Steigenberger, B., Schroder, A. S., Steinbacher, J., Kashiwazaki, G., Hofner, G., Wanner, K. T., Ochsenfeld, C., and Carell, T. (2013) Deamination, oxidation, and C-C bond cleavage reactivity of 5-hydroxymethylcytosine, 5-formylcytosine, and 5-carboxycytosine. *J. Am. Chem. Soc.*, ***135***, 14593-14599.

(32) Berthod, T., Cadet, J., and Molko, D. (1997) 5-Carboxy-2′ -deoxyuridine, a new photooxidation product of thymidine. *J. Photochem. Photobiol. A*, ***104***, 97-104.

(33) You, C., Dai, X., Yuan, B., and Wang, Y. (2012) Effects of 6-thioguanine and S6-methylthioguanine on transcription in vitro and in human cells. *J. Biol. Chem.*, ***287***, 40915-40923.

(34) Lech, T., and Sadlik, J. K. (2007) Copper concentration in body tissues and fluids in normal subjects of southern Poland. *Biol. Trace Elem. Res.*, ***118***, 10-15.

(35) Maiti, A., and Drohat, A. C. (2011) Thymine DNA glycosylase can rapidly excise 5-formylcytosine and 5-carboxylcytosine: potential implications for active demethylation of CpG sites. *J. Biol. Chem.*, ***286***, 35334-35338.

(36) Bennett, M. T., Rodgers, M. T., Hebert, A. S., Ruslander, L. E., Eisele, L., and Drohat, A. C. (2006) Specificity of human thymine DNA glycosylase depends on N-glycosidic bond stability. *J. Am. Chem. Soc.*, ***128***, 12510-12519.

(37) Zhang, L., Lu, X., Lu, J., Liang, H., Dai, Q., Xu, G. L., Luo, C., Jiang, H., and He, C. (2012) Thymine DNA glycosylase specifically recognizes 5-carboxylcytosine-modified DNA. *Nat. Chem. Biol.*, ***8***, 328-330.

(38) Yildirim, O., Li, R., Hung, J. H., Chen, P. B., Dong, X., Ee, L. S., Weng, Z., Rando, O. J., and Fazzio, T. G. (2011) Mbd3/NURD complex regulates expression of 5-hydroxymethylcytosine marked genes in embryonic stem cells. *Cell*, ***147***, 1498-1510.

Chapter 5

Concluding Remarks and Future Direction

In this dissertation, we utilized LC-MS/MS/MS coupled with the standard isotope-dilution method to accurately identify and quantify ROS-induced DNA lesions *in vitro* and *in vivo*. This method offers unambiguous identification and reliable quantification due to the nearly identical chemical properties and ionization efficiencies, as well as, analogous fragmentation patterns of the analytes and their corresponding isotope-labeled standards when subjected to LC-MS/MS analysis. In addition, we relied on off-line HPLC enrichment for the removal of salts and canonical nucleosides for improved efficiency in HPLC separation and electrospray ionization. The reliability and robustness in the detection and quantification of numerous ROS-induced DNA lesions *in vitro* (Chapter 1 and 4) and *in vivo* (Chapter 3) have opened possibilities of their use as biomarkers for assessing oxidative stress in cancer and other human diseases.

In Chapter 2, I assessed the induction of the (5'*R*) and (5'*S*) diastereomers of cdA and cdG in calf thymus DNA treated with Fenton-type reagents. Fenton-type reagents are a major source of endogenous ROS; thus, this transition metal-mediated reaction is highly restricted in cells through the regulation of transition metal ions, as well as, the regulation of cellular ROS via enzymatic and non-enzymatic means. Despite all these pathways in controlling cellular ROS generation, Fenton-type reactions can occur and the resulting damage can have catastrophic effects for the genome. Assessing what types of

DNA damage can occur and to what extent will increase our understanding of the role of ROS-induced DNA damage in aging, cancer and other human diseases. Here we demonstrated that elevated concentrations of Fenton-type reagents can induce increased generation of cdA and cdG. These results suggest that organisms with deficiencies in transition metal ion regulation could have adverse side-effects from accumulation of ROS-induced DNA damage.

In Chapter 3, building upon the study about the formation of Fenton reagent-induced cdA and cdG lesions *in vitro*, we examined the formation of these lesions in tissues of Long-Evans Cinnamon rats with a deletion of the *Atp7b* gene. Rats bearing a deletion of the *Atp7b* gene mimic the attributes of Wilson's disease. As stated in Chapter 3, patients with Wilson's disease have the inability to properly excrete copper into the bile. This often results in liver, neurological, and renal abnormities followed by copper toxicosis. In addition, it is not uncommon to find that the DNA damage arising from copper accumulation worsens with age. Here, we quantified cdA and cdG along with single-nucleobase lesions (5-fodU and 5-hmdU) in liver and brain tissues of LEC rats. Overall, we found age- and genotype-dependent accumulation of cdA, cdG, 5-fodU, and 5-hmdU. It would be interesting, to assess the levels of cdA and cdG in livers of patients with Wilson's disease. However, cdA and cdG lesions can be used as biomarkers for assessing oxidative stress in a multitude of models for disease and cancer.

Finally in Chapter 4, we changed directions to focus on the potential for 5-mdC being demethylated via ROS-induced oxidation of 5-mdC to 5-hmdC, 5-fodC, and 5-

cadC. Recently, it was demonstrated that 5-mdC could undergo active demethylation via a Tet/TDG-mediated base excision repair pathway, to dynamically regulate cytosine methylation during development. However, 5-hmdC and 5-fodC are known to be induced by ROS. Thus, the removal of the resulting 5-fodC and 5-cadC may be recognized by TDG and lead to inadvertent demethylation of 5-mdC. In addition, it remains unexplored whether 5-cadC could be induced by ROS. For this reason, we treated calf thymus DNA with increasing concentrations of Fenton-type reagents to investigate to what extent ROS could generate 5-hmdC, 5-fodC, and 5-cadC. Our results showed that all three oxidative lesions of 5-mdC could be generated, where 5-hmdC was produced at a level that is one order of magnitude higher than 5-fodC and 5-cadC. Because of their efficient cleavage by TDG, 5-fodC and 5-cadC, despite being induced a relatively low rates compared to 5-hmdC, could have the potential to impose detrimental consequences by resulting in aberrant cytosine demethylation. Future studies are needed for the investigation about the formation of these lesions by exogenous ROS from γ-rays. Furthermore, it is of interest to assess to what levels these lesions exist in tissues of LEC rats due to aberrant accumulation of copper ions in hepatocytes.

Appendix A

Supporting Information for Chapter 2

"Induction of 8,5'-Cyclopurine-2'-deoxynucleosides in Isolated DNA by Fenton-type Reagents"

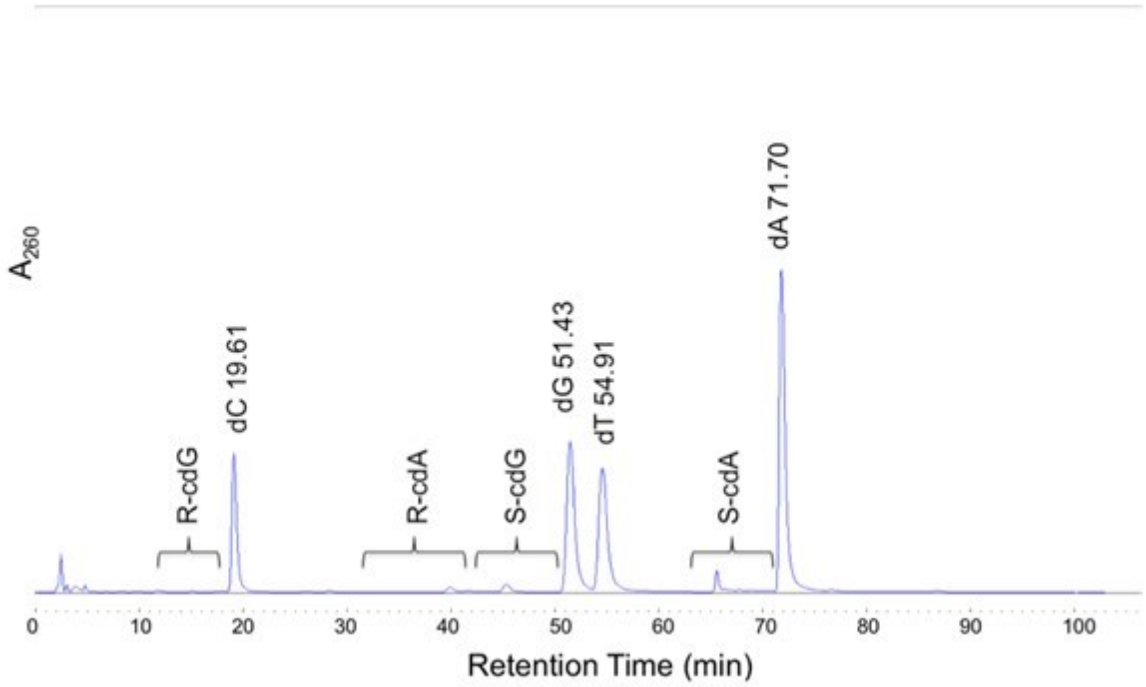

Figure A1. HPLC trace of the separation of enzymatic digestion mixture of Cu(II)/H_2O_2/ascorbate-treated calf thymus DNA.

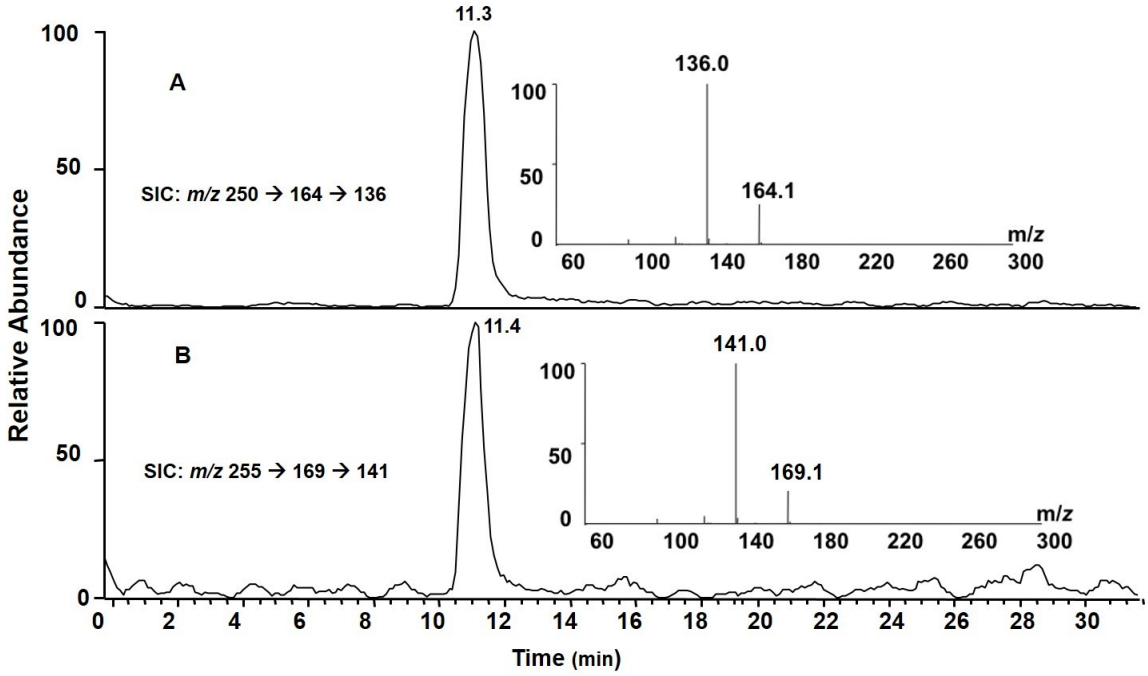

Figure A2. Selected-ion chromatograms (SICs) for monitoring the *m/z* 250→164→136 [A, for unlabeled *R*-cdA] and *m/z* 255→169→141 [B, for labeled *R*-cdA] transitions in the nucleoside mixture of Cu(II)/H_2O_2/ascorbate-treated calf thymus DNA. Shown in the insets are the positive-ion MS^3 spectra for the unlabeled and labeled *R*-cdA. The sample was treated under conditions B listed in Table 1.

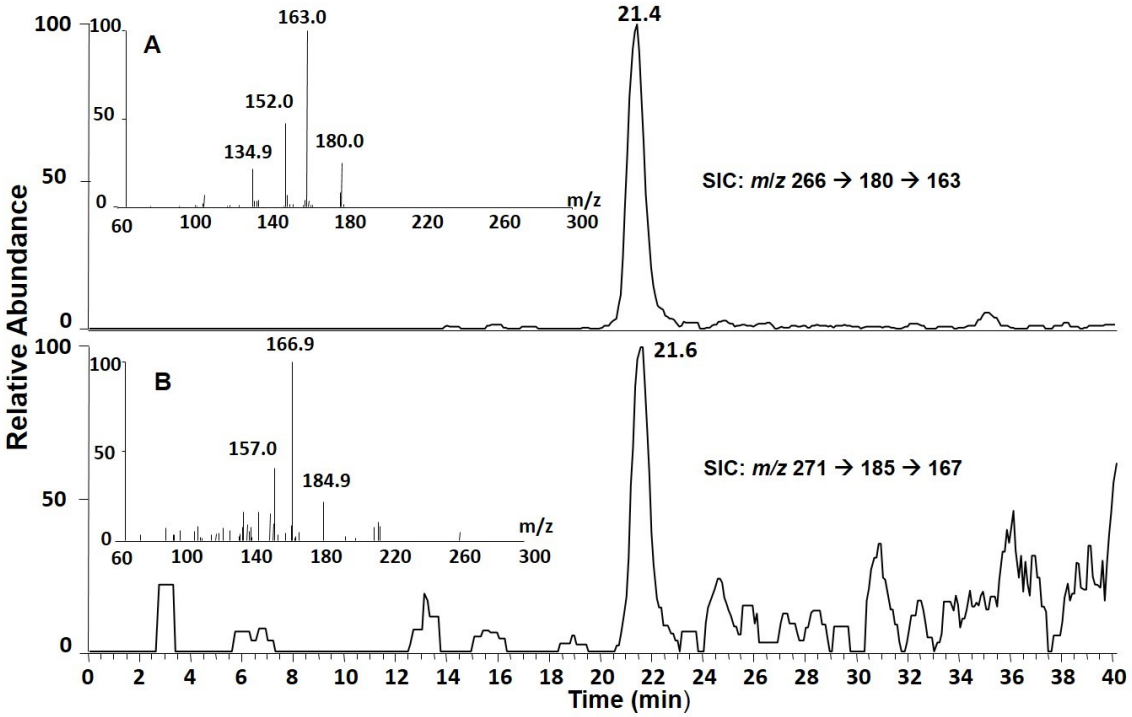

Figure A3. SICs for monitoring the *m/z* 266→180→163 [A, for unlabeled *S*-cdG] and *m/z* 271→185→167 [B, for labeled *S*-cdG] transitions in the nucleoside mixture of Cu(II)/H_2O_2/ascorbate-treated calf thymus DNA. Shown in the insets are the positive-ion MS^3 spectra for the unlabeled and labeled *S*-cdG. The sample was treated under conditions B listed in Table 1.

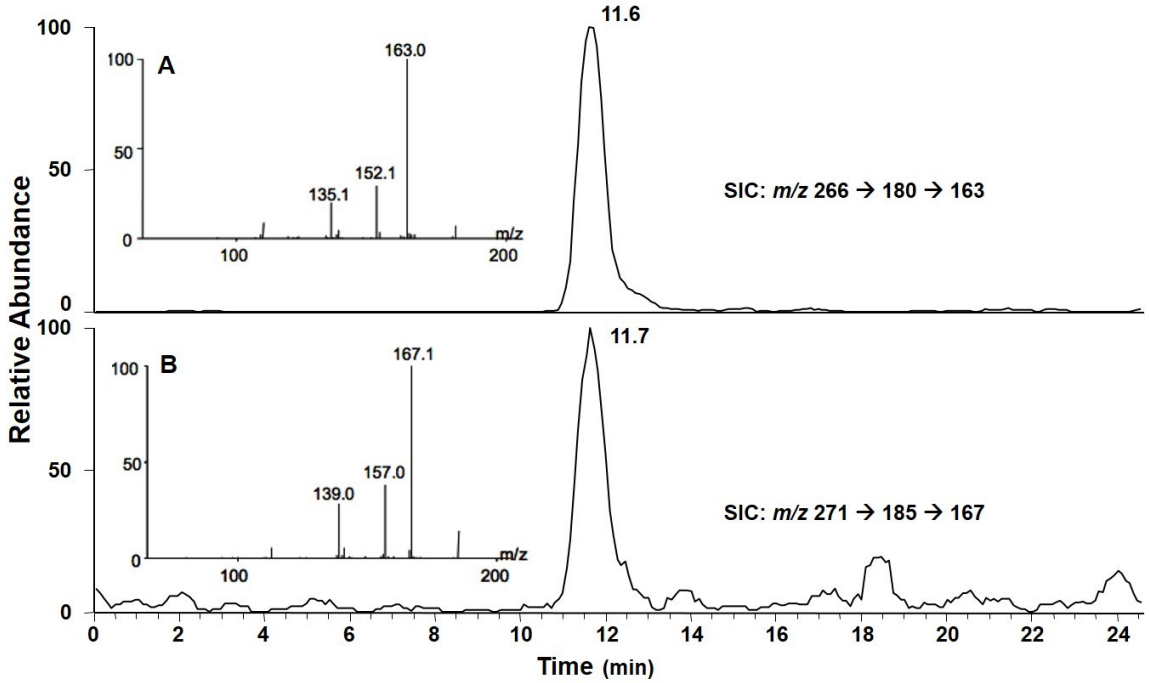

Figure A4. SICs for the monitoring the *m/z* 266→180→163 [A, for unlabeled *R*-cdG] and *m/z* 271→185→167 [B, for labeled *R*-cdG] transitions in the nucleoside mixture of Cu/H_2O_2/ascorbate-treated calf thymus DNA. Shown in the insets are the positive-ion MS^3 spectra for the unlabeled and labeled *R*-cdG.

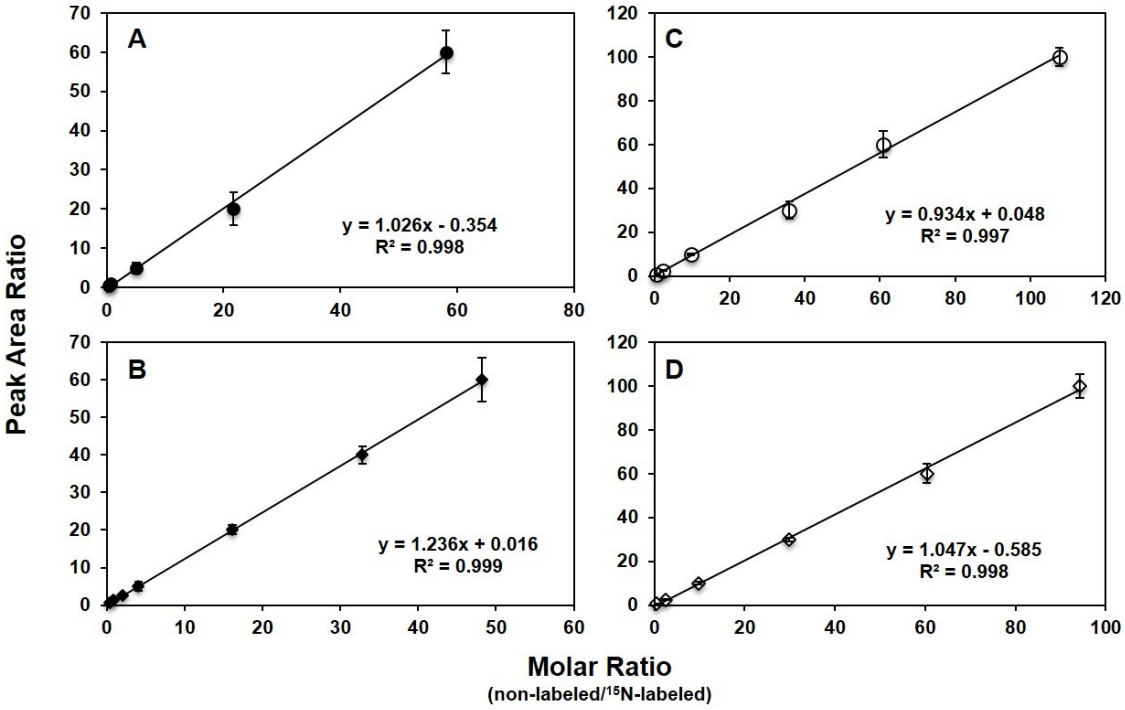

Figure A5. Calibration curves for the quantifications of A; *S*-cdG (filled circle), B; *S*-cdA (filled diamond), C; *R*-cdG (open circle), and D; *R*-cdA (open diamond) based on LC-MS/MS/MS analysis. The results reflect the means and standard deviations of data acquired from three independent LC-MS/MS/MS measurements. The amounts of labeled *S*-cdG, *S*-cdA, *R*-cdG, and *R*-cdA used for calibration were 20 fmol, 20 fmol, 40 fmol and 20 fmol, respectively.

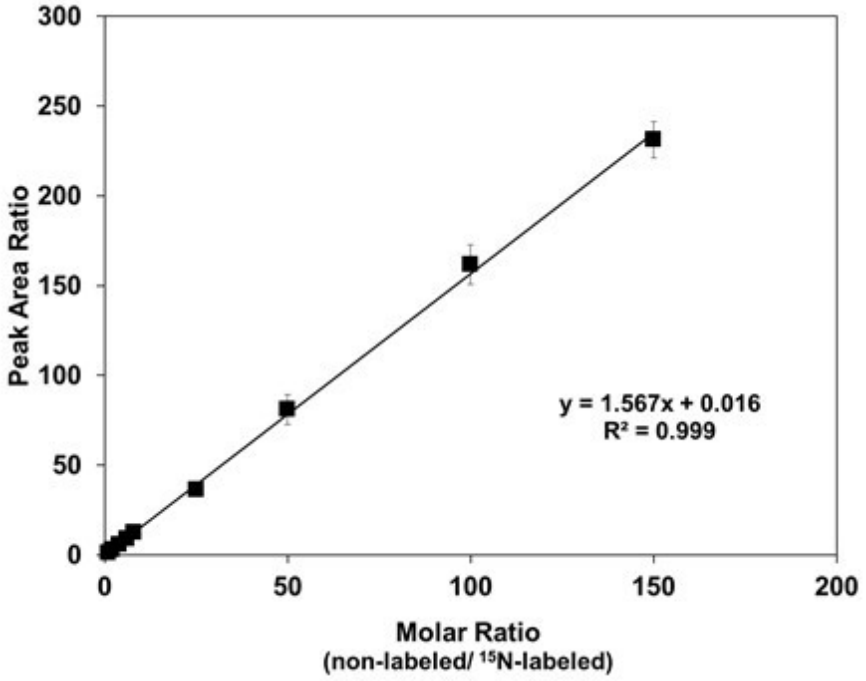

Figure A6. Calibration curve for the quantification of 8-oxodG based on LC-MS/MS analysis. The amount of labeled 8-oxodG used for the calibration was 500 fmol. The results reflect the means and standard deviations of data acquired from three independent LC-MS/MS measurements.

Table A1. A summary of the levels (in lesions per 10^6 nucleosides) of cdA and cdG in calf thymus DNA treated with Cu(II)/H_2O_2/ascorbate. The data represent the means and standard deviations of results from three independent oxidation and LC-MS/MS/MS quantification experiments.

	S-cdA	*S*-cdG	*R*-cdA	*R*-cdG
Control	0.07 ± 0.02	0.60 ± 0.07	0.93 ± 0.02	0.28 ± 0.03
A	0.17 ± 0.03	1.3 ± 0.3	2.8 ± 0.2	4.5 ± 0.4
B	0.45 ± 0.12	2.0 ± 0.3	17 ± 2	24 ± 2
C	2.5 ± 0.2	7.7 ± 1.5	60 ± 7	67 ± 9
D	18 ± 1	25 ± 4	128 ± 27	145 ± 15
E	44 ± 1	71 ± 11	440 ± 60	480 ± 67

Table A2. A summary of the levels (in lesions per 10^6 nucleosides) of cdA and cdG in calf thymus DNA treated with Fe(II)/H_2O_2/ascorbate. The data represent the means and standard deviations of results from three independent oxidation and LC-MS/MS/MS quantification experiments.

	S-cdA	*S*-cdG	*R*-cdA	*R*-cdG
Control	0.49 ± 0.07	1.1 ± 0.3	1.92 ± 0.04	1.9 ± 0.7
A	0.04 ± 0.12	1.5 ± 0. 8	2.0 ± 0.1	2.7 ± 0.3
B	0.76 ± 0.05	2.5 ± 1.1	2.1 ± 0.2	4.7 ± 0.6
C	1.3 ± 0.1	10 ± 5	15 ± 2	39 ± 13
D	42 ± 8	210 ± 60	460 ± 15	730 ± 180
E	125 ± 10	400 ± 10	860 ± 180	1190 ± 280

Table A3. A summary of the levels (in lesions per 10^6 nucleosides) of 8-oxodG in calf thymus DNA treated with Fe(II)/H_2O_2/ascorbate. The data represents the means and standard deviations of results from the measurements of three different oxidation and quantification experiments.

	8-oxodG
Control	600 ±170
A	1500 ± 110
B	3100± 720
C	12000 ± 2400
D	42000 ± 3000
E	57000 ± 7000

Appendix B

Supporting Information for Chapter 3

"Quantification of Oxidative DNA Lesions in Tissues of Long-Evans Cinnamon Rats by Capillary High-performance Liquid Chromatography-Tandem Mass Spectrometry Coupled with Stable Isotope-dilution Method"

Table B1. Optimized instrumental conditions of LC-ESI-MS^3 used for the analysis of the lesions measured in this study and detection limits of these lesions. The LOD and LOQ represent the means and standard deviations of the results from three measurements of the unlabeled lesion standards in three separate days. A constant activation time of 30 ms was employed for this experiment.

Lesion	Polarity	SIM (MS^3) of lesions		Optimized LTQ parameters		LOD, fmol	LOQ, fmol
		Unlabeled	Isotope-labeled	Normalized collision energy	Activation Q		
5-FodU	−	255 → 212	258 → 214	30	0.25	18 ± 2	59 ± 6
		212 → 140	214 → 142	33	0.25		
5-HmdU	−	257 → 214	260 → 216	30	0.25	24 ± 5	80 ± 15
		214 → 124	216 → 126	33	0.25		
R-cdG	+	266 → 180	271 → 185	40	0.27	1.5 ± 0.2	4.9 ± 0.7
		180 → 163	185 → 167	40	0.33		
S-cdG	+	266 → 180	271 → 185	40	0.27	0.50 ± 0.05	1.7 ± 0.2
		180 → 163	185 → 167	40	0.33		
R-cdA	+	250 → 164	255 → 169	40	0.27	0.61 ± 0.09	2.0 ± 0.3
		164 → 136	169 → 141	40	0.33		
S-cdA	+	250 → 164	255 → 169	40	0.27	0.27 ± 0.03	0.90 ± 0.10
		164 → 136	169 → 141	40	0.33		

Table B2. A summary of the levels (in lesions per 10^6 nucleosides) of oxidatively induced lesions in brain and liver tissues of rats. The data represent the means and standard deviations of results from the measurements of tissues of three different rats in each group (one technical replicate measurement was performed for each tissue DNA).

Lesion	Liver						Brain					
	LEA	LEC+/-			LEC-/-		LEA	LEC+/-			LEC-/-	
	3m	3m	12m	1m	3m	6m	3m	3m	12m	1m	3m	6m
5-FodU	7.0±1.6	7.8±1.6	13.5±2.2	12.7±1.8	31.4±8.6	12.1±2.9	18.8±1.5	20.3±2.7	36.3±7.0	19.7±4.1	26.3±0.6	33.5±5.2
5-HmdU	2.6±0.3	3.2±0.5	8.0±1.4	5.1±0.5	8.6±2.3	5.0±1.2	20.5±2.2	17.5±4.7	20.4±4.9	12.0±1.8	20.8±4.4	28.3±5.3
R-cdG	0.13±0.04	0.20±0.06	0.54±0.05	0.16±0.02	0.26±0.08	0.24±0.05	0.14±0.02	0.13±0.03	0.29±0.09	0.14±0.01	0.16±0.04	0.52±0.05
S-cdG	0.19±0.03	0.26±0.06	1.08±0.18	0.20±0.02	0.33±0.09	0.37±0.07	0.16±0.04	0.16±0.02	0.18±0.03	0.14±0.02	0.22±0.03	0.43±0.06
R-cdA	0.10±0.02	0.18±0.05	0.48±0.03	0.21±0.02	0.27±0.09	0.24±0.08	0.15±0.04	0.20±0.01	0.28±0.01	0.13±0.03	0.20±0.03	0.56±0.13
S-cdA	0.11±0.02	0.14±0.03	0.56±0.17	0.12±0.03	0.28±0.03	0.15±0.03	0.088±0.030	0.092±0.026	0.100±0.006	0.081±0.028	0.15±0.04	0.26±0.01

Table B3. List of primers used for Real-time qRT-PCR experiments.

NTHL1-RT-S	**5'-AGATGGCACACTTGGCTATGG-3'**
NTHL1-RT-AS	**5'-TCTTGGTCCACTTCAGTCTGTTG-3'**
NEIL1-RT-S	**5'-CGTAGACATCCGCCGCTTTG-3'**
NEIL1-RT-AS	**5'-TGCCGATTCCATTGAAGAACCTC-3'**
XPA-RT-S	**5'-TGAATGGCTCCCTGGCATAAC-3'**
XPA-RT-AS	**5'-GTGGCTCTGGTGTCTGTATGG-3'**
ERCC1-RT-S	**5'-GGAGGTGCTGGCGTTGTATC-3'**
ERCC1-RT-AS	**5'-CCTGGTGGGTGGTCCTGAG-3'**
CSA-RT-S	**5'-CAAGAACACAGCACAAGCACAG-3'**
CSA-RT-AS	**5'-CAGCAGTCAGAGCAGTCAGAG-3'**
CSB-RT-S	**5'-TGCCAGCAACAGAGACATCAAC-3'**
CSB-RT-AS	**5'-CCTCCGCTCCTCCGAGAATG-3'**
GAPDH-RT-S	**5'-AAGTTCAACGGCACAGTCAAGG-3'**
GAPDH-RT-AS	**5'-GACATACTCAGCACCAGCATCAC-3'**

Table B4. Histological grading of liver damage in rats

Animals	N	Histology grade (mean)
LEA rats	3	2 ± 0
3 mo old		
LEC+/- rats		
3 mo old	3	2 ± 0
12 mo old	3	2 ± 0
LEC-/- rats		
1 mo old	3	6 ± 2*
3 mo old	3	11 ± 1*
6 mo old	3	10 ± 2*

Histological grading of tissues was according to Malhi H, Bhargava KK, Afriyie MO, Volenberg I, Schilsky ML, Palestro CJ, Gupta S. ^{99m}Tc-mebrofenin scintigraphy for evaluating liver disease in a rat model of Wilson's disease. *J. Nucl. Med.* 2002;43:246-52.

Asterisks = $p<0.05$ versus LEA rats

Table B5. ESI-LC-MS^3 Data for constructing the calibration curve for the quantification of 5-FodU.

Concentrations of unlabeled lesion standard, nM	Molar ratios (Unlabeled/Isotope-labeled)	Integrated peak areas	
		Unlabeled	Isotope-labeled
29	0.04	$(2.7 \pm 0.3) \times 10^2$	$(5.7 \pm 0.5) \times 10^3$
86	0.12	$(6.4 \pm 2.4) \times 10^2$	$(4.2 \pm 1.7) \times 10^3$
2.9×10^2	0.40	$(2.1 \pm 1.0) \times 10^3$	$(4.3 \pm 2.1) \times 10^3$
8.6×10^2	1.2	$(7.1 \pm 2.5) \times 10^3$	$(4.3 \pm 1.5) \times 10^3$
2.0×10^3	2.8	$(1.6 \pm 0.6) \times 10^4$	$(4.0 \pm 1.6) \times 10^3$
4.3×10^3	6.0	$(4.0 \pm 1.4) \times 10^4$	$(5.1 \pm 1.5) \times 10^3$

The concentration of the isotope-labeled 5-FodU was 0.72 μM in all solutions used and the injection volume was 5.0 μL for each measurement.

Table B6. ESI-LC-MS^3 Data for constructing the calibration curve for the quantification of 5-HmdU.

Concentrations of unlabeled lesion standard, nM	Molar ratios (Unlabeled/Isotope-labeled)	Integrated peak areas	
		Unlabeled	Isotope-labeled
20	0.040	$(2.0 \pm 0.07) \times 10^2$	$(3.5 \pm 0.5) \times 10^3$
60	0.12	$(4.9 \pm 1.4) \times 10^2$	$(2.3 \pm 0.5) \times 10^3$
2.0×10^2	0.4	$(1.4 \pm 0.2) \times 10^3$	$(2.5 \pm 0.6) \times 10^3$
6.0×10^2	1.2	$(4.1 \pm 0.3) \times 10^3$	$(2.4 \pm 0.4) \times 10^3$
1.4×10^3	2.8	$(9.4 \pm 3.1) \times 10^3$	$(2.1 \pm 0.7) \times 10^3$
3.0×10^3	6.0	$(2.0 \pm 0.4) \times 10^4$	$(1.9 \pm 0.3) \times 10^3$

The concentration of the isotope-labeled 5-HmdU was 0.50 μM in all solutions used and the injection volume was 5.0 μL for each measurement.

Table B7. ESI-LC-MS^3 Data for constructing the calibration curve for the quantification of *R*-cdG.

Concentrations of unlabeled lesion standard, nM	Molar ratios (Unlabeled/Isotope-labeled)	Integrated peak areas	
		Unlabeled	Isotope-labeled
0.40	0.010	35 ± 20	$(3.9 \pm 1.6) \times 10^3$
0.80	0.020	48 ± 16	$(2.3 \pm 1.1) \times 10^3$
3.0	0.075	$(2.4 \pm 0.9) \times 10^2$	$(3.2 \pm 1.4) \times 10^3$
10	0.25	$(5.8 \pm 0.7) \times 10^2$	$(2.5 \pm 0.4) \times 10^3$
30	0.75	$(1.8 \pm 0.1) \times 10^3$	$(2.7 \pm 0.2) \times 10^3$
1.0×10^2	2.5	$(6.0 \pm 0.5) \times 10^3$	$(2.7 \pm 0.2) \times 10^3$

The concentration of the isotope-labeled *R*-cdG was 40 nM in all solutions used and the injection volume was 5.0 μL for each measurement.

Table B8. ESI-LC-MS^3 Data for constructing the calibration curve for the quantification of *S*-cdG.

Concentrations of unlabeled lesion standard, nM	Molar ratios (Unlabeled/Isotope-labeled)	Integrated peak areas	
		Unlabeled	Isotope-labeled
0.60	0.030	$(1.4 \pm 0.1) \times 10^2$	$(7.8 \pm 0.09) \times 10^3$
1.2	0.060	$(1.7 \pm 0.9) \times 10^2$	$(4.0 \pm 2.1) \times 10^3$
4.5	0.23	$(8.1 \pm 2.6) \times 10^2$	$(5.1 \pm 1.7) \times 10^3$
15	0.75	$(2.7 \pm 0.6) \times 10^3$	$(4.8 \pm 1.4) \times 10^3$
45	2.3	$(8.4 \pm 1.3) \times 10^3$	$(4.9 \pm 1.2) \times 10^3$
1.8×10^2	9.0	$(3.5 \pm 0.4) \times 10^4$	$(5.0 \pm 0.6) \times 10^3$

The concentration of the isotope-labeled *S*-cdG was 20 nM in all solutions used and the injection volume was 5.0 μL for each measurement.

Table B9. ESI-LC-MS^3 Data for constructing the calibration curve for the quantification of *R*-cdA.

Concentrations of unlabeled lesion standard, nM	Molar ratios (Unlabeled/Isotope-labeled)	Integrated peak areas	
		Unlabeled	Isotope-labeled
0.18	0.018	89 ± 24	$(4.7 \pm 1.3) \times 10^3$
0.36	0.036	80 ± 30	$(2.8 \pm 1.1) \times 10^3$
1.4	0.14	$(4.8 \pm 1.4) \times 10^2$	$(4.2 \pm 1.4) \times 10^3$
4.5	0.45	$(2.0 \pm 0.9) \times 10^3$	$(4.2 \pm 1.5) \times 10^3$
14	1.4	$(5.7 \pm 1.7) \times 10^3$	$(4.3 \pm 1.1) \times 10^3$
45	4.5	$(1.8 \pm 0.2) \times 10^4$	$(4.2 \pm 0.6) \times 10^3$

The concentration of the isotope-labeled *R*-cdA was 10 nM in all solutions used and the injection volume was 5.0 μL for each measurement.

Table B10. ESI-LC-MS^3 Data for constructing the calibration curve for the quantification of *S*-cdA.

Concentrations of unlabeled lesion standard, nM	Molar ratios (Unlabeled/Isotope-labeled)	Integrated peak areas	
		Unlabeled	Isotope-labeled
0.24	0.040	$(2.6 \pm 1.3) \times 10^2$	$(7.2 \pm 3.2) \times 10^3$
0.48	0.080	$(3.3 \pm 1.8) \times 10^2$	$(4.4 \pm 2.5) \times 10^3$
1.8	0.30	$(1.3 \pm 0.3) \times 10^3$	$(5.0 \pm 1.4) \times 10^3$
6.0	1.0	$(4.2 \pm 1.2) \times 10^3$	$(5.4 \pm 1.5) \times 10^3$
18	3.0	$(1.3 \pm 0.2) \times 10^4$	$(5.3 \pm 0.8) \times 10^3$
60	10	$(5.0 \pm 1.5) \times 10^4$	$(6.1 \pm 1.8) \times 10^3$

The concentration of the isotope-labeled *S*-cdA was 6.0 nM in all solutions used and the injection volume was 5.0 μL for each measurement.

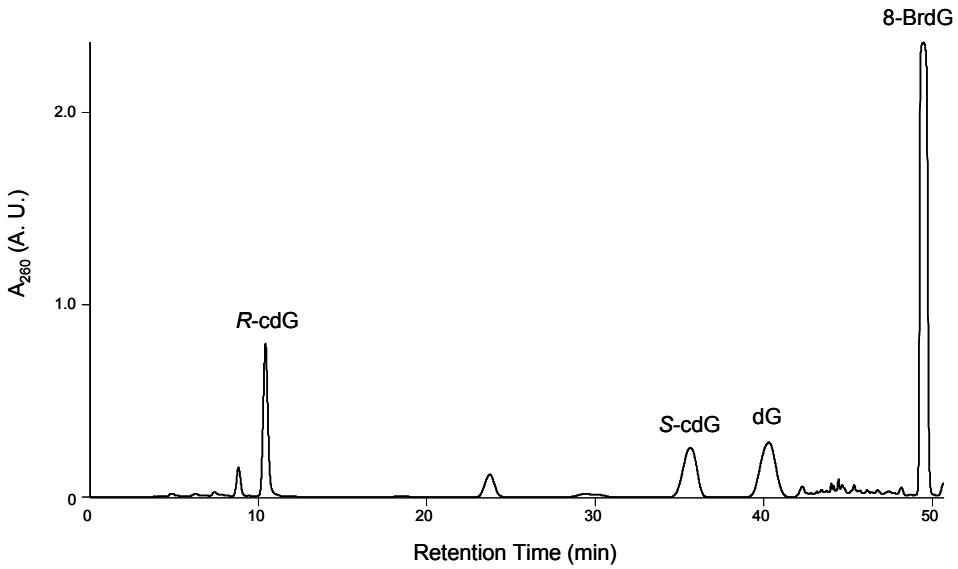

Figure B1. A representative HPLC trace for the separation of the synthetic mixture of the uniformly ^{15}N-labeled *R*- and *S*-cdG. Column, Alltima HP C18 column (5 μm in particle size, Grace Davison, Deerfield, IL), 4.6×250 mm; mobile phases, water (A) and methanol (B); flow rate, 1 mL/min; elution gradient, 0-25 min, 0% B; 25-26 min, 0-2% B; 26-36 min, 2% B; 26-40 min, 2-20% B; 40-60 min, 20% B.

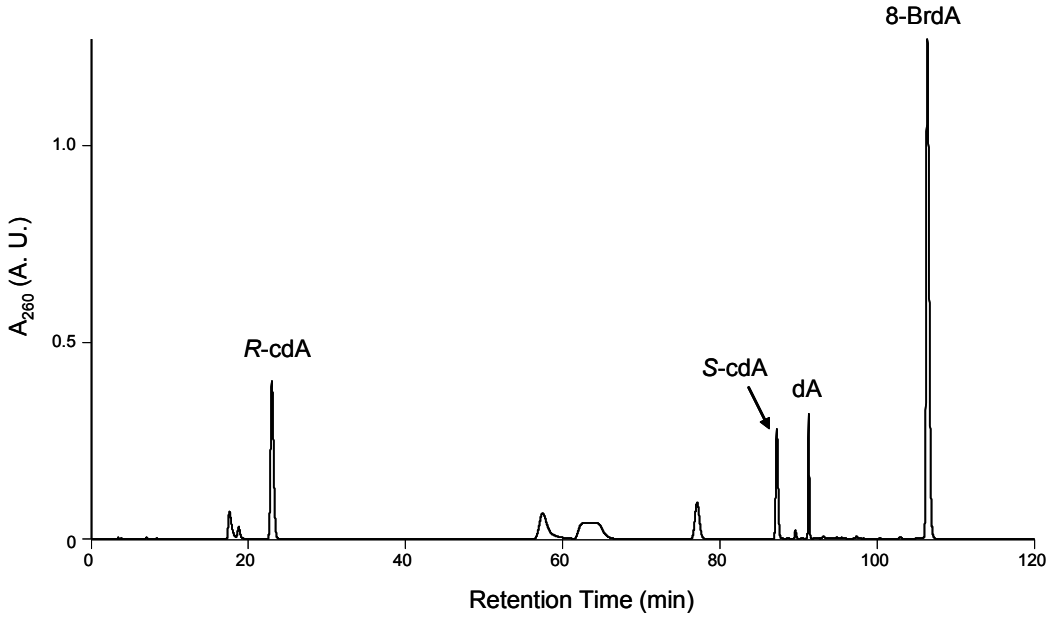

Figure B2. A representative HPLC trace for the separation of the synthetic mixture of the uniformly ^{15}N-labeled *R*- and *S*-cdA. Column, Alltima HP C18 column (5 μm in particle size, Grace Davison, Deerfield, IL), 4.6×250 mm; mobile phases, water (A) and methanol (B); flow rate, 1 mL/min; elution gradient, 0-40 min, 0% B; 40-41 min, 0-2% B; 41-60 min, 2% B; 60-61 min, 2-5% B; 61-80 min, 5% B; 80-90 min, 5-20% B; 90-120 min, 20% B.

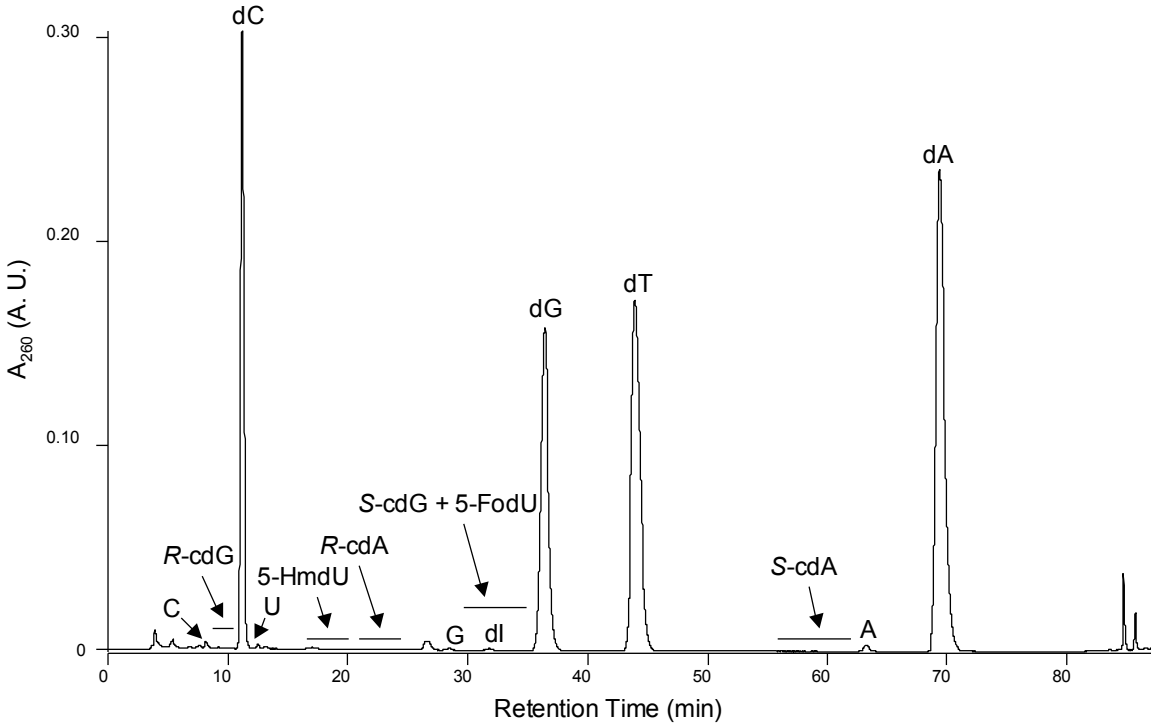

Figure B3. A representative HPLC trace for the separation of the enzymatic digestion mixture of genomic DNA from rat tissue.

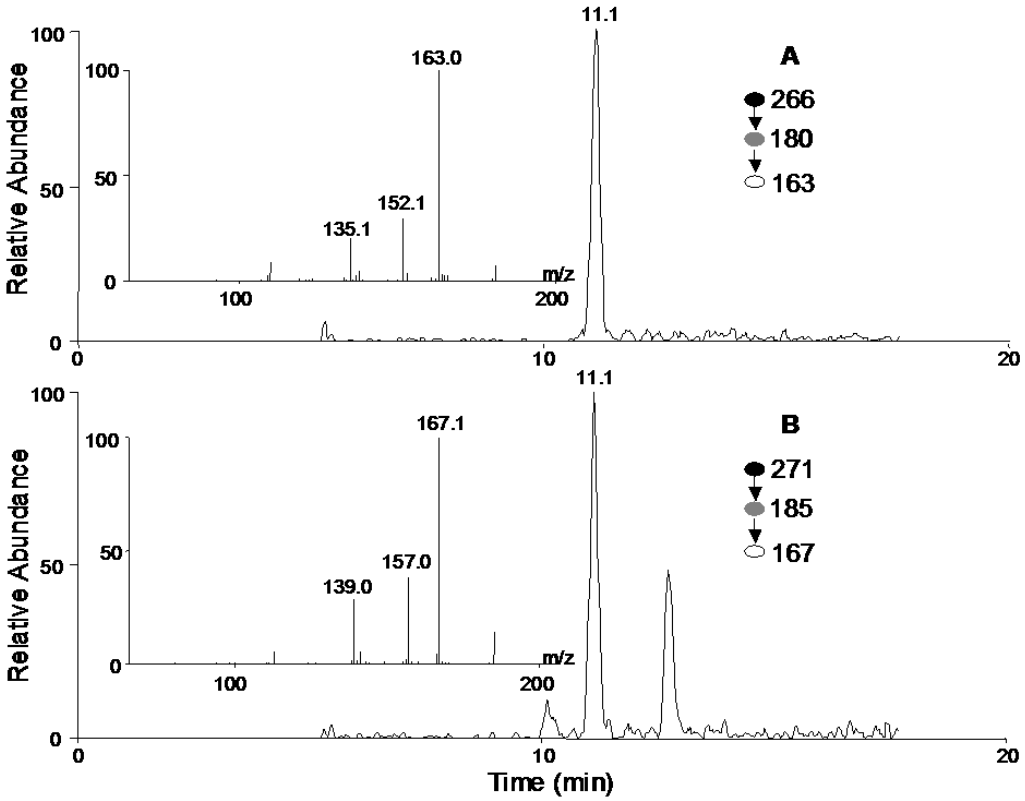

Figure B4. Selected-ion chromatograms (SICs) for monitoring the *m/z* 266→180→163 [A, for unlabeled *R*-cdG] and *m/z* 271→185→167 [B, for labeled *R*-cdG] transitions of the digestion mixture of genomic DNA from the liver tissue of a 3-month old LEC-/- rat. Shown in the insets are the positive-ion MS^3 spectra for the unlabeled and labeled *R*-cdG.

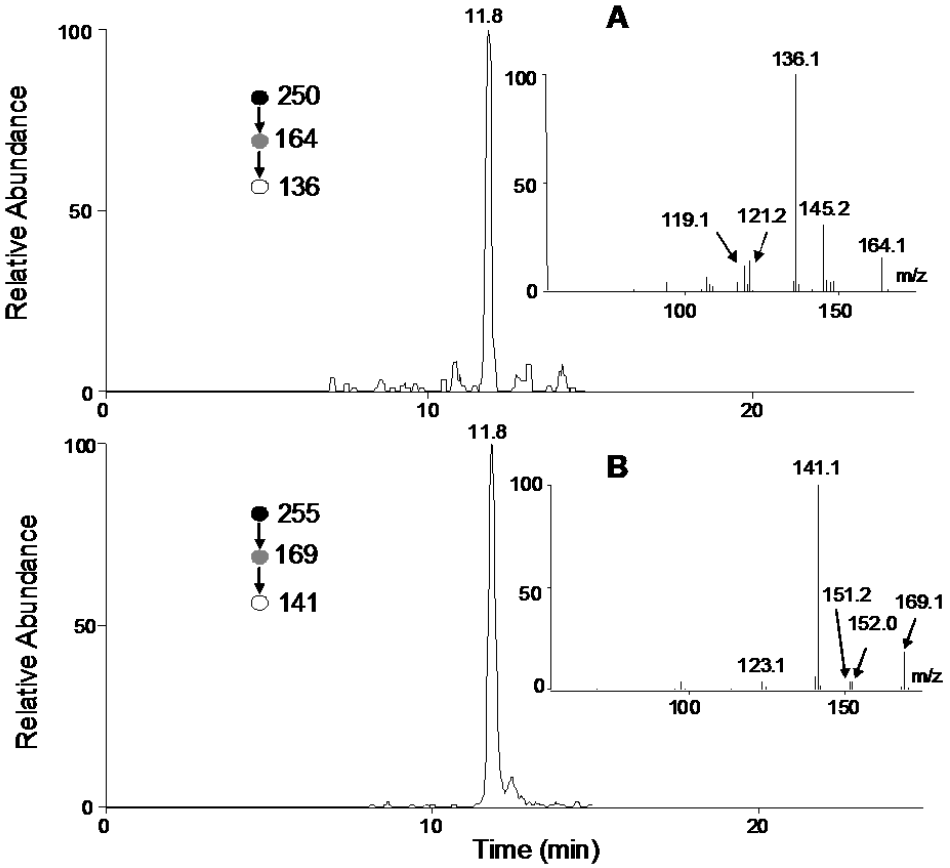

Figure B5. SICs for monitoring the *m/z* 250→164→136 [A, for unlabeled *S*-cdA] and *m/z* 255→169→141 [B, for labeled *S*-cdA] transitions of the digestion mixture of brain nuclear DNA of a 3-month old LEC-/- rat.

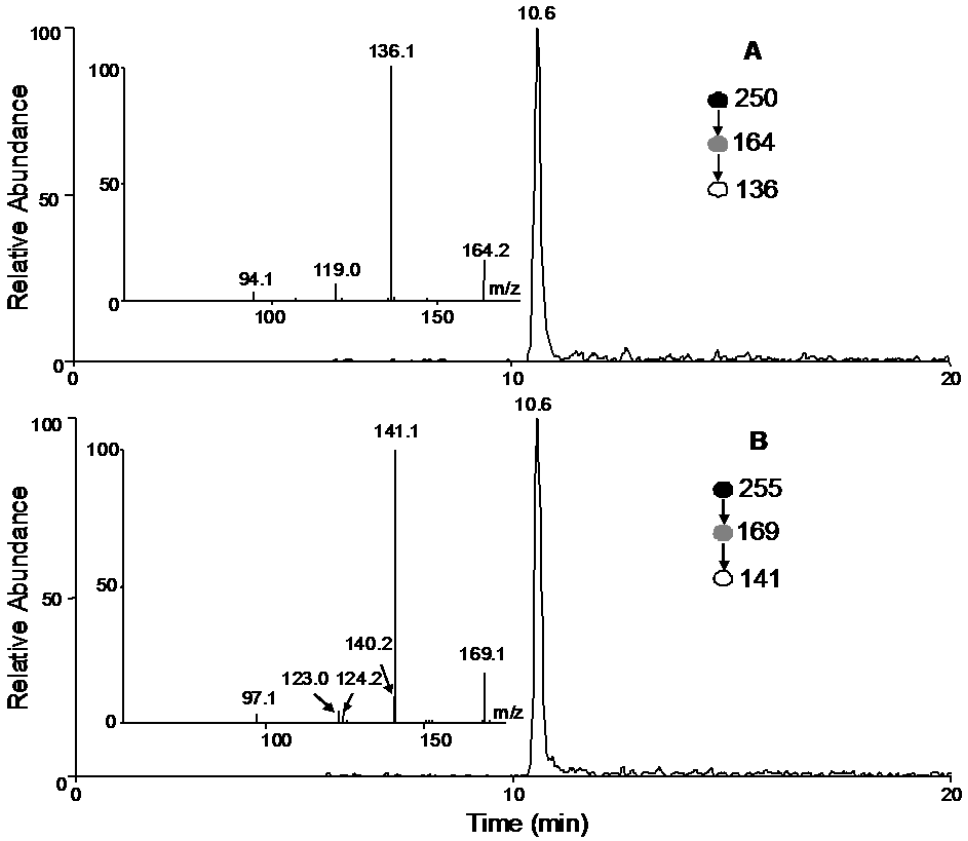

Figure B6. Selected-ion chromatograms (SICs) for monitoring the *m/z* 250→164→136 [A, for unlabeled *R*-cdA] and *m/z* 255→169→141 [B, for labeled *R*-cdA] transitions of the digestion mixture of genomic DNA from the liver tissue of a 6-month old LEC-/- rat. Shown in the insets are the positive-ion MS^3 spectra for the unlabeled and labeled *R*-cdA.

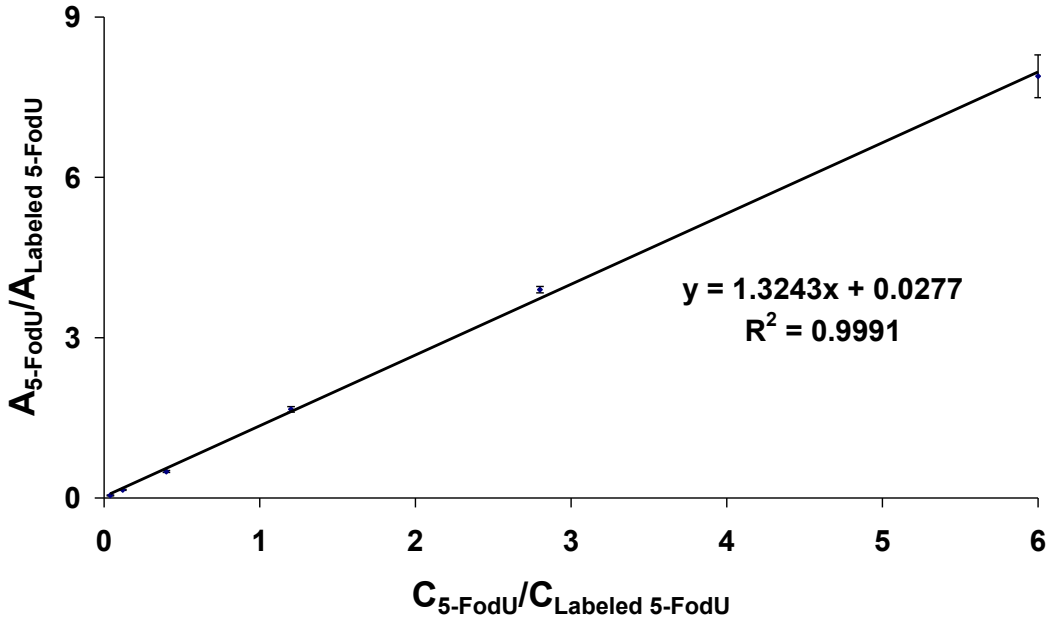

Figure B7. Calibration curve for the quantification of 5-FodU. X axis is the molar ratio and Y axis is the peak area ratio.

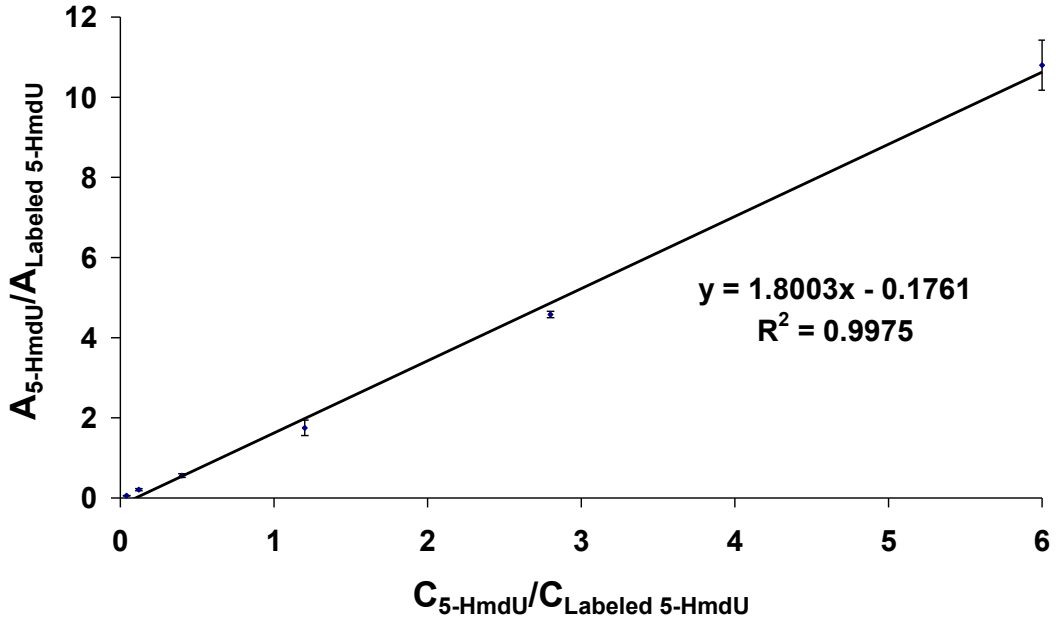

Figure B8. Calibration curve for the quantification of 5-HmdU.

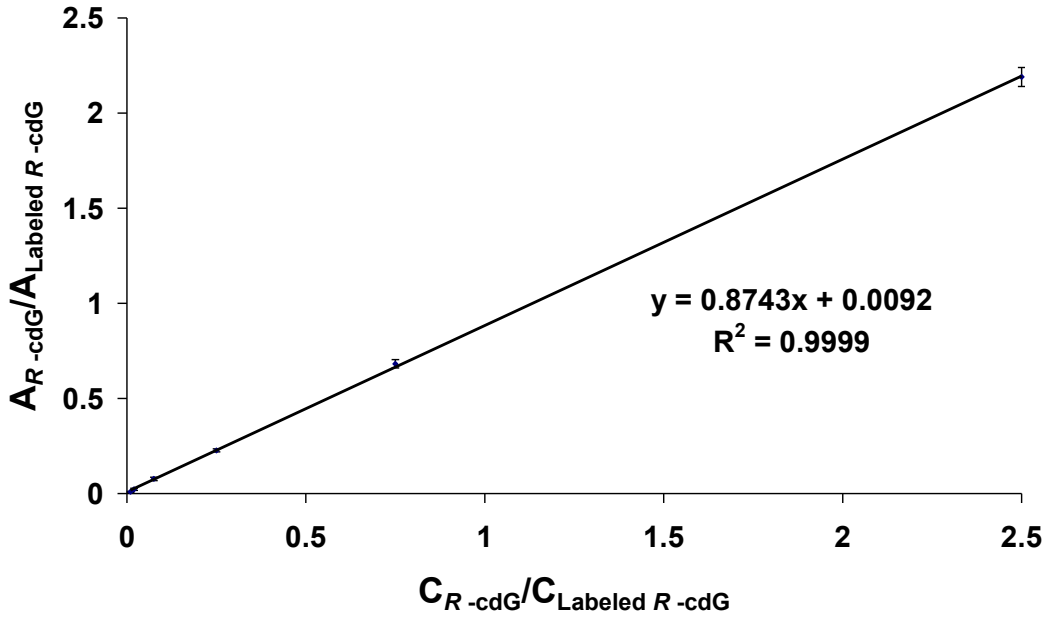

Figure B9. Calibration curve for the quantification of *R*-cdG.

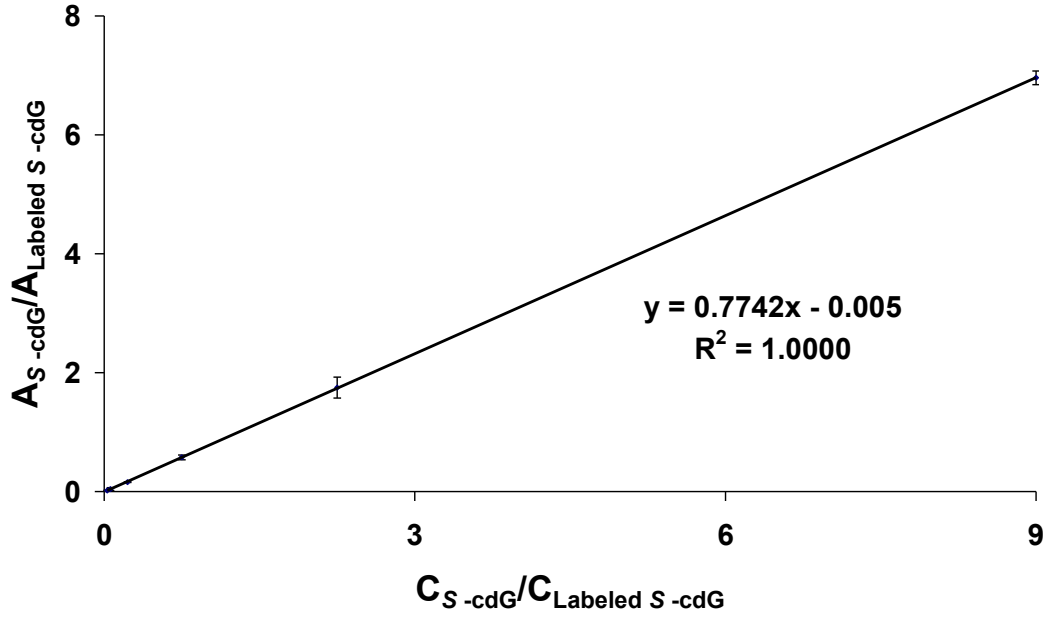

Figure B10. Calibration curve for the quantification of *S*-cdG.

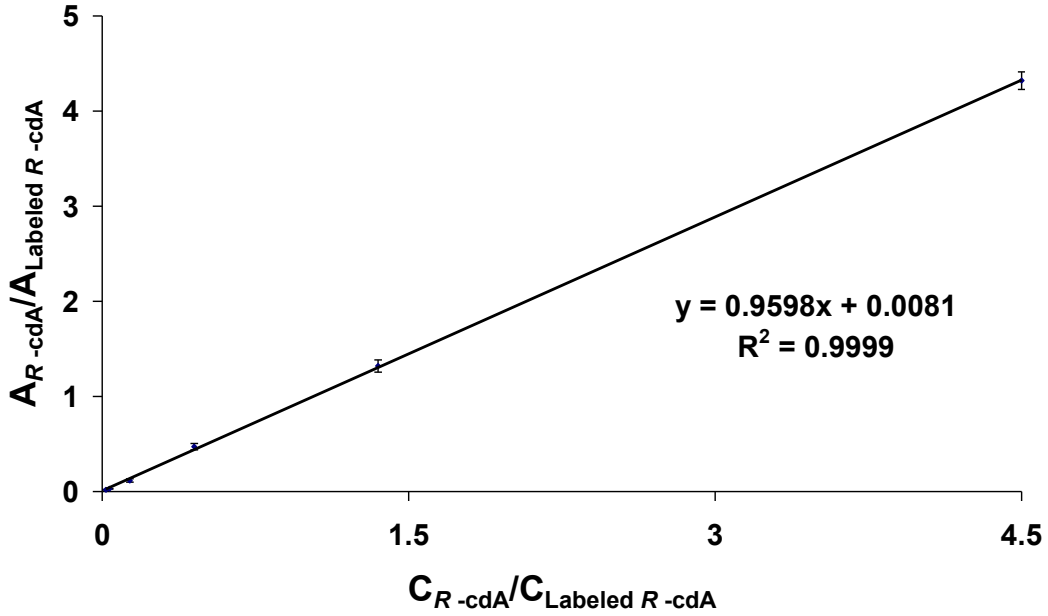

Figure B11. Calibration curve for the quantification of *R*-cdA.

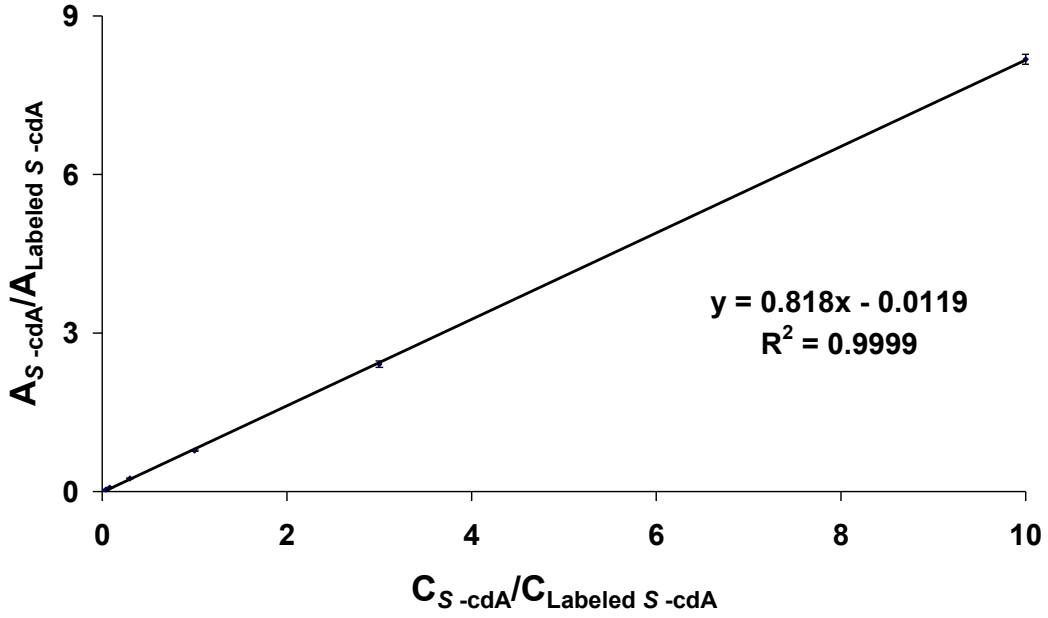

Figure B12. Calibration curve for the quantification of *S*-cdA.

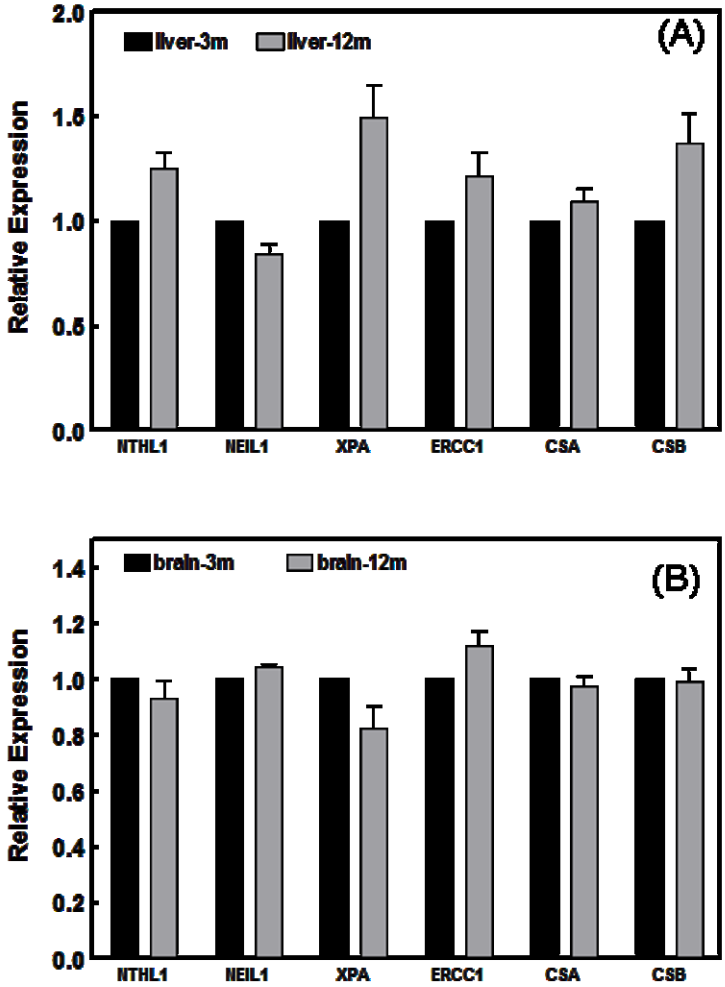

Figure B13. The mRNA levels of NTHL1, NEIL1, XPA, ERCC1, CSA and CSB in the livers (A) and brains (B) of LEC+/- (3m or 12m) rats. The results were obtained by real-time qRT-PCR with the use of GAPDH as standard. The data represent the mean ± S.D. of three separate experiments.

Appendix C

Supporting Information for Chapter 4

"Induction of 8,5'-Cyclopurine-2'-deoxynucleosides in Isolated DNA by Fenton-Type Reagents"

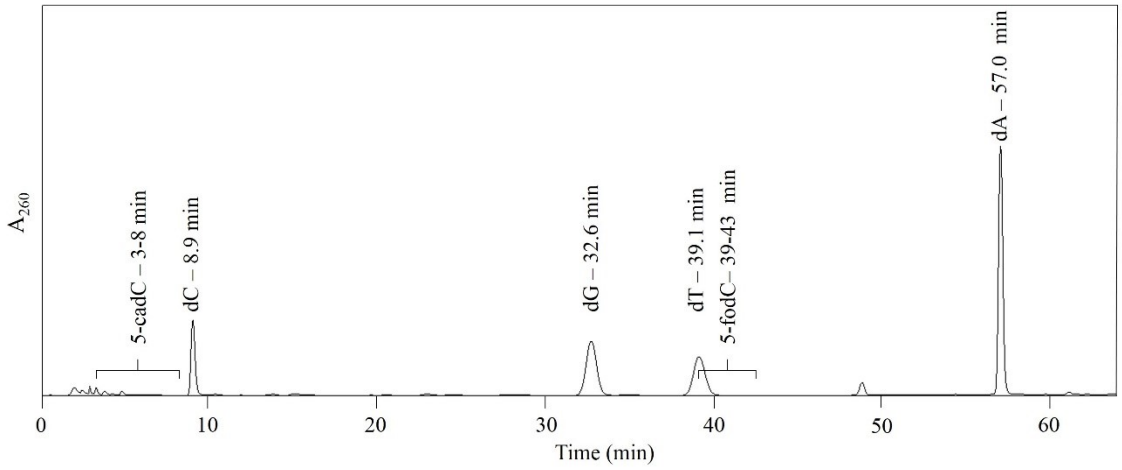

Figure C1. Representative HPLC trace for the enrichment of 5-fodC and 5-hmdC from the enzymatic digestion mixture from isolated Calf Thymus DNA treated with Cu(II)/H_2O_2/ascorbate.

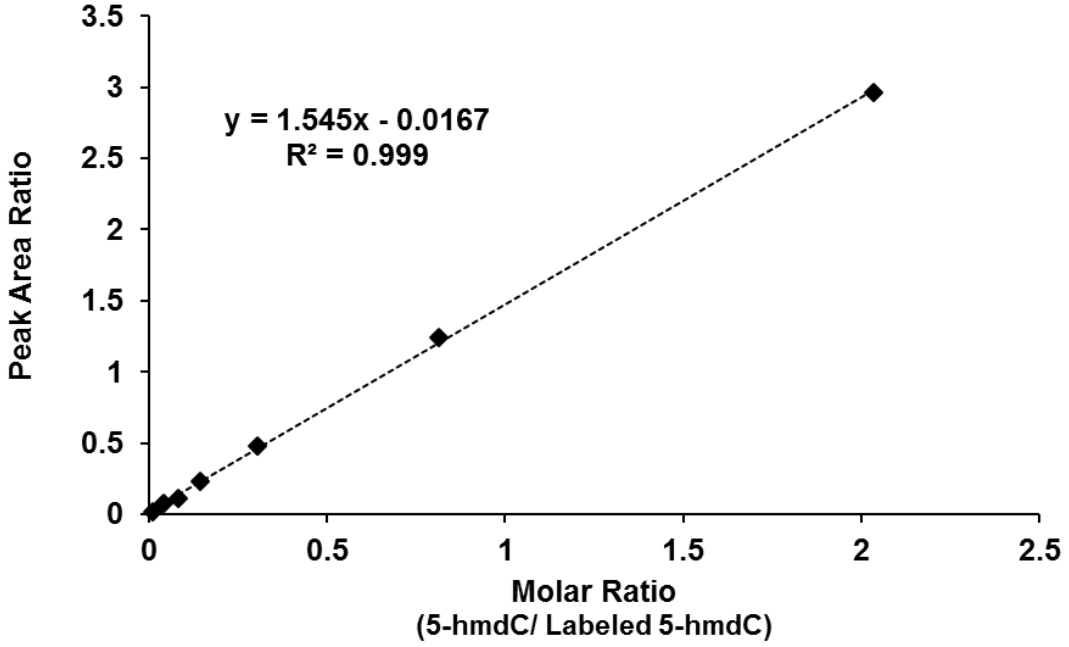

Figure C2. Calibration curve for the quantification of 5-hmdC by LC-MS/MS/MS with stable isotope dilution method. Plotted is the peak are ratios (5-hmdC/labeled 5-hmdC) with respect to the molar ratio of the unlabeled nucleoside over that of the corresponding stable isotope-labeled standard of 5-hmdC (30 fmol).

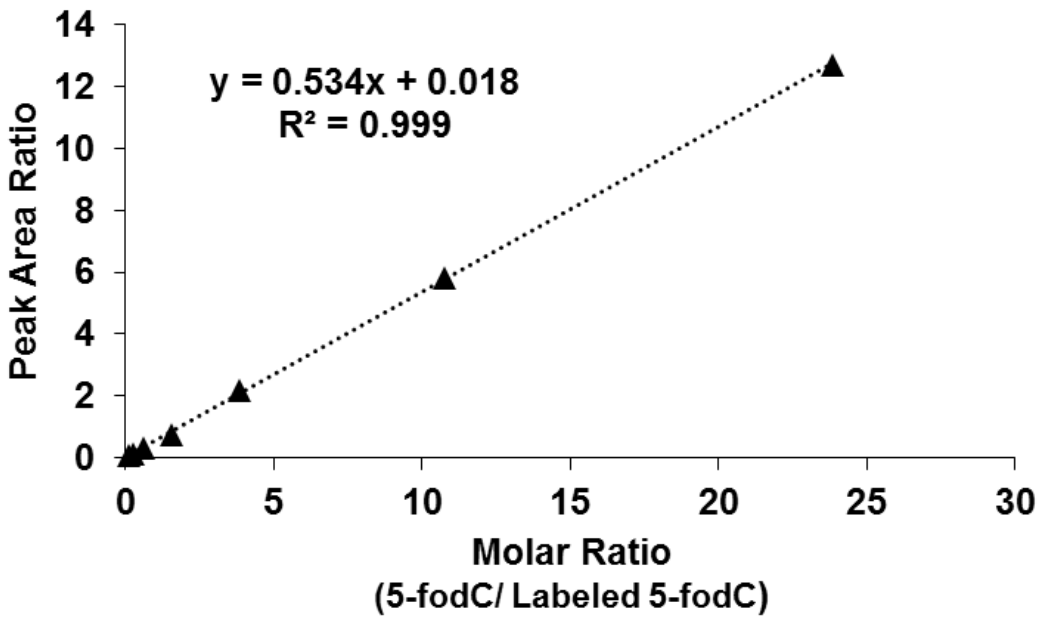

Figure C3. Calibration curve for the quantification of 5-fodC by LC-MS/MS/MS with stable isotope dilution method. Plotted is the peak are ratios (5-fodC/labeled 5-fodC) with respect to the molar ratio of the unlabeled nucleoside over that of the corresponding stable isotope-labeled standard of 5-fodC (30 fmol).

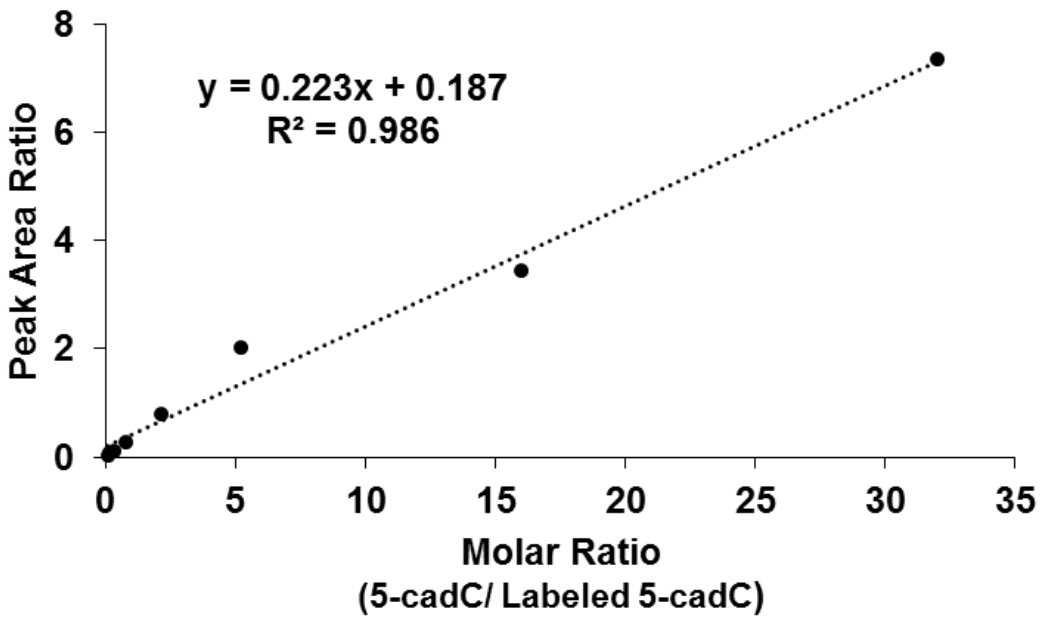

Figure C4. Calibration curve for the quantification of 5-cadC by LC-MS/MS/MS with stable isotope dilution method. Plotted is the peak are ratios (5-cadC/labeled 5-cadC) with respect to the molar ratio of the unlabeled nucleoside over that of the corresponding stable isotope-labeled standard of 5-cadC (25 fmol).

Table C1: A summary of the levels (in lesions per 10^6 nucleosides) of cdA and cdG in calf thymus DNA treated with Cu(II)/H_2O_2/ascorbate. The data represent the means and standard deviations of results from three independent oxidation and LC-MS/MS/MS quantification experiments.

	5-hmdC	5-fodC	5-cadC
Control	61 ± 10	0.87 ± 0.47	1.2 ± 0.1
A	179 ± 29	7.6 ± 1.1	3.1 ± 0.3
B	285 ± 51	12.2 ± 3.8	9.7 ± 2.4
C	442 ± 46	28.0 ± 8.8	29.2 ± 5.9
D	683 ± 38	46.8 ± 6.0	67 ± 18